Preparation of antifouling poly(vinyl chloride) membranes for application in wastewater treartment

Zhou, Zhung

(Degree)
博士（学術）

(Date of Degree)
2017-03-25

(Date of Publication)
2019-03-25

(Resource Type)
doctoral thesis

(Report Number)
甲第6909号

(URL)
https://hdl.handle.net/20.500.14094/D1006909

Doctoral Dissertation

Preparation of antifouling poly(vinyl chloride) membranes for application in wastewater treatment

（水処理用耐ファウリングポリ塩化ビニル膜の作製）

January 2017

Graduate School of Engineering

Kobe University

Zhuang Zhou

Contents

Chapter I

Introduction

I.1MEMBRANE PROCESS

I.1.1 Overview of membrane separation

Membrane separation has become a valuable and rapidly developing technology in the past decades. It is widely used in various separation fields, such as wastewater treatment, artificial organs and energy storage systems [1]. A membrane can simply be considered as a selective barrier between two phases. The membrane separation process is schematically represented in Fig. I. 1 [2]. As shown in Fig. I. 1, when the membrane comes into contact with phases 1 and 2, components in the feed solution can be transported through the membrane at different rates, owing to the driving force and the different physical/chemical interactions between the membrane and each component. The driving force can be attributed to the difference of pressure, concentration, temperature, electricity potential, and so on. The membrane separation process can also be considered to be a process of energy exchange. The separation process requires energy from the outside, because the free enthalpy of the mixture is usually lower than that of the pure substance. Therefore, the cost of the separation process depends on the energy consumption over the whole process. Generally speaking, the energy consumption increases as the concentration and the particle size in the feed solutions decrease. Today, researchers are working to develop membranes that can separate substances with smaller particle sizes by consuming lower energy.

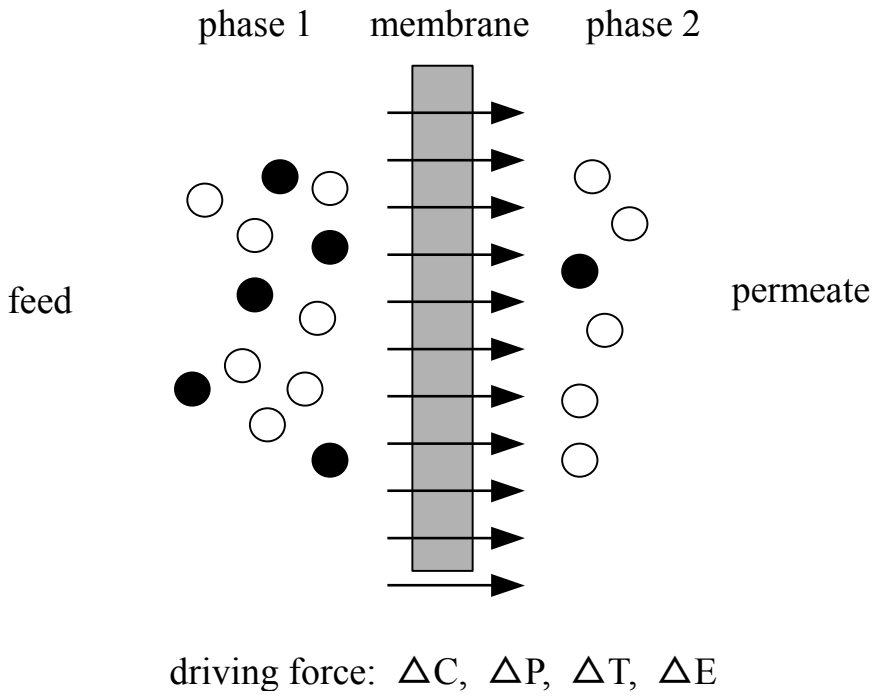

Fig.I.1 Membrane separation process in a two-phase system [1].

I.1.2 Classification of membranes

Membranes can be classified in different ways [1]. In terms of materials, they can be classified as organic, inorganic or organic/inorganic composited membranes. In terms of shapes, they can be classified as either flat sheet or hollow fiber membranes. In terms of morphologies, they can be classified as either symmetric or asymmetric membranes. Also, based on the properties of the feed solutions, they can be classified as gas separation, liquid separation, or solid separation membranes, etc. Usually, the membranes are divided based on the applied fields and the separation principles, including microfiltration (MF), ultrafiltration (UF), nanofiltration (NF), reverse osmosis (RO), forward osmosis (FO), electrodialysis (ED), membrane electrolysis (ME), diffusion dialysis (DD), pervaporation (PV), membrane distillation (MD) and membrane contactors (MC) [3]. The general membrane applications and the most used membranes are listed in Fig. I. 2.

MF, UF, NF and RO are the most widely used separation processes for water treatment. MF membranes with pore sizes ranging from 0.1 to 10 micrometers (µm) have been used for municipal water treatment since 1987 [4]. They can remove turbidity spikes and bacteria with high permeate fluxes and considerable separation precision. UF membranes with pore sizes

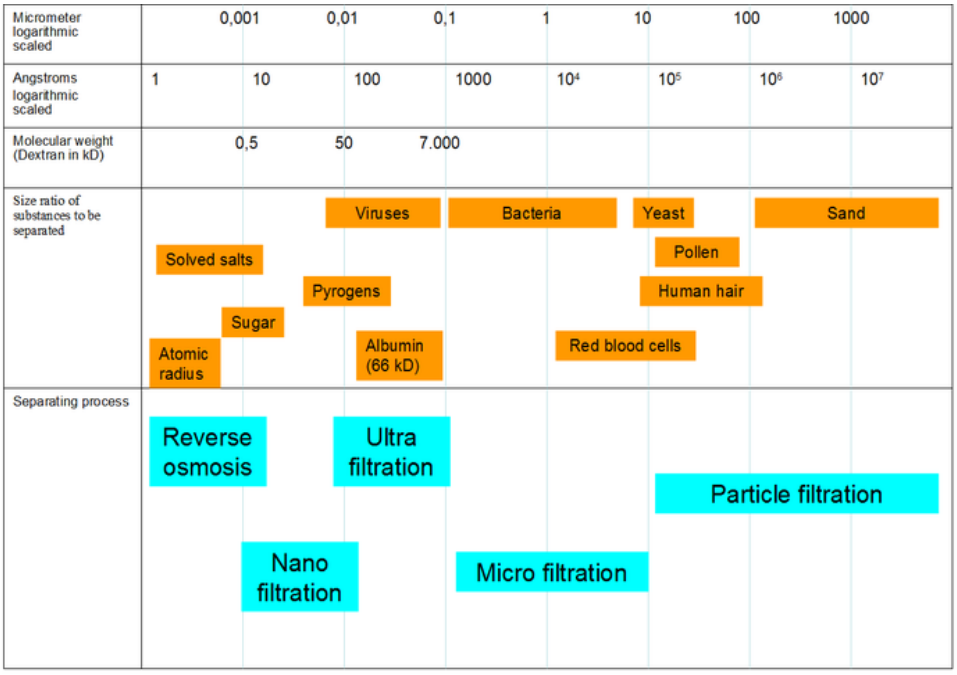

Fig. I. 2 General membrane applications and the most used membranes [3].

ranging from 1 nanometers (nm) to 0.1 µm can retain solutes with higher molecular weights (10^3 - 10^6 Da), whereas solutes with lower molecular weights can still penetrate such membranes when pressure drops. In industrial applications, UF membranes are mostly used for the purification of proteins or colloid solutions. NF membranes can effectively separate dye molecules or matter with low molecular weight (lower than10^3 Da) from wastewater. NF membranes show the good perspective on the application to the softening of groundwater or the concentration unit in food processing. RO membranes are semipermeable membranes that have a dense non-pore skin layer. It can remove ions and other molecules from drinking water by applying a pressure that exceeds the osmotic pressure. In general, industrial separation

processes are composed of multiple separation units. For example, drinking water purification processes usually include MF, UF, NF and RO processes to remove macro particles, bacteria, metal ions and salt, respectively. After these units, clean water can be obtained. Suitable membrane processes should be designed to meet the quality of the permeate production.

I.2 PREPARATION OF POLYMER MEMBRANES

Numerous techniques are used to fabricate membranes (as shown in Table I. 1) [1]. Sintering, stretching, track-etching, and phase inversion are usually used to prepare polymer membranes. Template leaching and sol-gel processes are mostly used to prepare inorganic membranes. In the following chapters, I introduce the preparation methods of polymer materials only.

I.2.1 Introduction of general preparation methods

Generally speaking, porous membranes can be obtained from sintering, stretching, track-etching, and phase inversion methods. Sintering methods that fabricate only MF membranes with low porosity (around 10-20 %) are carried out by compressing polymeric particles and then sintering at high temperature. Therefore, only polymers with high chemical and thermal resistance, such as polyethylene and polytetrafluoroethylene, can be used in such a method. Stretching methods can fabricate MF membranes with small pore sizes (~0.1 μm) and high

Table I. 1 Several methods for preparing porous membranes.

Preparation processes		Applicable material examples	UF	MF	Properties
Phase inversion	Nonsolvent induced phase separation (NIPS)	Polysulfone Polyethersulfone Polyacrylonitrile Cellulose derivatives Polyvinylidene fluoride	○	○	Asymmetric structures High permeability High porosity
	Thermally induced phase separation (TIPS)	Polyethylene Polypropylene Polyvinylidene fluoride		○	Generally high strength High porosity
Stretching (semicrystalline)		Polyethylene Polypropylene Polytetrafluoroethylene		○	Slit-like pores

Uniform and porosity (~90%), respectively. However, only semi-crystalline polymers can be used for this method. Track-etching methods can be used to fabricate various membranes with pore sizes ranging from 0.02 to 10 μm. However, the surface porosity is low (only 10%). Phase inversion is a versatile method that can prepare various types of membranes. Membranes prepared from phase inversion are mostly composed of dense skin layers and finger-like or spongy sublayers. The skin layer works as an effective separation layer, and largely determines the membrane's permeability and selectivity.

I.2.2 Phase inversion

Phase inversion is a controlled process of transforming polymers from a liquid state to a solid state. Firstly, one liquid phase is transformed into two liquid phases (liquid-liquid demixing) or one liquid phase and one solid phase (liquid-solid demixing). Then, the liquid phase with high polymer concentration solidifies and forms the membrane matrix, while the liquid phase with low polymer concentration forms the membrane pores when the liquid is exchanged by the solution and removed out of the membrane structure. Phase inversion processes are often classified as follows: (a) precipitation from the vapor phase (vapor-induced phase separation (VIPS)), (b) precipitation by controlled evaporation, (c) immersion precipitation (liquid-induced phase separation), and (d) thermal precipitation (thermally induced phase separation (TIPS)) [1]. Except for (d), such methods are also classified as nonsolvent induced phase separation (NIPS). The structures of the resultant membranes can be varied by manipulating the properties of the polymer materials and the conditions of the preparation processes.

I.2.3 NIPS process

Since Loeb and Sourirajan first developed a cellulose acetate (CA) membrane via the NIPS method in the 1960s, NIPS has become one of the most widely used methods for commercial membrane preparation because it is cheap and simple to prepare, requires low operating temperatures, and because of the wide number of polymer materials that are available [4].

The polymer dope solution for the NIPS method is usually composed of at least three components, including a polymer, solvent and nonsolvent. The nonsolvent and the solvent must be miscible under the preparation conditions. NIPS could be considered as a process that associates the penetration of the nonsolvent into the polymer dope solution with the leaching

of the solvent. The procedures to prepare flat-sheet membranes via the NIPS method can be briefly described as follows:

(a) Dissolve polymers into the solvent to obtain a homogeneous dope solution.
(b) Shape the homogeneous dope solution into a desired shape, such as a flat sheet or hollow fiber.
(c) Immerse the shaped dope solution into the coagulation bath, inducing phase separation by the exchange of solvent and nonsolvent, and forming the membrane structure.

The system of the NIPS process can be described by a ternary phase diagram. As shown in Fig.I.3, three corners in the triangle represent the polymer, solvent, and nonsolvent; three axes indicate the combinations of any two components; and each point inside the triangle shows the ternary composition [1]. When the change of composition in dope solution follows Path a in the Fig. I.3, a sufficient amount of nonsolvent enters the dope solution, leading to the liquid-liquid phase separation and the formation of a porous membrane. On the other hand, the solid-liquid phase separation will occur and form a dense membrane when the change in composition follows the direction of Path b.

The advantages of the NIPS method are summarized as follows [4]: (a) it can be carried out at room temperature via a simple and cheap process; (b) the prepared membranes contain asymmetric structures and high porosity; (c) a broad range of polymer materials are available. The NIPS method is widely used in the preparation of various membranes, such as RO membranes, UF membranes, MF membranes, membranes for gas separation, etc.

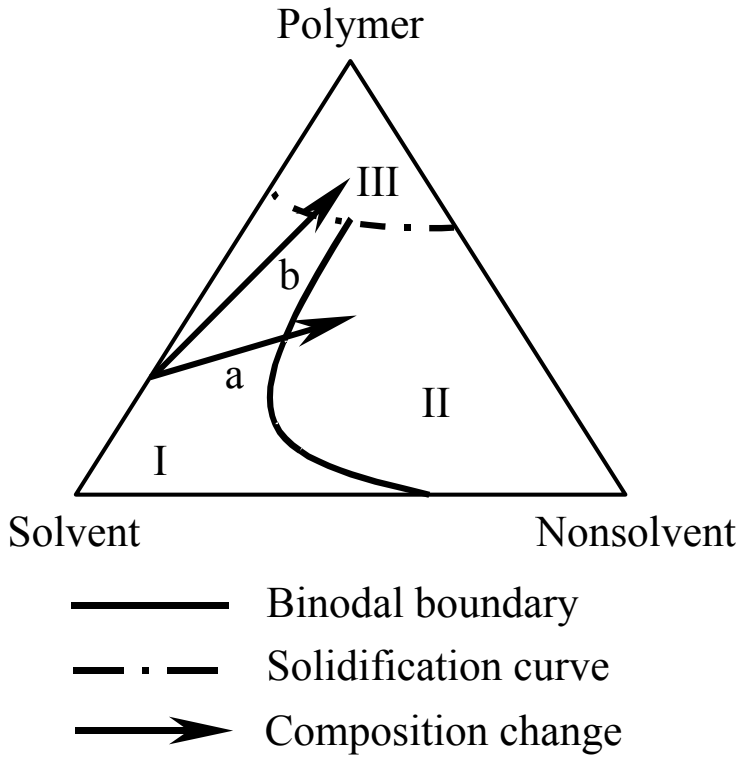

Fig. I. 3 Ternary phase diagram for the NIPS process. I: One liquid phase region; II: Two phases region; III: One solid phase region.

I.3 MEMBRANE FOULING AND ANTIFOULING MODIFICATION

I.3.1 Membrane fouling phenomenon

The membrane performance, especially the water flux, decreases over the filtration time during the membrane filtration process (in Fig. I.4). Such flux decline can mainly be attributed to the membrane fouling phenomenon, which is defined as the deposition of macromolecules, retained particles, emulsions, colloids, etc. on/in the membrane structures [5-7]. Membrane fouling is mainly classified as pore narrowing, pore plugging and cake layer formation. Compared with non-pore membranes, porous MF and UF membranes are more susceptible to fouling during the filtration process.

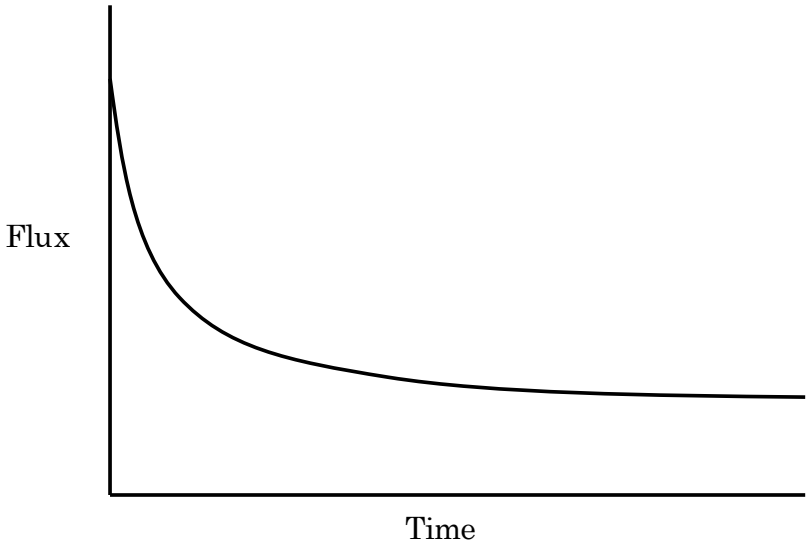

Fig. I. 4 Flux decline behavior as a function of time during the filtration process.

I.3.2 Three modes of membrane fouling

Fouling is a very complex phenomenon that is difficult to control in membrane systems [8]. In order to theoretically describe fouling phenomena, membrane fouling is generally separated into three primary modes based on the size of the foulant and the size of the membrane pores. The three modes, pore narrowing, pore plugging, and cake layer formation, are schematically shown in Fig. I. 5.

When the diameter of the foulant in the feed solution is much smaller than that of the membrane pores ($d_{particle} << d_{pore}$), the membrane pores are constricted or narrowed by foulant adsorption on the surface or inside the pores during the filtration process. The extent of pore narrowing in this case is highly dependent upon the membranes morphologies. In general, porous membranes with high porosity have a higher fouling propensity, because foulant particles are more likely to attach to the membrane surfaces and to be retained in the membrane structures.

When the diameter of the foulant in the feed solutions is smaller or similar to that of the membrane pores ($d_{particle} \leq d_{pore}$), the foulant blocks the pores and induces pore plugging. Because the pore narrowing and pore plugging usually occur at the same time in real filtration processes, these two modes are together named pore clogging. Pore clogging in MF and UF membranes leads to the decline of membrane porosity and blocked flow in the channel [9]. Significant pore clogging of the fouled membranes can be difficult to recover from, even with back flushing or chemical cleaning [10].

When the diameter of the foulant in the feed solutions is much larger than that of the membrane pores ($d_{particle} > d_{pore}$), all the foulants will be retained on the membrane surface, forming a cake layer on the surface. The cake layer mainly results from the aggregation or deposition of proteins, microparticle colloids, microorganisms, etc. This then causes the membrane's permeation flux to decrease significantly or even fall to zero, as the cake layer grows in thickness during the filtration process. The cake layer meanwhile can inhibit particles in feed solutions from passing through the membrane, increasing membrane selectivity.

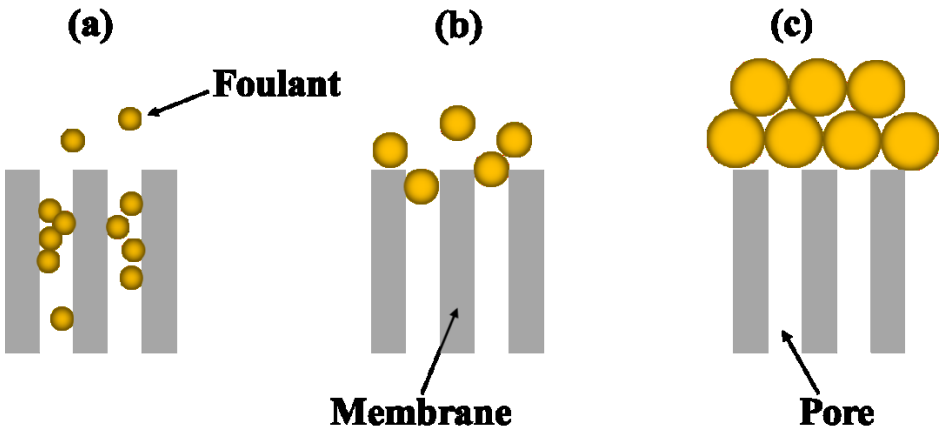

Fig. 1. 5 Illustration of particle fouling mechanisms. (a) Pore narrowing, $d_{particle} << d_{pore}$, (b) Complete pore blockage or pore plugging, $d_p \leq d_{pore}$, and (c) Cake layer formation, $d_{particle} > d_{pore}$.

In addition to the above-mentioned modes, membrane fouling can also be classified according to whether the fouling is reversible or irreversible. Irreversible fouling mainly results from pore narrowing and pore plugging, whereas reversible fouling is mainly attributed to the formation of a cake layer. The occurrence of irreversible fouling is generally inevitable in MF and UF membranes. The use of techniques to limit irreversible fouling has become a crucial issue in membrane applications.

I.3.3 Factors affecting membrane fouling

Membrane fouling depends upon the interaction between the foulant and the membrane, which mainly results from factors such as the foulant's properties, operating conditions, membrane properties, etc.

I.3.3.1 Effect of feed properties

The properties of the foulants in the feed solution, such as the lability, aggregation, shapes, and the net charge of the foulants, are all important factors affecting membrane fouling. It should be noted that water resources are usually composed of various kinds of foulants. Moreover, these foulants may interact with each other and may significantly affect the fouling propensity in water treatments. Membrane fouling can also be affected by the environments of the water resources, such as the pH, temperature, ion strength, viscosity, etc.

I.3.3.2 Effect of operating conditions

The operating conditions of the water treatment, such as the flow velocity, the flow turbulence, initial flux, and the operating pressure, control the membrane fouling. The fouling can be suspended by increasing flow velocity and turbulence, because turbulent flow can sweep

off the deposited foulants on the membrane surfaces. The initial flux and operating pressure in the filtration process also significantly changes the fouling propensity. The membrane has stable performance over a long-term filtration when the initial flux is lower than the critical flux, whereas severe fouling rapidly occurs when the initial flux is higher than such critical flux [11, 12].

I.3.3.3 Effect of membrane properties

The membrane properties, including surface hydrophobicity, surface charge, pore size, and surface roughness, largely determine membrane fouling [13].

The particles in the feed solution can be adsorbed on the membrane surface when the particles and membrane surface have the opposite charge. When the membrane and the particles in the feed solution have the same charge, the antifouling performance in the filtration process is improved because of the electrostatic repulsive force [14]. Membranes with a negatively charged surface exhibit good resistance to negatively charged humic acids (HA) [15], bovine serum albumin (BSA), and bacteria [16], while positively charged membrane surfaces effectively resist the adsorption of lysozyme [17]. Therefore, membrane surfaces with balanced positive and negative charges have better antifouling performance in wastewater treatment because of the complex components in wastewater [17].

The fouling of porous membranes (MF, UF, etc.) becomes more serious when the membrane surface has large pore sizes or a wide pore size distribution [18]. Surface roughness is also an important factor related to membrane fouling [13, 19]. Generally speaking, rougher membrane surfaces can induce severe fouling because the foulant can deposit and accumulate in the valleys between projection structures on the membrane surface [19]. Therefore, membranes with the smooth surfaces are desired for inhibiting fouling problems.

Membranes with hydrophilic surfaces can foul less than those with hydrophobic surfaces because of the hydrophobic-hydrophobic interaction between foulants and membrane surfaces [20]. For example, proteins are more easily adsorbed on hydrophobic membrane surfaces than on hydrophilic surfaces. Therefore, increasing the hydrophilicity of membrane surfaces has become an important subject in membrane engineering for improving membrane performance and expanding membrane applications [21]. The following sections will briefly introduce the general methods that are used to obtain a hydrophilic membrane with antifouling properties.

I.3.4 Preparation of antifouling membranes using hydrophilic materials

Hydrophilic membranes can be prepared directly using hydrophilic polymer materials, such as cellulose and its derivatives [4]. In a previous study, cellulose acetate (CA), cellulose acetate butyrate (CAB), and cellulose acetate propionate (CAP) were used to prepare hollow fiber membranes via the phase inversion method [22]. Three membranes, particularly the CA membrane, had a hydrophilic surface and showed good antifouling performance when filtering HA and BSA solutions.

With the exception of natural hydrophilic polymer materials, modified or synthesized polymers can also be used to prepare hydrophilic membranes. Sulfonation is frequently used for polymer modification to increase hydrophilicity [23, 24]. For example, the membrane prepared using sulfonated polyethersulfone (SPES) [24] or sulfonated polyethersulfone Cardo [25] exhibited a hydrophilic surface and antifouling properties, whereas those prepared from PES or PSF obtained a hydrophobic surface with a high fouling propensity. Recently, amphiphilic copolymers resulting from the polymerization of hydrophobic and hydrophilic monomers have shown good potential as membrane materials [26-28]. Chen et al. [26] used a

series of polyacrylonitrile-block-polyethylene glycol (PAN-b-PEG) copolymers to prepare UF membranes via the NIPS method. The prepared membranes exhibited high hydrophilicity and considerable fouling resistance to the BSA solution. Moreover, they reported that antifouling properties increased with increasing PEG segment content rather than PEG chain length.

Although hydrophilic and antifouling membranes can be directly prepared from hydrophilic polymer materials, it should be noted that such polymers are generally soft materials and resultant membranes have low mechanical properties which would limit membrane applications. Therefore, these soft hydrophilic polymer materials are seldom directly used in the fabrication of commercial membranes [29].

I.3.5 Hydrophilic modification of hydrophobic membranes for antifouling

The most commercial polymer membranes are prepared by hydrophobic materials, such as PES, PVDF, etc., owing to their high mechanical properties, chemical resistance and thermal stability. However, hydrophobic-hydrophobic interactions between the foulant and the membrane surface lead to the severe membrane fouling problem. Therefore, it is necessary to incorporate hydrophilic or polar groups onto the hydrophobic membrane surface to endow the modified membrane surface with antifouling properties.

I.3.5.1 General hydrophilic modification methods

To improve membrane antifouling properties, coating, grafting and blending are the generally used approaches in membrane engineering [4].

Coating is one of the most popular methods to improve membrane surface antifouling properties. In this method, a hydrophilic or fouling resistance layer is simply coated and formed on the top surface of the virgin polymer membranes. Versatile polymers, such as the

zwitterionic copolymers, hydrophilic copolymers and negatively charged polymers, can be used to form the coating layer with different surface properties [30]. However, the antifouling performance of the modified membranes usually decreases during the membrane separation process. The coating layer can easily peel off, due to the low interaction between the thin coating layer and the virgin membrane surface. Moreover, only the top surface can be modified via the coating method, whereas the wall surface of the membrane pores hardly changes. In addition, coating methods decrease membrane water permeability, owing to the inevitable accumulation of the coating layer on the pore surface.

Grafting is a promising method to generate a fouling-resistant brush layer on the membrane surface via covalent bonds. Compared with the physical surface coating methods, grafted membranes usually show long-term durability, owing to the strongly covalent attachment of the chains on the surface [31]. High energy irradiation, plasma and enzymatic, etc. are common approaches to initiating surface grafting [32]. In the grafting process, these approaches are selected by considering both the chemical composition of the virgin membranes and the expected characteristics of the modified surface. However, an inevitable problem for grafting technology is that the pure water permeability of the modified membranes declines, because the grafted chains plug membrane pores and decrease the surface porosity [32]. It is worth pointing out that the grafting method is mainly used in post-treatment of the flat-sheet membranes rather than hollow fiber membranes, limiting its application in industral production [30].

Blending is a relatively easy and effective way to endow the membrane surface and the walls of the pores with hydrophilicity and fouling resistance [8]. Blending modification is also the most practical method in industrial production applications [33]. A blending approach can be used to obtain an antifouling or hydrophilic surface during the membrane preparation

process [30]. The major additives used in the blending method are hydrophilic homopolymers and amphiphilic copolymers. In the following sections, these two types of additives will be briefly introduced.

I.3.5.2 Blending method using homopolymers

Polyethylene glycol (PEG) and polyvinylpyrrolidone (PVP) are the most frequently used hydrophilic homopolymer additives used in blending modification to improve the membrane surface hydrophilicity and antifouling properties. Adding hydrophilic homopolymer additives to polymer dope solutions not only increases membrane hydrophilicity, but also affects membrane formation, leading to different membranes morphologies. The concentration and molecular weight of the additives affect the properties of the blend membranes [34-36]. Generally speaking, when increasing the blend ratio or molecular weight of the PEG/PVP, the thermodynamic stability of the polymer dope solution will decrease, leading to the instantaneous demixing of the precipitation and usually forming the porous membranes with higher pure water permeability. However, if the blend ratio or the molecular weight is higher, the exchange rate of the solvent and non-solvent can be decreased due to the increased viscosity of the dope solution, leading to a delayed demixing. Consequently, membranes with less porous surfaces and lower pure water permeability can be obtained [37]. However, using PEG and PVP, it is difficult to obtain a long-term hydrophilic/antifouling membrane, because these additives are water-soluble and can leach out during membrane preparation and the filtration process. Therefore, PEG and PVP are mainly regarded as pore-forming additives and used to modify the membranes morphologies.

I.3.5.3 Blending method using amphiphilic copolymers

Ever since Mayes first used an amphiphilic copolymer poly(methyl methacrylate-*r*-polyoxyethylene methacrylate) (P(MMA-*r*-POEM)) to improve the antifouling properties of the PVDF membrane, the use of amphiphilic copolymers as blending additives in the preparation of antifouling membranes has attracted worldwide attention [38]. Amphiphilic copolymers are composed of hydrophilic and hydrophobic segments. The general types of amphiphilic copolymers are shown in Fig. I. 6. Because of the unique chemical structures, amphiphilic copolymers show much potential for use in blending modification. The hydrophobic segments of these copolymers make them compatible with the membrane matrix and help to retain them in the membrane, while hydrophilic segments endow the membrane

with hydrophilicity and antifouling properties [39]. The hydrophilic segments of the copolymer are spontaneously enriched on the membrane surface during the phase separation process, because of the strong interaction between hydrophilic segments and water molecules in the coagulation bath [40]. Consequently, a stable layer of hydrophilic chains can be obtained on the surfaces of the membrane and pore walls, protecting the membrane surface from the

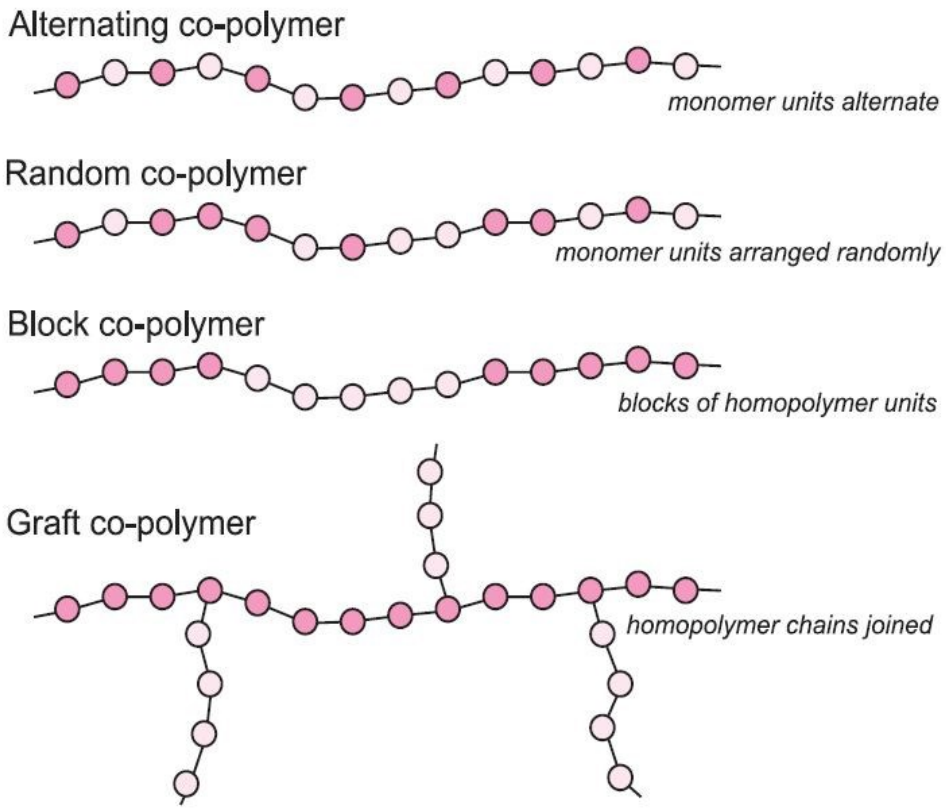

Fig. I.6 Structures of different copolymers [43].

approaching foulant [41]. Among the developed copolymers, PEG-based copolymers exhibit good antifouling performance. This is because PEG chains have large excluded volume, hydrophilicity, and unique coordination with surrounding water molecules in the aqueous solution, resulting in a strong capacity to form hydration layers that resist foulant adsorption [42]. In addition, the antifouling properties of PEG chains that have been incorporated on the

membrane surface can be further improved by increasing the density or the length of the PEG chains [41, 42].

I.4 PVC MEMBRANES AND MODIFICATIONS

I.4.1 PVC membranes

Poly(vinyl chloride) (PVC) is a promising alternative material for membrane preparation because of its excellent mechanical strength, high corrosion resistance, and low cost [44-46]. Various PVC membranes for commercial use have already been produced by some companies, such as Litree Corp (China). However, severe fouling problems occur in PVC membranes because of their hydrophobic nature [47]. Therefore, it is necessary to improve membrane antifouling properties to further their development and application. Moreover, considering that membrane mechanical properties also limit membrane lifetime and membrane applications, it is also necessary to design and prepare robust PVC membranes for use in harsh conditions.

I.4.2 Antifouling modification of PVC membranes

The hydrophobic nature of PVC leads to severe membrane fouling due to the adsorption and the accumulation of foulants on membrane surfaces [48]. Increasing membrane surface hydrophilicity effectively inhibits membrane fouling [49]. Therefore, several surface modification methods have been developed to increase the hydrophilicity and antifouling properties of PVC membranes, including blending [50-52], surface coating [53-55], and surface grafting [56-59]. Surface coating and grafting methods usually involve extra steps in membrane preparation and have difficulty in modifying the walls of the membrane's internal pores. Polymer blending is a convenient and versatile approach to improving both the membrane surface and internal pore walls. Homopolymers, including carboxylated poly(vinyl

chloride) (CPVC) [60], PVP [61], polyvinyl formal (PVF) [50], cellulose acetate (CA) [62], etc., have been used to prepare hydrophilic blend PVC membranes. However, the blending method is limited by the low compatibility between such homopolymers and PVC and the low durability of the additives.

Using amphiphilic copolymers as blending additives has also been investigated for the preparation of antifouling PVC membranes [63, 64]. The hydrophilic segments of the amphiphilic copolymer segregate on the membrane surface, making the membrane hydrophilic with good fouling resistance. Also, the hydrophobic segments provide compatibility with the membrane matrix and improve copolymer retention in the membrane matrix. For example, copolymers containing PEG chains easily form a hydration layer, which is resistant to foulant adsorption [51, 65]. Various PEG-based copolymers have been proposed for the hydrophilic modification of PVC membranes, such as Pluronic F-127 [51, 65], poly(ether sulfone-g-poly(ethylene glycol)methyl ether methacrylate) (PES-*g*-PEGMA) [64]. In those works, the copolymer/PVC blend membranes showed desirable stability and antifouling properties.

I.4.3 Mechanical enhancement of PVC membranes

Blending PEG-based polymer materials effectively improves the PVC membrane surface's antifouling properties. However, increasing the PEG-based copolymer content in PVC membranes can decrease the mechanical strength [66], owing to the softness of the PEG material [67]. The membrane's low mechanical strength can limit its application. For example, severe aeration or a backflush process can damage the membrane structure during wastewater treatment [68]. Therefore, PVC hollow fiber pmembranes having both antifouling properties and considerable mechanical strength are desirable for membrane engineering.

Several methods have been developed to increase the mechanical strength of PVC membranes. These methods include the incorporation of nano-size particles [69, 70] and the preparation of mechanical enhanced dual-layer PVC hollow fiber membranes [71-73]. However, these methods suffer from increasing costs and changing membrane properties. Recently, braid-reinforced hollow fiber membranes have attracted significant attention [74-76]. Braid-reinforced hollow fiber membranes are prepared by coating the dope solution onto low-cost tubular braids. Fan et al. [77] used the hydrophilic homopolymer CA as the coating material to prepare braid-reinforced hollow fiber membranes. This kind of membrane showed high mechanical properties and low fouling propensity when filtering a milk solution. Braid-reinforced membranes show much promise for the preparation of hydrophilic membranes with high mechanical strength.

I.5 PURPOSE OF THIS STUDY

Membrane separation technology has become one of the most promising methods for drinking water and wastewater treatment. The membrane market has grown rapidly because of increasing demands for safe water. MF and UF membranes (porous membranes) have dominated market share for commercial membranes. For membranes used in wastewater treatment, such as PES, PVDF, etc., are popular membrane materials because of their good processing requirements, robust mechanical strength, high chemical and thermal resistance, etc. Recently, PVC has also attracted attention as a potential membrane material, owing to its low cost and high chemical resistance. However, the hydrophobic nature of such polymer materials leads to severe fouling problems, limiting the membrane's application.

The purpose of this study is to prepare advanced PVC membranes with antifouling properties by using amphiphilic copolymers and the blending method. A series of amphiphilic

copolymer poly(vinyl chloride-*co*-poly(ethylene glycol)methyl ether methacrylate) (poly(VC-*co*-PEGMA)) with varying PEGMA segment percentages were first used to prepare antifouling membranes using the NIPS method, and applied to BSA filtration for evaluating the antifouling properties. The effect of the membrane material, pore size, and initial water permeability on the fouling tendency of the prepared membranes was investigated. Molecular dynamics (MD) simulation was also carried out to determine the membrane surface state.

Furthermore, in order to improve the mechanical strength of the pure poly(VC-*co*-PEGMA) membranes, poly(VC-*co*-PEGMA)/PVC blend membranes with appropriate mechanical strength and antifouling were prepared via the NIPS method. The effect of the copolymer/PVC blend ratios on the surface morphology, hydrophilicity, mechanical strength, and, in particular, the fouling propensity of the prepared membranes was evaluated. To understand the mechanism of membrane fouling, MD simulations were carried out to assess the distribution of the copolymer in the membrane matrix in the presence of water.

Finally, I proposed an effective approach to obtain a robust hollow fiber membrane with considerable antifouling surface using soft hydrophilic polymeric material. Braid-reinforced hollow fiber membrane with superior mechanical properties was prepared by using PVC as the coating material, and poly(VC-*co*-PEGMA) was blended into the coating layer to endow the membrane surface with antifouling properties. To the best of our knowledge, the preparation of braid-reinforced PVC hollow fiber membranes with antifouling surface to prevent actual foulants deposition has not been studied yet. Novel braid-reinforced poly(VC-*co*-PEGMA)/PVC hollow fiber membranes were prepared. For exploring the optimal preparation conditions of the braid-reinforced membranes, the effect of the chemical-physical properties of the PET braids on the membrane properties was studied. By investigating the membrane mechanical properties and antifouling properties for the filtration of activated sludge solution,

I aim to develop an advanced ultrafiltration hollow fiber membrane for application in wastewater treatment.

I.6 SCOPE OF THIS THESIS

This thesis is divided into 5 parts. Each part is described briefly as shown below:

Chapter 1 introduces the background and the purpose of this study. A review of the previous work and the scope of the thesis are also given.

In **Chapter II**, two series of antifouling MF membranes with different pure water permeabilities were fabricated using poly(vinyl chloride-*co*-poly(ethylene glycol)methyl ether methacrylate) (poly(VC-*co*-PEGMA)) copolymers with different PEGMA segment percentages via the NIPS method. Membranes with similar water permeability were obtained for each series by changing the dope solution composition. Bovine serum albumin (BSA) adsorption on copolymer films decreased and membrane surface pore size, hydrophilicity, and antifouling properties increased by increasing the PEGMA segment percentage. BSA filtration results revealed that the membrane material and the initial water flux in the filtration more strongly affected the fouling propensity than the membrane surface pore size. Molecular dynamics simulation was carried out to investigate the state of the PEGMA on the membrane surface for clarifying the fouling mechanism.

In **Chapter III**, several membranes with low fouling properties were prepared by blending PVC with poly(VC-*co*-PEGMA) copolymer via the NIPS method. BSA adsorption on polymer films decreased and the membrane surface pore sizes, hydrophilicity, and antifouling properties increased on increasing the poly(VC-*co*-PEGMA)/PVC blending ratio. Membrane surface PEGMA coverage increased on increasing the poly(VC-*co*-PEGMA)/PVC blending ratio, resulting in higher hydrophilicity and lower fouling propensities. Membranes with similar

water permeabilities were prepared by adjusting the dope solution composition to eliminate the effect of hydrodynamic conditions on membrane fouling performance. The effect of the membrane material on the membrane fouling propensity was much stronger than that of the membrane surface structure. Molecular dynamics simulations were performed to evaluate the surface chemical composition of the membrane matrix and results were compared with results obtained from XPS measurements.

In Chapter IV, braid-reinforced hollow fiber membranes with high mechanical properties and considerable antifouling surface were prepared by blending PVC with poly(VC-*co*-PEGMA) copolymer via NIPS method. The tensile strength of the braid-reinforced PVC hollow fiber membranes was significantly larger than that of previously reported various types of PVC hollow fiber membranes. The high interfacial bonding strength indicated the good compatibility between the coating materials and the surface of polyethylene terephthalate (PET)-braid. Owing to the surface segregation phenomena, the membrane surface PEGMA coverage increased with the increase of the poly(VC-*co*-PEGMA)/PVC blending ratio, resulting in higher hydrophilicity and BSA repulsion. To compare the fouling properties, membranes with similar PWPs were prepared by adjusting the dope solution composition to eliminate the effect of hydrodynamic conditions on the membrane fouling performance. The blend membrane surfaces exhibited considerable fouling resistance to the molecular adsorption from both BSA solution and activated sludge solution. In both cases, the flux recovered to almost 80% of the initial flux using only water backflush. Considering their great mechanical properties and antifouling resistance to activated sludge solution, these novel membranes show good potential for application in wastewater treatment.

Chapter V summarized the main conclusions of this dissertation.

REFERENCES

[1] M. Mulder, Basic Principles of Membrane Technology, Kluwer Academic Publisher, Dordrencht, 1997.

[2] B. Nicolaisen, Developments in membrane technology for water treatment, Desalination, 153 (2003) 355-360.

[3] P. van de Witte, P.J. Dijkstra, J.W.A. van den Berg, J. Feijen, Phase separation processes in polymer solutions in relation to membrane formation, J. Membr. Sci., 117 (1996) 1-31.

[4] J. Ren, R. Wang, Preparation of Polymeric Membranes, L.K. Wang, J.P. Chen, Y.T. Hung, N.K. Shammas (Eds.), Membrane and Desalination Technologies, Humana Press, Inc., Totowa, NJ, USA (2010).

[5] W. Yuan, A.L. Zydney, Humic acid fouling during microfiltration, J. Membr. Sci., 157 (1999) 1-12.

[6] J.E. Kilduff, S. Mattaraj, M. Zhou, G. Belfort, Kinetics of Membrane Flux Decline: The Role of Natural Colloids and Mitigation via Membrane Surface Modification, J. Nanopart. Res. , 7 (2005) 525-544.

[7] Y.Q. Wang, T. Wang, Y.L. Su, F.B. Peng, H. Wu, Z.Y. Jiang, Remarkable reduction of irreversible fouling and improvement of the permeation properties of poly(ether sulfone) ultrafiltration membranes by blending with pluronic F127, Langmuir, 21 (2005) 11856-11862.

[8] R. Kumar, A.F. Ismail, Fouling control on microfiltration/ultrafiltration membranes: Effects of morphology, hydrophilicity, and charge, J. Appl. Polym. Sci., 132 (2015) app. 42042.

[9] J. Busch, A. Cruse, W. Marquardt, Modeling submerged hollow-fiber membrane filtration for wastewater treatment, J. Membr. Sci., 288 (2007) 94-111.

[10] K. Kimura, Y. Hane, Y. Watanabe, G. Amy, N. Ohkuma, Irreversible membrane fouling during ultrafiltration of surface water, Water Res. , 38 (2004) 3431-3441.

[11] Q. She, C.Y. Tang, Y.-N. Wang, Z. Zhang, The role of hydrodynamic conditions and solution chemistry on protein fouling during ultrafiltration, Desalination, 249 (2009) 1079-1087.

[12] R.W. Field, D. Wu, J.A. Howell, B.B. Gupta, Critical flux concept for microfiltration fouling, J. Membr. Sci., 100 (1995) 259-272.

[13] D. Rana, T. Matsuura, Surface Modifications for Antifouling Membranes, Chem. Rev. , 110 (2010) 2448-2471.

[14] G.D. Kang, Y.M. Cao, Development of antifouling reverse osmosis membranes for water treatment: A review, Water Res. , 46 (2012) 584-600.

[15] L.L. Hwang, H.H. Tseng, J.C. Chen, Fabrication of polyphenylsulfone/polyetherimide blend membranes for ultrafiltration applications: The effects of blending ratio on membrane properties and humic acid removal performance, J. Membr. Sci., 384 (2011) 72-81.

[16] R.S. Kane, P. Deschatelets, G.M. Whitesides, Kosmotropes Form the Basis of Protein-Resistant Surfaces, Langmuir, 19 (2003) 2388-2391.

[17] Y.H. Zhao, X.Y. Zhu, K.H. Wee, R.B. Bai, Achieving highly effective non-biofouling performance for polypropylene membranes modified by UV-induced surface graft polymerization of two oppositely charged monomers, J. Phys. Chem. B , 114 (2010) 2422-2429.

[18] X. Fu, T. Maruyama, T. Sotani, H. Matsuyama, Effect of surface morphology on membrane fouling by humic acid with the use of cellulose acetate butyrate hollow fiber membranes, J. Membr. Sci., 320 (2008) 483-491.

[19] M. Hashino, T. Katagiri, N. Kubota, Y. Ohmukai, T. Maruyama, H. Matsuyama, Effect of surface roughness of hollow fiber membranes with gear-shaped structure on membrane fouling by sodium alginate, J. Membr. Sci., 366 (2011) 389-397.

[20] K.C. Khulbe, C. Feng, T. Matsuura, The art of surface modification of synthetic polymeric membranes, J. Appl. Polym. Sci., 115 (2010) 855-895.

[21] V.M. Kochkodan, N. Hilal, V.V. Goncharuk, L. Al-Khatib, T.I. Levadna, Effect of the surface modification of polymer membranes on their microbiological fouling, Colloid J. , 68 (2006) 267-273.

[22] T. Shibutani, T. Kitaura, Y. Ohmukai, T. Maruyama, S. Nakatsuka, T. Watabe, H. Matsuyama, Membrane fouling properties of hollow fiber membranes prepared from cellulose acetate derivatives, J. Membr. Sci., 376 (2011) 102-109.

[23] R. Guan, H. Zou, D. Lu, C. Gong, Y. Liu, Polyethersulfone sulfonated by chlorosulfonic acid and its membrane characteristics, Eur. Polym. J. , 41 (2005) 1554-1560.

[24] B. Van der Bruggen, Chemical modification of polyethersulfone nanofiltration membranes: A Review, J. Appl. Polym. Sci., 114 (2009) 630-642.

[25] J.F. Blanco, Q.T. Nguyen, P. Schaetzel, Novel hydrophilic membrane materials: sulfonated polyethersulfone Cardo, J. Membr. Sci., 186 (2001) 267-279.

[26] X.R. Chen, Y. Su, F. Shen, Y.H. Wan, Antifouling ultrafiltration membranes made from PAN-b-PEG copolymers: Effect of copolymer composition and PEG chain length, J. Membr. Sci., 384 (2011) 44-51.

[27] S. Molina, P. Carretero, S.B. Teli, J.G. de la Campa, A.E. Lozano, J. Abajo, Hydrophilic porous asymmetric ultrafiltration membranes of aramid-g-PEO copolymers, J. Membr. Sci., 454 (2014) 233-242.

[28] Z. Zhou, S. Rajabzadeh, A. Rajjak Shaikh, Y. Kakihana, T. Ishigami, R. Sano, H. Matsuyama, Preparation and characterization of antifouling poly(vinyl chloride-co-poly(ethylene glycol)methyl ether methacrylate) membranes, J. Membr. Sci., (2016) 414-422

[29] I.S. Chang, P. Le Clech, B. Jefferson, S. Judd, Membrane fouling in membrane bioreactors for wastewater treatment, J. Eviron. Eng., 128 (2002) 1018-1029.

[30] F. Liu, N.A. Hashim, Y. Liu, M.R.M. Abed, K. Li, Progress in the production and modification of PVDF membranes, J. Membr. Sci., 375 (2011) 1-27.

[31] A. Asatekin, S. Kang, M. Elimelech, A.M. Mayes, Anti-fouling ultrafiltration membranes containing polyacrylonitrile-graft-poly(ethylene oxide) comb copolymer additives, J. Membr. Sci., 298 (2007) 136-146.

[32] N. Hilal, O.O. Ogunbiyi, N.J. Miles, R. Nigmatullin, Methods employed for control of fouling in MF and UF membranes: A comprehensive review, Sep. Sci. Tech. , 40 (2005) 1957-2005.

[33] K.K. Sirkar, Membrane separation technologies: Current developments, Sep. Sci. Technol., 6 (2007) 145-184.

[34] H. Susanto, M. Ulbricht, Characteristics, performance and stability of polyethersulfone ultrafiltration membranes prepared by phase separation method using different macromolecular additives, J. Membr. Sci., 327 (2009) 125-135.

[35] G. Arthanareeswaran, D. Mohan, M. Raajenthiren, Preparation, characterization and performance studies of ultrafiltration membranes with polymeric additive, J. Membr. Sci., 350 (2010) 130-138.

[36] Y.H. Zhao, B.K. Zhu, X.T. Ma, Y.Y. Xu, Porous membranes modified by hyperbranched polymers: I. Preparation and characterization of PVDF membrane using hyperbranched polyglycerol as additive, J. Membr. Sci., 290 (2007) 222-229.

[37] B.J. Cha, J.M. Yang, Effect of high-temperature spinning and PVP additive on the properties of PVDF hollow fiber membranes for microfiltration, Macromol. Res., 14 (2006) 596-602.

[38] J.F. Hester, P. Banerjee, A.M. Mayes, Preparation of protein-resistant surfaces on poly(vinylidene fluoride) membranes via surface segregation, Macromolecules, 32 (1999) 1643-1650.

[39] J.F. Hester, P. Banerjee, Y.Y. Won, A. Akthakul, M.H. Acar, A.M. Mayes, ATRP of amphiphilic graft copolymers based on PVDF and their use as membrane additives, Macromolecules, 35 (2002) 7652-7661.

[40] Q. Shi, Y.L. Su, S.P. Zhu, C. Li, Y.Y. Zhao, Z.Y. Jiang, A facile method for synthesis of pegylated polyethersulfone and its application in fabrication of antifouling ultrafiltration membrane, J. Membr. Sci., 303 (2007) 204-212.

[41] W. Zhao, Y. Su, C. Li, Q. Shi, X. Ning, Z. Jiang, Fabrication of antifouling polyethersulfone ultrafiltration membranes using Pluronic F127 as both surface modifier and pore-forming agent, J. Membr. Sci., 318 (2008) 405-412.

[42] S. Kang, A. Asatekin, A.M. Mayes, M. Elimelech, Protein antifouling mechanisms of PAN UF membranes incorporating PAN-g-PEO additive, J. Membr. Sci., 296 (2007) 42-50.

[43] A. Clements, The Essential Chemical Industry, University of York, Chemical Industry Education Centre, 2010.

[44] M. Bodzek, K. Konieczny, The influence of molecular mass of poly (vinyl chloride) on the structure and transport characteristics of ultrafiltration membranes, J. Membr. Sci., 61 (1991) 131-156.

[45] H. Okuno, K. Renzo, T. Uragami, Influence of casting solution additive, degree of polymerization, and polymer concentration on poly (vinyl chloride) membrane properties and performance , J. Membr. Sci., 83 (1993) 199-209.

[46] S. Mei, C.F. Xiao, X.Y. Hu, Preparation of porous PVC membrane via a phase inversion method from PVC/DMAc/Water/Additives, J. Appl. Polym. Sci., 120 (2011) 557-562.

[47] W.D. Liu, Y.H. Zhang, L.F. Fang, B.K. Zhu, L.P. Zhu, Antifouling properties of poly(vinyl chloride) membranes modified by amphiphilic copolymers P(MMA-b-MAA), Chin. J. Polym. Sci. , 30 (2012) 568-577.

[48] A.D. Marshall, P.A. Munro, G. Trägårdh, The effect of protein fouling in microfiltration and ultrafiltration on permeate flux, protein retention and selectivity: A literature review, Desalination, 91 (1993) 65-108.

[49] S. Kang, A. Asatekin, A.M. Mayes, M. Elimelech, Protein antifouling mechanisms of PAN UF membranes incorporating PAN-g-PEO additive, J. Membr. Sci., 296 (2007) 42-50.

[50] X. Fan, Y. Su, X. Zhao, Y. Li, R. Zhang, J. Zhao, Z. Jiang, J. Zhu, Y. Ma, Y. Liu, Fabrication of polyvinyl chloride ultrafiltration membranes with stable antifouling property by exploring the pore formation and surface modification capabilities of polyvinyl formal, J. Membr. Sci., 464 (2014) 100-109.

[51] B. Liu, C. Chen, W. Zhang, J. Crittenden, Y. Chen, Low-cost antifouling PVC ultrafiltration membrane fabrication with Pluronic F 127: Effect of additives on properties and performance, Desalination, 307 (2012) 26-33.

[52] R. Patel, W.S. Chi, S.H. Ahn, C.H. Park, H.-K. Lee, J.H.z. Kim, Synthesis of poly(vinyl chloride)-g-poly(3-sulfopropyl methacrylate) graft copolymers and their use in pressure retarded osmosis (PRO) membranes, Chem. Eng. J. , 247 (2014) 1-8.

[53] J. Chapman, A. Lawlor, E. Weir, B. Quilty, F. Regan, Phthalate doped PVC membranes for the inhibition of fouling, J. Membr. Sci., 365 (2010) 180-187.

[54] S.M. Hosseini, S.S. Madaeni, A. Zendehnam, A.R. Moghadassi, A.R. Khodabakhshi, H. Sanaeepur, Preparation and characterization of PVC based heterogeneous ion exchange membrane coated with Ag nanoparticles by (thermal-plasma) treatment assisted surface modification, J. Ind. Eng.Chem, 19 (2013) 854-862.

[55] M.J. Berrocal, R.D. Johnson, I.H.A. Badr, M.D. Liu, D.Y. Gao, L.G. Bachas, Improving the blood compatibility of ion-selective electrodes by employing poly(MPC-co-BMA), a copolymer containing phosphorylcholine, as a membrane coating, Anal. Chem., 74 (2002) 3644-3648.

[56] M. Yoshikawa, K. Tsubouchi, Specialty polymeric membranes. 9. Separation of benzene cyclohexane mixtures through poly(vinyl chloride)-graft-poly(butyl methacrylate), J. Membr. Sci., 158 (1999) 269-276.

[57] R. Patel, M. Patel, S.H. Ahn, Y.K. Sung, H.K. Lee, J.H. Kim, J.S. Sung, Bioinert membranes prepared from amphiphilic poly(vinyl chloride)-g-poly(oxyethylene methacrylate) graft copolymers, Mater. Sci. Eng., C, 33 (2013) 1662-1670.

[58] F. Liu, B. K. Zhu, Y. Y. Xu, Preparation and characterization of poly(vinyl chloride)-graft-acrylic acid membrane by electron beam, J. Appl. Polym. Sci., 105 (2007) 291-296.

[59] S. Rajabzadeh, R. Sano, T. Ishigami, Y. Kakihana, Y. Ohmukai, H. Matsuyama, Preparation of hydrophilic vinyl chloride copolymer hollow fiber membranes with antifouling properties, Appl. Surf. Sci. , 324 (2015) 718-724.

[60] P.R. Babu, V.G. Gaikar, Preparation, structure, and transport properties of ultrafiltration membranes of poly(vinyl chloride) (PVC), carboxylated poly(vinyl chloride) (CPVC), and PVC CPVC blends, J. Appl. Polym. Sci., 73 (1999) 1117-1130.

[61] P.R. Babu, V.G. Gaikar, Preparation, structure, and transport properties of ultrafiltration membranes of poly(vinyl chloride) and poly(vinyl pyrrolidone) blends, J. Appl. Polym. Sci., 77 (2000) 2606-2620.

[62] L. Krishnamoorthy, P. M. Arif, R. Ahmedkhan, Separation of proteins from aqueous solution using cellulose acetate/poly (vinyl chloride) blend ultrafiltration membrane, J. Mater. Sci., 46 (2011) 2914-2921.

[63] J. Liu, Y. Su, J. Peng, X. Zhao, Y. Zhang, Y. Dong, Z. Jiang, Preparation and Performance of Antifouling PVC/CPVC Blend Ultrafiltration Membranes, Ind. Eng. Chem. Res., 51 (2012) 8308-8314.

[64] S. Jiang, J. Wang, J. Wu, Y. Chen, Poly(vinyl chloride) and poly(ether sulfone)-g-poly(ether glycol) methyl ether methacrylate blend membranes with improved ultrafiltration performance and fouling resistance, J. Appl. Polym. Sci., 132 (2015), pp. 41726–41735.

[65] M.C. Shen, L. Martinson, M.S. Wagner, D.G. Castner, B.D. Ratner, T.A. Horbett, PEO-like plasma polymerized tetraglyme surface interactions with leukocytes and proteins: in vitro and in vivo studies, J. Biomater. Sci. Ed., 13 (2002), pp. 367–390.

[66] Z. Zhou, S. Rajabzadeh, A.R. Shaikh, Y. Kakihana, W. Ma, H. Matsuyama, Effect of surface properties on antifouling performance of poly(vinyl chloride-co-poly(ethylene glycol)methyl ether methacrylate)/PVC blend membrane, J. Membr. Sci., 514 (2016) 537-546.

[67] L.T.J. Korley, B.D. Pate, E.L. Thomas, P.T. Hammond, Effect of the degree of soft and hard segment ordering on the morphology and mechanical behavior of semicrystalline segmented polyurethanes, Polymer, 47 (2006) 3073-3082.

[68] C. Psoch, S. Schiewer, Anti-fouling application of air sparging and backflushing for MBR, J. Membr. Sci., 283 (2006) 273-280.

[69] A. Behboudi, Y. Jafarzadeh, R. Yegani, Preparation and characterization of TiO2 embedded PVC ultrafiltration membranes, Chem. Eng. Res. Des., 114 (2016) 96-107.

[70] Y. Zhao, J. Lu, X. Liu, Y. Wang, J. Lin, N. Peng, J. Li, F. Zhao, Performance enhancement of polyvinyl chloride ultrafiltration membrane modified with graphene oxide, J. Colloid Interface Sci., 480 (2016) 1-8.

[71] H. Liu, C. Xiao, Q. Huang, X. Hu, W. Shu, Preparation and interface structure study on dual-layer polyvinyl chloride matrix reinforced hollow fiber membranes, J. Membr. Sci., 472 (2014) 210-221.

[72] H.L. Liu, C.F. Xiao, Q.L. Huang, X.Y. Hu, Structure design and performance study on homogeneous-reinforced polyvinyl chloride hollow fiber membranes, Desalination, 331 (2013) 35-45.

[73] H. Liu, C. Xiao, Q. Huang, Z. Fan, X. Hu, W. Shu, Study on interface structure and performance of homogeneous-reinforced polyvinyl chloride hollow fiber membranes, Iran. Polym. J, 24 (2015) 491-503.

[74] Q. Quan, C.F. Xiao, H.L. Liu, Q.L. Huang, W. Zhao, X.Y. Hu, G.L. Huan, Preparation and characterization of braided tube reinforced polyacrylonitrile hollow fiber membranes, J. Appl. Polym. Sci., 132 (2015), app. 41795.

[75] Z.W. Fan, C.F. Xiao, H.L. Liu, Q.L. Huang, J. Zhao, Structure design and performance study on braid-reinforced cellulose acetate hollow fiber membranes, J. Membr. Sci., 486 (2015) 248-256.

[76] Z.W. Fan, C.F. Xiao, H.L. Liu, Q.L. Huang, Preparation and performance of homogeneous braid reinforced cellulose acetate hollow fiber membranes, Cellulose, 22 (2015) 695-707.

[77] Z. Fan, C. Xiao, H. Liu, Q. Huang, J. Zhao, Structure design and performance study on braid-reinforced cellulose acetate hollow fiber membranes, J. Membr. Sci., 486 (2015) 248-256.

Chapter II

Preparation and characterization of antifouling poly(vinyl chloride-*co*-poly(ethylene glycol)methyl ether methacrylate) membranes

II.1 INTRODUCTION

Poly(vinyl chloride) (PVC) has attracted attention because of its excellent mechanical strength, high resistance to corrosion, and low cost [1-4]. However, PVC membranes suffer from a serious problem of membrane fouling owing to their hydrophobicity. [5]. Efforts have been made to improve the antifouling properties of PVC membranes by grafting them with hydrophilic chains [6-9]. Recently, Rajabzadeh et al. investigated the effects of different grafting chains such as poly(ethylene glycol)methyl ether methacrylate (PEGMA) and zwitterionic monomers, and concluded that the grafting of PEGMA was more effective in decreasing the fouling than the grafting of zwitterionic monomers [9]. Although the grafting is an effective method to decrease membrane fouling, it usually involves an extra step for modifying the surface of the prepared membranes.

Blending of PVC with hydrophilic polymers was used as an alternative method to prepare antifouling membranes [10-13]. Babu and Gaikar prepared PVC/carboxylated poly(vinyl chloride) (CPVC) [10] and PVC/polyvinyl pyrrolidone (PVP) [11] flat sheet blend membranes, and evaluated the effects of the filtration process conditions on the membrane fouling performance. However, the effect of the membrane material has not been investigated adequately. Fan et al. [12] prepared PVC/polyvinyl formal (PVF) blend flat sheet ultrafiltration membranes. They reported that the membrane surface hydrophilicity and antifouling property

increased sharply, because PVF segregated to the membrane surface during phase separation. Xu et al. [13] prepared a PVC hollow fiber membrane by adding poly(ethylene glycol) (PEG), and evaluated the effect of dope composition and membrane preparation conditions on the properties of the prepared membranes. However, PVP and PEG, mostly used as pore former additives, tend to easily wash away and the membrane hydrophilicity decreases during filtration [14]. In addition, some PVC blends with hydrophilic polymers such as PVC/PAN [15], PVC/cellulose acetate (CA) [16], and PVC/polystyrene [17] have compatibility issues.

In some studies, amphiphilic copolymers have been used as blending polymers to prepare antifouling membranes because of the unique chemical structure of the copolymers [18-21]. The hydrophobic segments of such amphiphilic copolymers make them compatible with the membrane matrix and help in their retention in the membrane, while their hydrophilic segments endow the membrane with good hydrophilicity and antifouling properties. Copolymers containing PEG chains exhibit better hydrophilicity and antifouling properties because of the strong capacity of the PEG chains to form a hydration layer [22, 23]. Liu et al. [24] prepared membrane with superior antifouling properties by blending a commercial Poly(ethylene oxide) (PEO) based amphiphilic copolymer (Pluronic F 127) with a PVC dope solution. They found that the antifouling properties and water permeability of the prepared membranes improved on increasing the copolymer concentration to up to 8 wt%; however, further increase in the copolymer concentration decreased the water permeability.

To the best of our knowledge, no study has been conducted on the membrane preparation of only PVC-based copolymer for antifouling improvement. This issue becomes important if consider that PVC is not sufficiently compatible with some hydrophilic polymers, which makes it difficult to prepare a PVC blend membrane with adequate antifouling properties. To overcome these disadvantages, poly(vinyl chloride-co-poly(ethylene glycol)methyl ether

methacrylate) (poly(VC-co-PEGMA)) with varying PEGMA segment percentage was used as a material for membrane preparation by using the conventional NIPS method, and was applied to BSA filtration for evaluating the antifouling properties. The effects of the membrane material, pore size, and initial water permeability on the fouling tendency of the prepared membrane were evaluated. Molecular dynamics (MD) simulation was also carried out to determine the membrane surface state and experimental results were explained based on the MD calculations.

II.2 COMPUTATIONAL METHODS

II.2.1 Model building

The poly(VC-*co*-PEGMA) copolymer molecule (structure shown in Fig. II. 1) is constructed by using the polymer builder module in Material Studio 7.0.1 suite (BIOVIA Inc., USA) by using the experimental information about the PEGMA concentration in a copolymer. The atomistic structure of each copolymer was also built by using Material Studio 7.0.1 suite and energy minimization was carried out. The *ab initio* force field COMPASS [25] was used for all atomistic simulations. The amorphous atomistic structures of the copolymers were constructed by using a three-dimensional (3D) cubic unit cell subject to periodic boundary conditions by an "Amorphous Cell" module. The module builds molecules in a cell in a Monte Carlo fashion by minimizing the close contacts between atoms, until a realistic distribution of torsion angles for any given forcefield is reached [26]. Using this algorithm, an amorphous polymer structure can be built with realistic conformations, while minimizing the number of close contacts between atoms [26, 27]. Further, each chain was replicated to obtain the desired chain numbers.

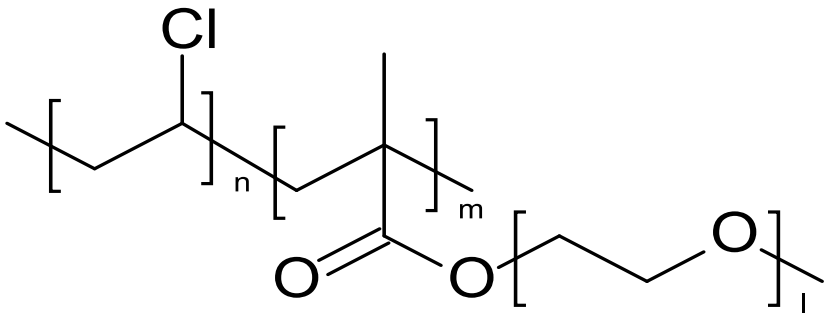

Fig. II.1. Chemical structure of poly (VC-*co*-PEGMA).

II.2.2 Molecular dynamics

The MD simulation was performed with the Material Studio package using the Forcite Plus module, which uses the velocity Verlet integrator method for computing the positions and velocities of atoms. The MD simulation was carried out in two steps; the first step included molecular mechanics (MM) and MD with the canonical ensemble (NVT) and isothermal-isobaric ensemble (NPT). All MD simulations are run with a 1.0 fs time step. In the second step, equilibration was carried out using the NVT ensemble on a velocity-scale thermostat at 300 K. Further, the production run was carried out for 20 ns using the Nose thermostat [28] and Berendsen barostat [29], and the pressure was maintained at 0.1 MPas bar. Periodic boundary conditions were applied in three dimensions so that the simulation cell is effectively repeated infinitely in each direction. The nonbonded electrostatic and van der Waals forces are controlled by “atom-based” summation and a cutoff value of 10.0 Å is used.

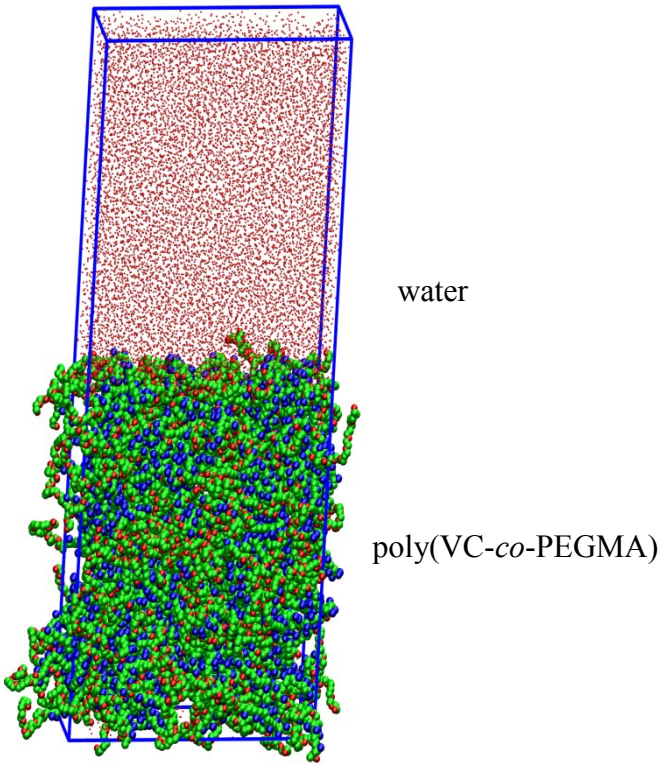

Fig. II.2. A representative snapshot of poly(VC-*co*-PEGMA) (PEGMA 9.8 mol%) in presence of water. Poly(VC-co-PEGMA) is shown in ball and stick model. Atom color coding are as follows: C-green, Cl-blue, O-red.

After calculations on the bulk sample, I extended the cell axis perpendicular to the surface of interest, leaving an empty space above the polymer. Using the program Amorphous Cell, these surfaces were then solvated by filling the empty space above them with water molecules at a density of 1 g/cm^3. Minimization was carried out, followed by NVT and NPT simulations. The simulation conditions were similar to those used for the copolymer membrane in the presence of air. The MD runs lasted for 20 ns after an initial equilibration of 5 ns. No additional

constraints were applied, and all molecules were allowed to move freely during the simulation. A representative snapshot after 20 ns of the production run is shown in Fig. II. 2. In this figure, poly(VC-*co*-PEGMA) is shown as a ball and stick model. Only the oxygen of water is shown for clarity.

II.3 EXPERIMENTAL

II 3.1 Material

PVC (Mw = 55000) and three kinds of poly(VC-co-PEGMA) (with PEGMA segment percentages of 2.4, 6.1, and 9.8 mol%, respectively, and Mw of 100,000, 360,000, and 180,000, respectively) were kindly supplied by Sekisui Chemical Co., Ltd. BSA, sodium dihydrogen phosphate (NaH2PO4), disodium hydrogen phosphate (Na2HPO4), and dimethylacetamide (DMAc) were purchased from Wako Pure Chemical Industries. The BSA solution was prepared by dissolving BSA in 0.1 mol/L phosphate buffer solution (PBS). polystyrene latex particles (diameter = 100 nm) used for the rejection measurement were purchased from Duke Scientific Corporation (Thermo Fisher Scientific, Waltham, MA). Deionized water was produced in a Millipore Milli-Q unit. All reagents were used as received.

II.3.2 Flat sheet membrane preparation

Two types of MF membranes with high and low water permeabilities, referred to as H and L series membranes, were prepared by a NIPS method by using three copolymers with different PEGMA segment percentages. To distinguish the H- and L-type membranes prepared by using different copolymers, these membranes were labeled with H and L followed by numbers 0, 1, 2, and 3, corresponding to the copolymer containing 0, 2.4, 6.1, and 9.8 mol% PEGMA. The

composition of the dope solutions used for membrane casting is shown in Table 1. For two series of H- and L-type membranes, the dope polymer compositions were adjusted so that they have similar pure water permeabilities to enable a better comparison of the fouling properties.

Table II.1. Composition of dope solutions for membrane casting.

Membrane	poly(VC-*co*-PEGMA)		Solvent weight fraction [wt%]
	PEGMA segment percentage [mol%]	Weight fraction [wt%]	
H0	0.0 (PVC homopolymer)	11	89
H1	2.4	13	87
H2	6.1	15	85
H3	9.8	18	82
L0	0.0 (PVC homopolymer)	14	86
L1	2.4	20	80
L2	6.1	20	80
L3	9.8	20	80

To prepare flat sheet membranes, the polymers were dissolved in DMAc by stirring at 45 °C for one day to obtain homogeneous solutions, and then degassed overnight at 25 °C. Then, the solution was cast on a glass plate with a nonwoven support by a steel knife with thickness of 200 μm to obtain a nascent polymeric film. The plate with the film was subsequently immersed in a nonsolvent bath of deionized water at 24±1 °C, leading to phase separation and formation of porous membranes. All membranes were washed thoroughly with deionized water to remove residual solvent, and were kept in deionized water before use.

II.3.3 BSA adsorption on polymer films

The amount of BSA adsorbed on the polymer film surface was measured using a quartz crystal microbalance with dissipation monitoring (QCM-D, Q-Sense E1, MEIWAFOSIS Co. Ltd, Japan). Piezoelectric quartz crystal sensors with a fundamental resonant frequency of around 5 MHz and a diameter of 14 mm (QSX 301, Q-Sense Co., Sweden) were used. Before each measurement, the sensor was cleaned by using an ultraviolet/ozone cleaner (Pro Cleaner 110; BioForce Nanosciences Co., USA). After spin coating with a 1.0 wt% polymer solution at 3000 rpm for 1 min and drying on a hot stage (KATHERM C-MAG HP4' Kampmann GmbH, Germany) at 80 °C for 20 min, the sensor was placed in the QCM flow chamber. Then, the PBS solution was injected into the flow chamber at a flow rate of 50 μL/min for more than 1 h to stabilize the sensor and obtain the baseline. Next, the PBS solution was substituted with a 1000 ppm BSA solution. In accordance with the Sauerbrey equation (Eq. 1), the total amount of BSA adsorbed on the polymeric film surface was calculated by varying the sensor oscillation frequency during a parallel flow of BSA solution at a constant temperature (25 °C) [30].

$$\Delta m = -C\,\Delta f/n \qquad (1)$$

In Eq. 1, Δm is the adsorption amount ($ng \cdot cm^{-2}$), C is the mass sensitivity constant (17.7 $ng \cdot cm^{-2} \cdot Hz\text{-}1$ at f = 4.95 MHz), Δf is the variation of frequency (Hz), and n is the overtone number (n = 7).

II.3.4 Membrane characterization

II.3.4.1 X-ray photoelectron spectroscopy analysis

X-ray photoelectron spectroscopy (XPS, PHI X-tool, ULVAC-PHI, Japan) was used to evaluate the surface chemical composition of the polymeric membranes. The system was equipped with an AI Kα radiation source (280 eV). Survey spectra were recorded over the

range 0–700 eV. The surface elemental composition was calculated from the peak area with a correction for atomic sensitivity. The take-off angle of the photoelectron was set at 45°.

II.3.4.2 Air bubble contact angle measurement

The air bubble contact angle of each membrane was measured with a contact angle goniometer (Drop Master 300, Kyowa Interface Science Co., Japan). A sample was prepared by cutting off a random part of the membrane in a suitable size and placed in a glass cell filled with deionized water. By using a special L-shaped syringe needle, an air bubble (1.5 μL) was released below the sample, and the air bubble contact angle with the surface was measured automatically upon contact. To minimize the experimental error, at least seven measurements were carried out at different locations of the sample.

II.3.4.3 Membrane morphology observation

A field emission scanning electronic microscope (JSF-7500F, JEOL Co. Ltd., Japan) was used to observe the surface morphology of the membranes. The prepared flat membranes were freeze-dried using a freeze dryer (FD-1000, EYELA, Japan), and then sputter coated with a 5 nm osmium tetroxide (OsO4) layer using an osmium coater (Neoc-STB; MEIWAFOSIS Co. Ltd., Japan). The coated samples were examined at an accelerating voltage of 8 kV at different magnifications.

II.3.4.4 Water permeability measurement

Water permeability was evaluated using a two-parallel-plate cross-flow module (C10-T; Nitto Denko Co. Ltd., Japan). The module channel had a clearance of 2.5 mm, a width of 45 mm, and a length of 180 mm. The flat membrane was installed on a permeable support. The

effective membrane area inside the footprint of the O-ring was 6×10^{-3} m^2. The ultrapure water was pumped into the module using a peristaltic pump. The operating pressure at filtration was adjusted by a needle valve at the outlet. The mean pressure value at the inlet and outlet of the membrane module was taken as the operating pressure. The feed water flow rate at the entrance of the membrane module was maintained at 190 $mL \cdot min^{-1}$. Before starting the measurement, the membrane was compacted at 0.1 MPa until the water flux became stable. Then, the membrane permeability was measured at 0.05 MPa every 3 min.

II.3.4.5 Polystyrene particle rejection measurement

The polystyrene particle rejection experiment was conducted in a cross-flow stainless cell with an effective filtration area of 8×10^{-4} m^2 using a 300 ppm latex particles. The feed solution was prepared by adding the monodisperse latex particles in an aqueous nonionic surfactant (mass fraction 0.1%, Triton X-100), and was then forced to permeate through the membrane under 0.05 MPa; the filtrate was collected after 15 min of feed circulation. The concentrations of the feed and the filtrate were measured via a UV-vis spectrophotometer (U-2000, Hitachi Co., Tokyo, Japan) at a wavelength of 385 nm. The membrane rejection was calculated by the following equation:

$$R(\%) = (1 - \frac{C_p}{C_f}) \times 100 \qquad (2)$$

where R, C_p, and C_f were the rejection, latex particle concentration of permeate, and feed solution concentration, respectively.

II.3.5 Membrane fouling experiment

The membrane fouling experiment was carried out using the same apparatus as that used for the membrane water permeability measurement. First, the membrane was compacted with

Milli-Q water at a pressure of 0.12 MPa and a flow rate of 190 mL/min for at least 15 min until the flux stabilized. Then, the initial water fluxes were set to 500 and 80 L/(m^2·h) for H- and L-type membranes, respectively, by adjusting the filtration pressure. As described below, H and L series membranes had similar water permeabilities, and thus, their adjusted pressures did not differ very much. Subsequently, the BSA fouling experiment was performed by replacing Milli-Q water by a 50 ppm BSA solution (pH 7.0 in PBS), and the flux was measured over the filtration time. The retentate was recycled into the feed tank, while the permeate was collected and weighed. The collected permeate was returned to the feed tank every 10 min for maintaining a constant concentration of the feed solution. After continuing the BSA filtration for 70 min, the fouled membrane was backflushed with Milli-Q water at 0.01 MPa for 2 min. Subsequently, the fouling experiment was restarted for another 40 min.

II.4 RESULTS AND DISCUSSION

II.4.1 MD simulation results

MD simulation is a powerful technique for computing the equilibrium and dynamic properties of polymeric materials. MD simulation was mainly carried out to understand the surface properties of the polymer in the presence of air and water. Hence, I restricted our analysis to clarifying the surface properties and their comparison with the experimental results. Radial distribution function analysis was carried out to understand the interactions between PEGMA and VC, and to assess how it varies on varying the PEGMA segment concentration. Figure 3 shows radial distribution functions of the O atom of PEGMA with the Cl atom of PVC. For all the copolymers, the first large peak was observed at 0.5 nm on varying the peak intensity according to the PEGMA concentration. It is clear that on increasing the PEGMA segment

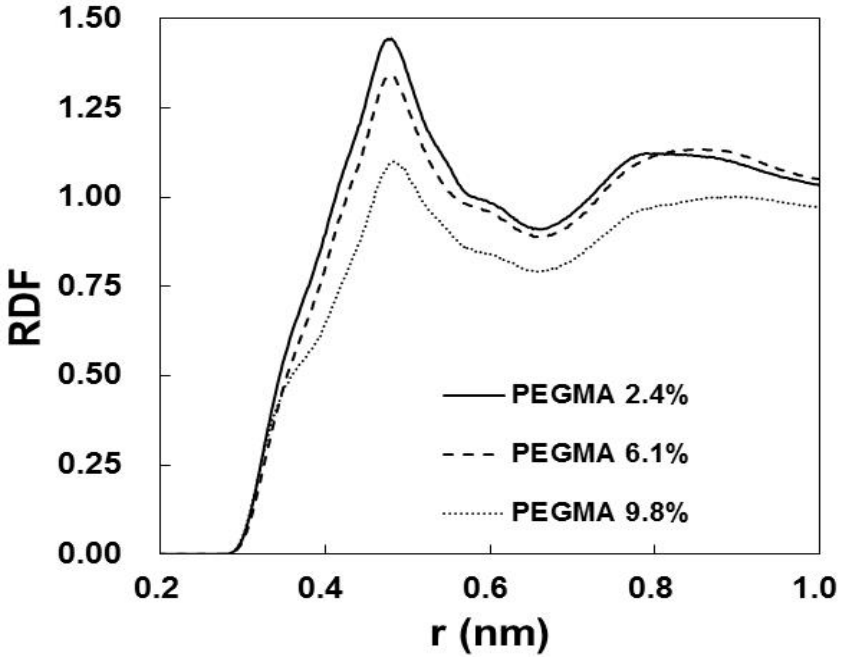

Fig.II.3. Radial distribution functions of O of PEGMA with Cl of VC.

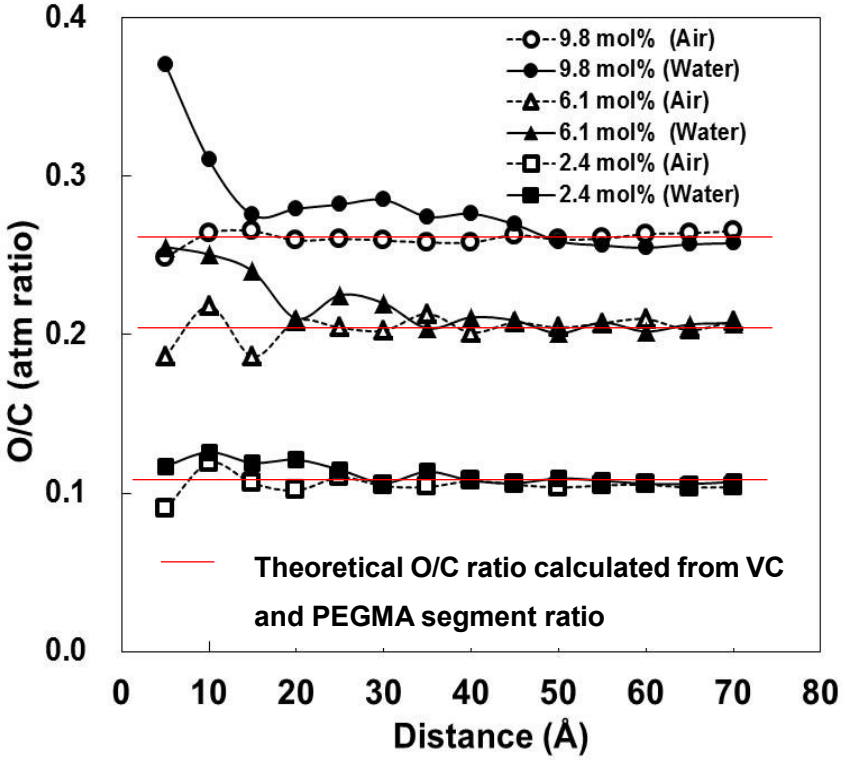

Fig.II.4. Surface chemical ratios for poly **(**VC-co-PEGMA) with different PEGMA segment percentage in presence of air (A) and water (W). Zero of the horizontal axis corresponds to the membrane surface.

concentration, the interaction between the Cl and O atoms decreases. This means that the PEGMA segment becomes more flexible with the increase in the PEGMA segment percentage. This high flexibility of the PEGMA segment is favorable for improving the membrane antifouling property.

The surface properties of copolymers are often characterized at the macroscopic level to determine their hydrophilic or hydrophobic property. In polymers, wettability mainly depends on the chemical nature and possible mobility of the exposed groups that undergo significant surface rearrangement, depending on their environment such as air or water [31]. As protein adsorption can be controlled by surface properties, I analyzed the surface properties to determine how different environments affect the surface functional groups of the copolymer. Surface chemical composition analysis was carried out along the z-axis, perpendicular to the polymer surface, in both the air and water environments; the results are shown in Fig.II.4. The Figure shows the comparison of the oxygen to carbon molar ratio (O/C) of different copolymers with different PEGMA segment percentages to understand the distribution of PEGMA in the membrane in the presence of water and air. From Fig. II. 4, it is clear that in the presence of water, the O/C ratio at the surface increases for every copolymer. This means that the PEGMA concentration at the surface is higher than that in the bulk, because the hydrophilic PEGMA segment is more likely to approach the surface in the presence of water. The distribution of PEGMA in the copolymer matrix becomes more pronounced on increasing the PEGMA segment percentage in the copolymer structure, which, as explained above, will decrease the interaction between oxygen and chlorine in the copolymer structure. Thus, in the presence of water, it is more likely that in copolymers with higher PEGMA segment percentage, the PEGMA segments move to the water-copolymer interface and hence increase the surface PEGMA concentration. In the presence of air, the O/C ratio at the surface decreases, which

means that the PEGMA concentration at the surface is lower than that in the bulk of the copolymer. This is because the vinyl chloride (VC) segment is likely to approach the surface connected to hydrophobic air.

II.4.2 BSA adsorption on polymeric films

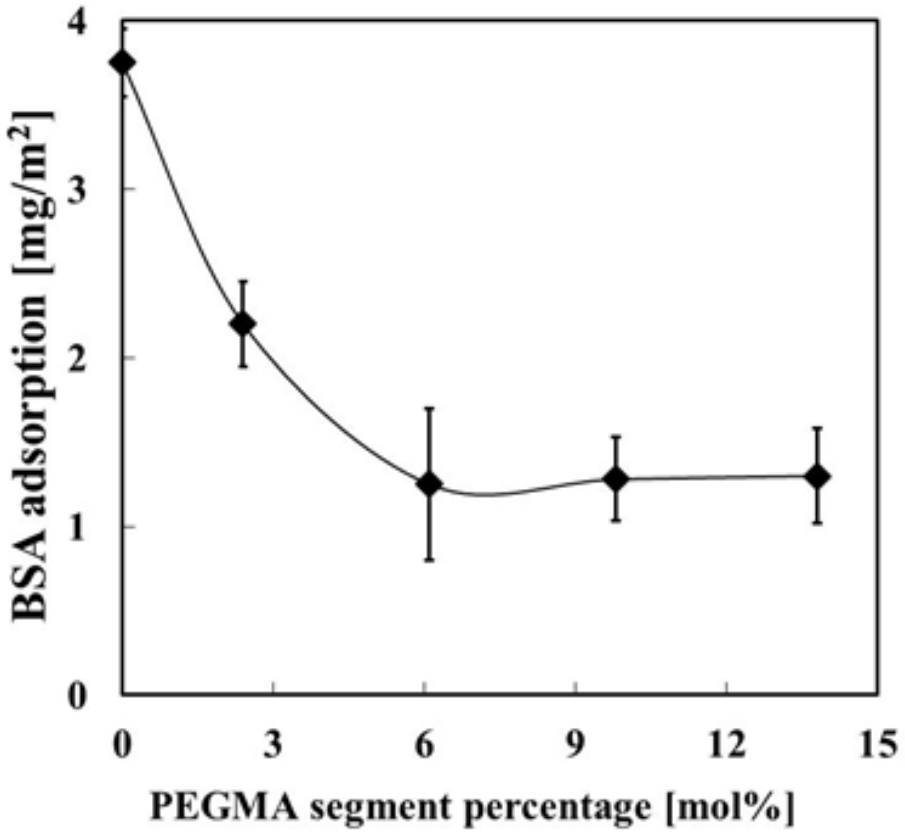

Fig. II. 5. BSA adsorption on copolymer films with different PEGMA segment percentage.

QCM-D analysis was conducted to evaluate the adsorption tendency of BSA on polymeric films prepared from four poly(VC-*co*-PEGMA) copolymers with different PEGMA segment percentages. The adsorption results are shown in Fig. II. 5. BSA adsorption decreased sharply on increasing the PEGMA segment percentage from 0 to 6.1 mol%, owing to the increase in the concentration of PEGMA molecules on the film surface. It has been well reported that

PEGMA effectively decreases protein adsorption [32-34]. Further increase in the PEGMA segment percentage had no effect on the BSA adsorption intensity. From the QCM results, it is expected that membranes prepared by using copolymers with a PEGMA segment percentage of ≥6.1 mol% show noticeable antifouling properties for protein solutions.

4.3. XPS measurements

The membrane surface chemical compositions of copolymer membranes were examined by using XPS wide scans; the results are shown in Fig. 6. It can be observed clearly that the copolymer membranes show four major emission peaks at 530 eV for O 1s, 284 eV for C 1s, 270 eV for Cl 2s, and 201 eV for Cl 2p. Because the VC segment has no oxygen atom in its structure, the O 1s peak at the membrane surface is considered as representative of PEGMA. The appearance of the O1s peak of the PVC membrane is related to surface oxidation by environmental oxygen [35]. I believe that surface oxidation occurs in all the prepared membranes, including the copolymer membranes.

The surface composition of the prepared membranes was evaluated by considering the O/C ratio. Figure 7 shows the composition of the measured results and the theoretical ratios calculated from the VC and PEGMA segment ratio. The experimental results showed that the O/C ratios increased for both the H- and L-type membranes on increasing the PEGMA segment percentage of the copolymer. In contrast, a comparison of the O/C ratios for the respective H and L types of the membranes showed that both the ratios were almost the same. For all the prepared copolymer membranes, the measured O/C ratios were higher than the theoretical values. This phenomenon can be explained by considering that the PEGMA segments of the copolymer enrich the membrane surface during the membrane preparation process because of the strong interaction between the PEGMA segments with water in the coagulation bath [36].

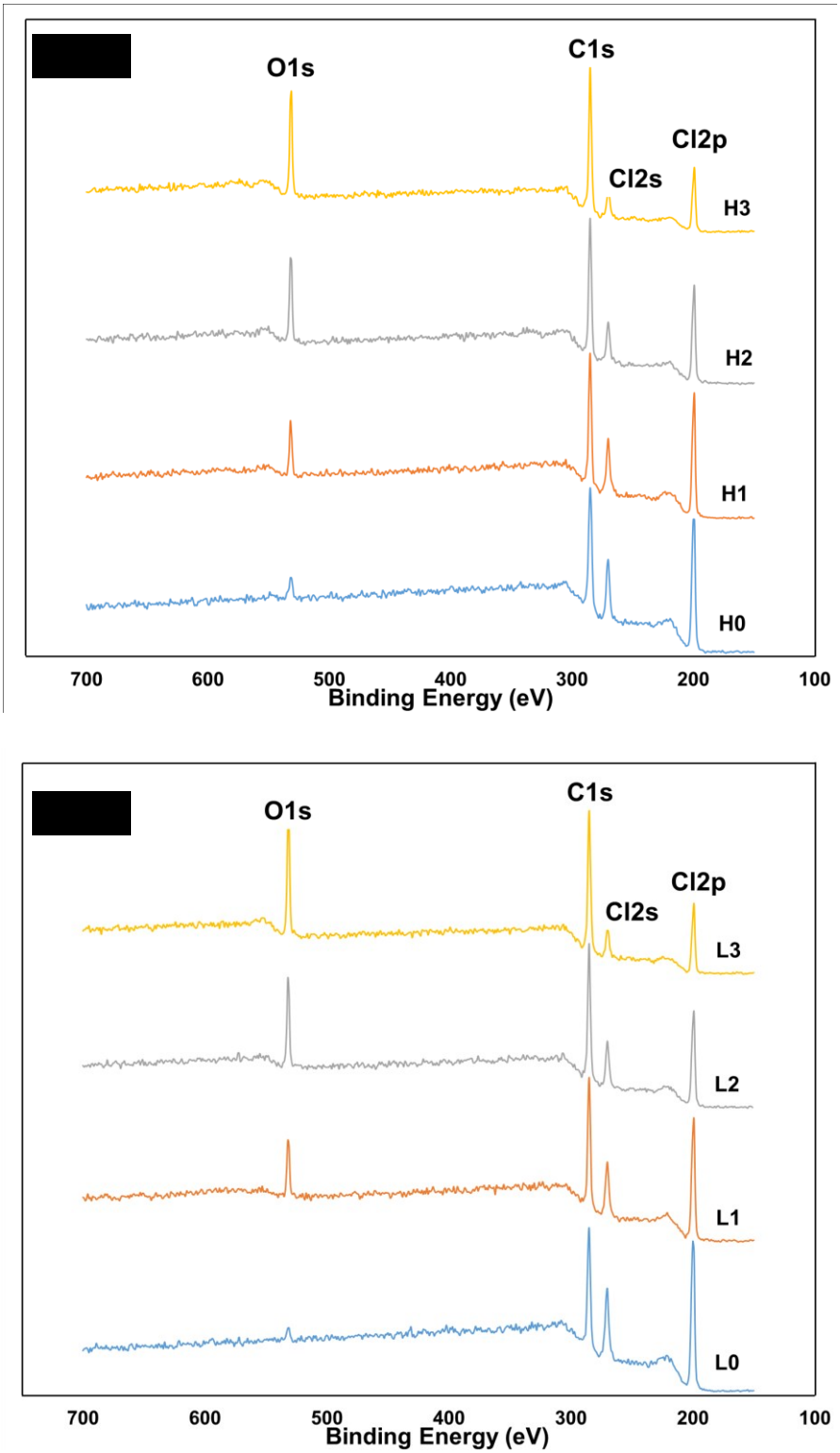

Fig. II.6. XPS spectra for (a) H type membranes and (b) L type membranes.

A comparison of the O/C ratios obtained from the XPS measurement with those obtained from the MD simulation in the presence of water (Fig. 4) shows that both the ratios have similar values. It was expected that the O/C ratios calculated from MD simulation would be higher than the

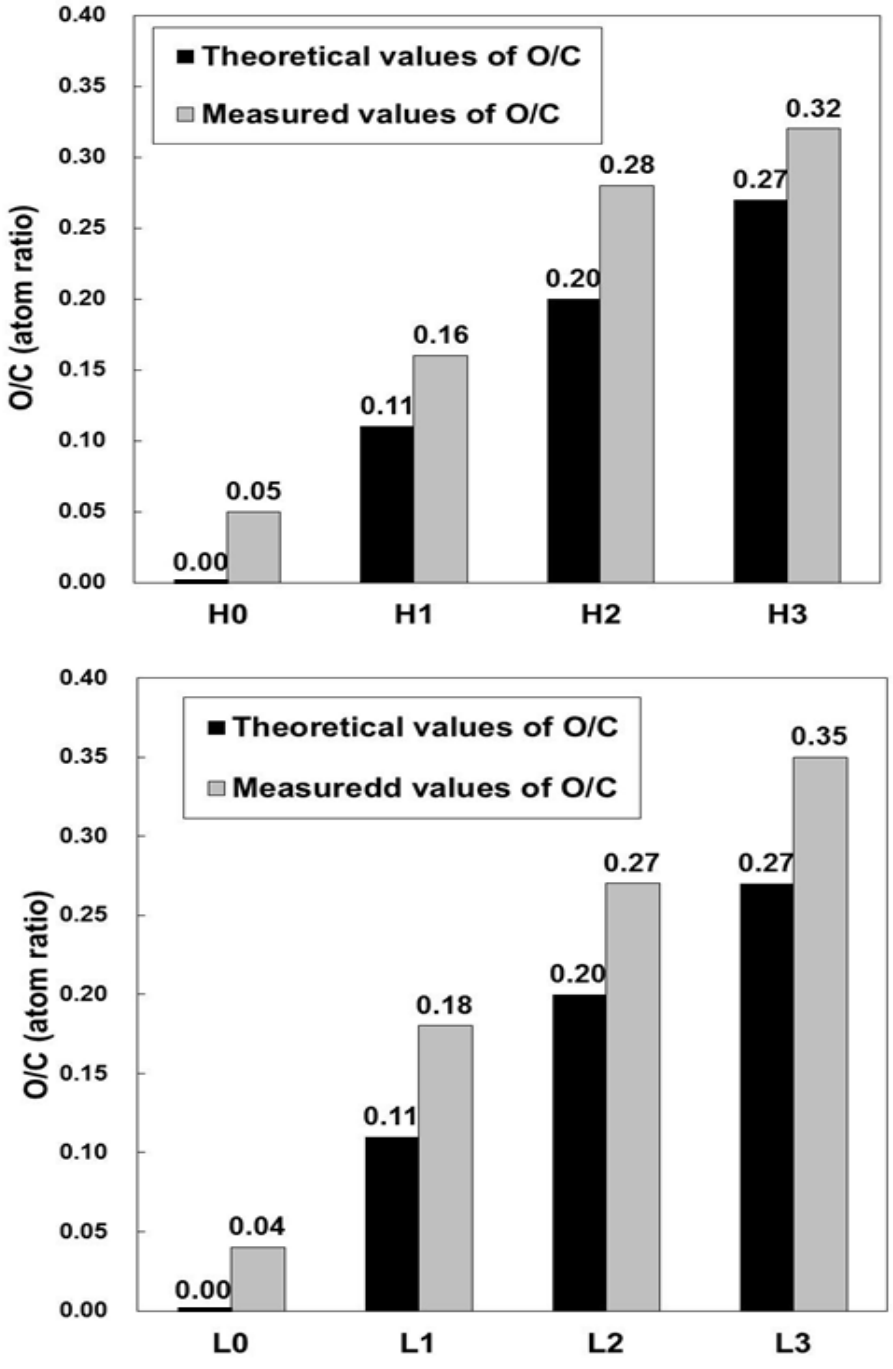

Fig.II.7. Surface O/C atom ratios of the different H and L type membranes

experimental results for the following reasons. Firstly, MD simulation results are valid for a completely stable equilibrium state situation. However, it is very difficult to obtain completely stable conditions during membrane preparation. A complete segregation of the PEGMA polymers from the membrane surface cannot be accomplished because of polymer solidification during membrane preparation. On the other hand, it should be considered that, the average compositions of the elements at a depth of several tens of angstrom from the surface are obtained by XPS measurements [37]. Therefore, it was expected that O/C ratios at the surface obtained from MD simulation would be higher than the results obtained from XPS. However, because of membrane oxidation caused by environmental oxygen, the O/C ratios measured with XPS are higher than those owing to PEGMA molecules. Since these factors counterbalance each other, the O/C ratios from the XPS results and those of MD simulation were found to be almost the same.

II.4.4 Hydrophilicity of the membranes

The surface hydrophilicity of the prepared membranes was evaluated by air bubble contact angle measurements. The results are shown in Fig. 8. For both the H- and L-type membranes, the air bubble contact angle increased on increasing the PEGMA segment percentage owing to the increase in the PEGMA concentration at the membrane surface, as explained in Sections 4.1 and 4.3. The contact angle increases slightly when the PEGMA segment percentage exceeds 6.1 mol%. This result is in agreement with the QCM-D analysis result shown in Fig. 5, in which BSA adsorption hardly shows a further decrease when the PEGMA segment percentage exceeds 6.1 mol%. Therefore, it can be expected that membrane antifouling properties increase slightly when the PEGMA segment percentage is higher than 6.1 mol%.

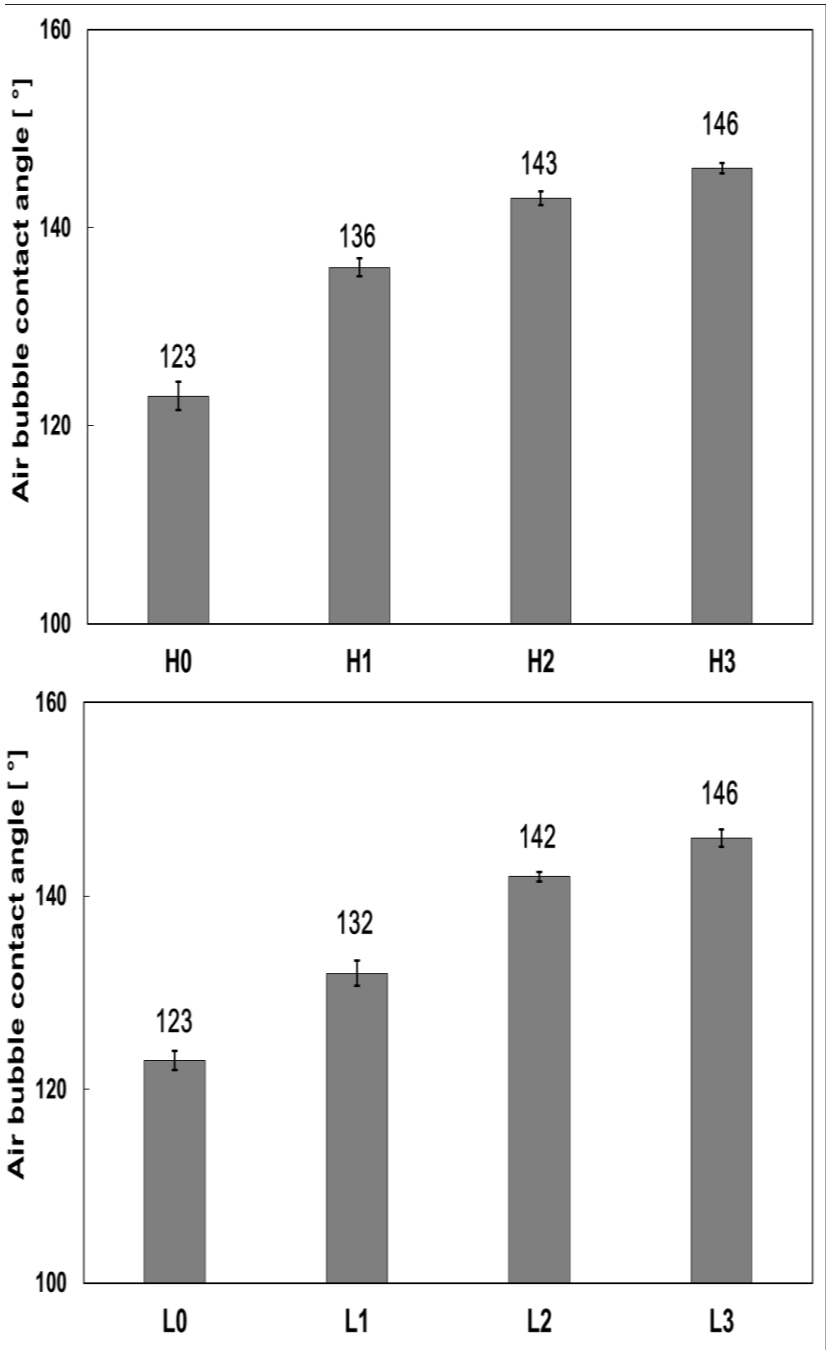

Fig.II.8. Air bubble contact angle results of (a) H type membranes and (b) L type membranes.

II.4.5 Membrane surface morphology

The surface structures of the prepared membranes are shown in Fig. 9. For an accurate comparison of the pore size and pore density of the prepared membranes, SEM images at two different magnifications (10,000× and 50,000×) are shown in Fig. 9. As explained in Section

(a) 10,000×Magnification (b) 50,000× Magnification

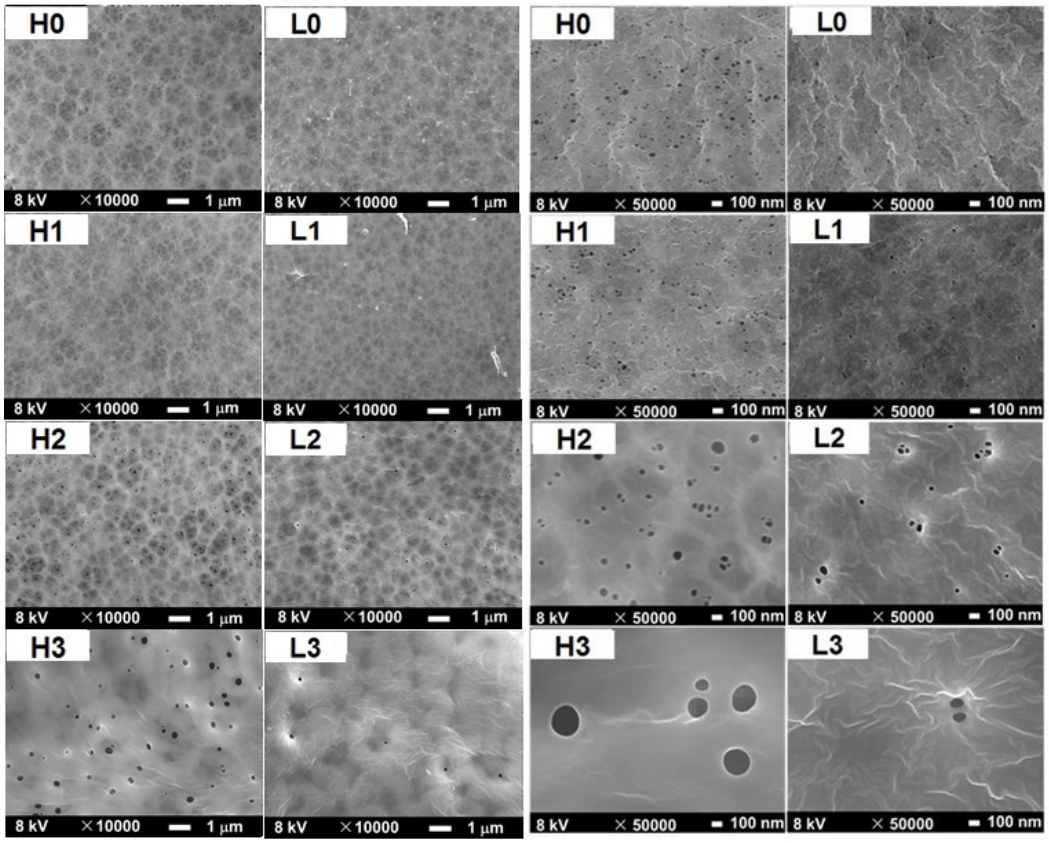

Fig.II.9. Surface SEM images of the prepared membranes.

(a) lower magnification

(b) higher magnification

2.3, the copolymer weight fractions in dope solution were changed to obtain membranes with similar water permeability for each series of the membranes. It is clear from Fig. 9 that for the same type of the used polymer, the porosity of the H series membranes is higher than that of the L-type membranes because of the lower polymer concentration in the former. Moreover,

for both the H- and L-type membranes, the pore size increased and the pore density decreased on increasing the PEGMA segment percentage in the copolymers. The increase in the PEGMA segment percentage increases the hydrophilicity of the polymer, which enhances the influx of water to the polymer solution during the membrane formation. It is well understood that a higher exchange rate of solvent with water results in larger pores at the membrane surface [38].

II.4.6. Pure water permeability and polystyrene particle rejection

Pure water permeabilities for both the H and L types of the prepared membranes are shown in Fig. 10 (a) and (b), respectively. Pure water permeabilities of H-type membranes were around 1150±200 L/(m^2·atm·h) and those of L-type membranes were around 169±20 L/(m^2·atm·h). Since water permeability can influence membrane fouling, I prepared membranes with similar water permeabilities to evaluate only the effect of the PEGMA segment percentage in the copolymers. From the SEM results shown in Fig. 9, it can be concluded that for H- and L-type membranes, the pore size increased and the pore density decreased with increase in the PEGMA segment percentage. While for H0 and L0 membranes, small pores were formed in much larger amounts, for H3 and L3 membranes, the number of the larger pores was much lower. Thus, these membranes seems to have similar surface porosity, and hence, similar pure water permeabilities.

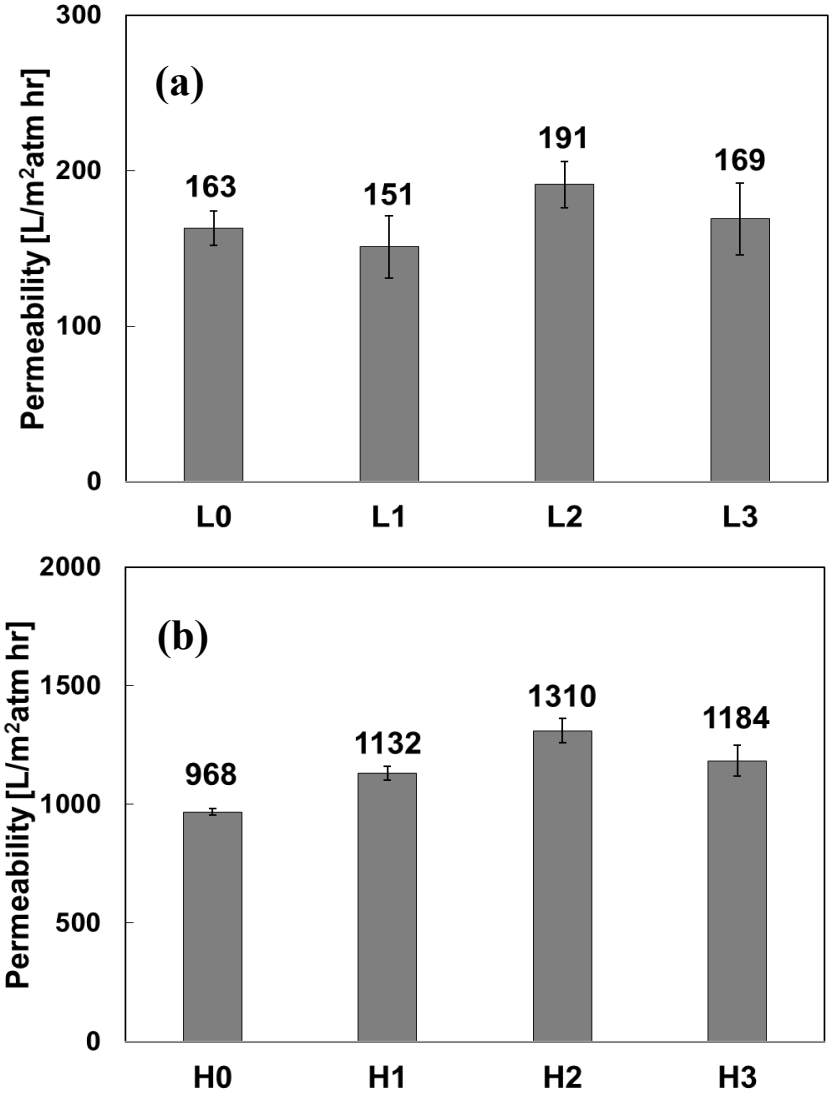

Fig. 10. Pure water permeabilities of (a) H type membranes and (b) L type membranes.

The rejection properties of the prepared membranes were evaluated using polystyrene latex particles with 100 nm diameter; the results are shown in Fig. 11(a) and (b) for the H- and L-type membranes, respectively. Particle rejection decreased slowly from 98% for H0 to 89% for H1 and H2 membranes, and then rejection showed a sharp decrease to 40% for H3 membrane. In contrast, the rejection was high at around 99% for L0, L1, and L2 membranes, and it

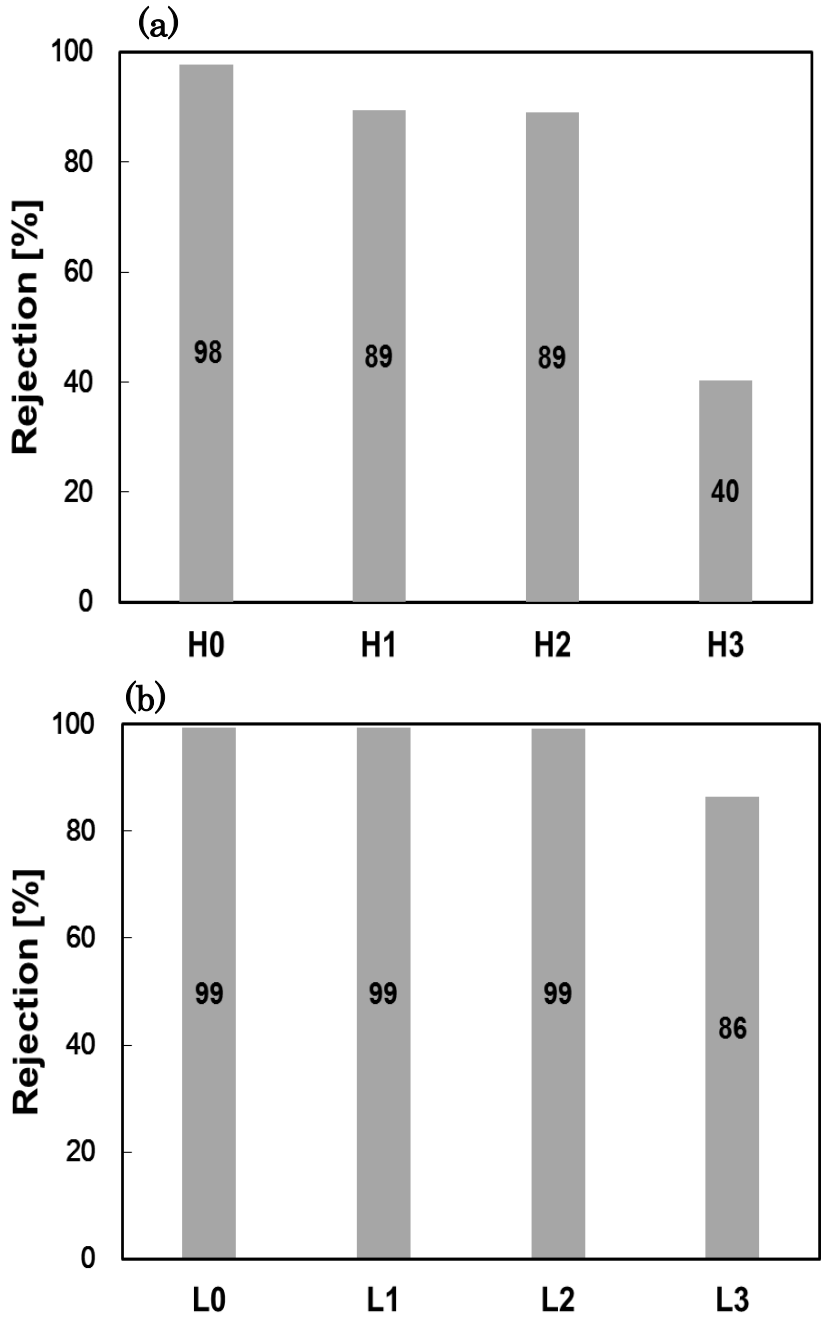

Fig. II.11. Polystyrene rejection results of (a) H type membranes and (b) L type membranes.

decreased to 86% for the L3 membrane. As explained in Section 4.5, the membrane surface pore size increased on increasing the PEGMA segment percentage (from L0 to L3 and from

H0 to H3 membranes). Thus, it is reasonable that rejection properties deteriorated on increasing the pore size.

II.4.7. Antifouling property evaluation

The antifouling properties of the prepared membranes were investigated by filtration experiments using 50 ppm BSA solution. The water fluxes observed during filtration for the H- and L-type membranes are shown in Fig. 12 (a) and (b), respectively. The initial water fluxes for the H- and L-type membranes were set at 500 and 80 L/(m^2·h), respectively. As depicted in Fig. 12 (a), the antifouling performances of the H-type membranes increased on increasing the PEGMA segment percentage. After 70 min of BSA filtration, the permeation fluxes of the H3 and H2 membranes were around 80% and 60% of its initial flux, respectively, whereas that of the H0 membrane (PVC control) reduced sharply to nearly 45% of the initial flux. After backflushing, the water fluxes of the H3 and H2 membranes recovered to 96% and 80% of the initial flux, whereas that of the H0 membrane recovered only to 54%. This improvement in the antifouling property of poly(VC-*co*-PEGMA) membranes is consistent with the increased hydrophilicity revealed by the air bubble contact angle measurement (Fig. 8 (a)), and can be attributed to the existence of a PEG layer at the surface of the membrane and pores [39]. Because the hydrated PEG chains have a large excluded volume in an aqueous environment, the PEG layer tends to repel protein molecules that approach the surface, serving as a steric barrier to protein adsorption [40, 41]. Moreover, it is well understood that protein adsorption can be prevented more effectively by increasing the density of the PEG layer on the membrane surface [42-45]. Therefore, antifouling properties of the prepared membranes increased on increasing the PEGMA segment percentage. Conversely, it is worth mentioning

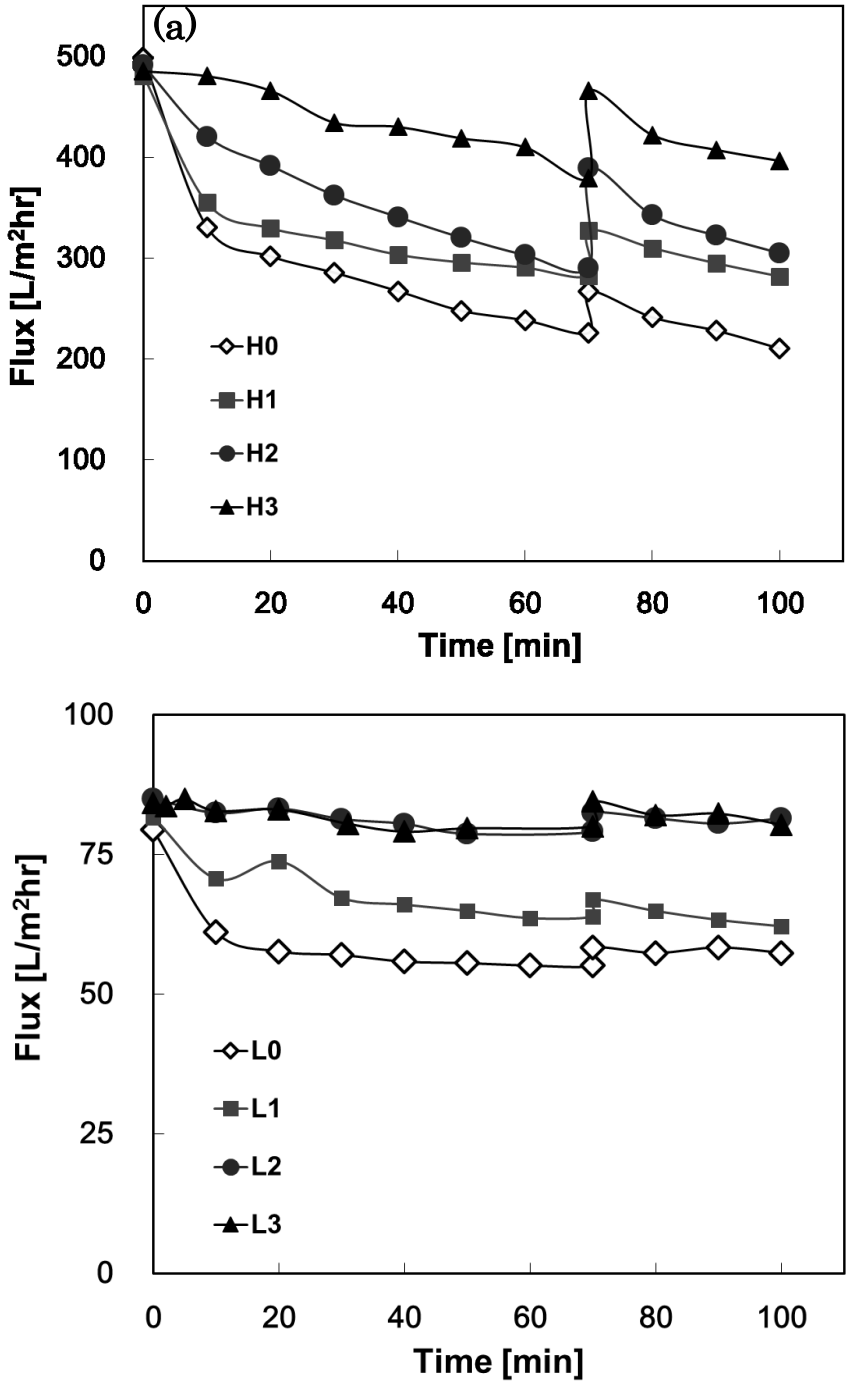

Fig.II.12. BSA fouling results of (a) H type membranes and (b) L type

that the membrane surface morphology strongly affects the membrane fouling tendency. Fu et al. indicated that when the pore size increased at the membrane surface, the fouling tendency also increased [46]. Considering that the pore size of the H3 membrane was much larger than

that of the H0 membrane (Fig. 9 (b)), I expected that more severe fouling would occur for the H3 membrane if only the effect of surface morphology is considered. However, the H3 membrane showed much better antifouling performance than H0 membrane, proving that the observed difference in the fouling performance is related to the change in the membrane material properties, rather than surface morphology.

II.5. CONCLUSTIONS

Poly(VC-co-PEGMA) copolymer membranes were successfully prepared via a NIPS method. The membrane characterization was performed using XPS, air contact angle, QCM, and SEM observation. MD simulation was carried out to study the state of PEGMA segment at the membrane surface. XPS measurement and MD simulation showed that the PEGMA segment was more likely to be present at the membrane surface. The copolymer membrane hydrophilicity and antifouling property considerably improved because of the higher concentration of PEGMA segment on the membrane surface. When the PEGMA segment percentage was around 9.8 mol%, the copolymer membrane showed very good antifouling property and restrained irreversible fouling, despite showing low membrane rejection to BSA molecules.

REFERENCE

[1] M. Mulder, Basic Principles of Membrane Technology, Kluwer Academic Publisher, Dordrencht, 1997.

[2] H. Okuno, K. Renzo, T. Uragami, Influence of casting solution additive, degree of polymerization, and polymer concentration on poly (vinyl chloride) membrane properties and performance, J. Membr. Sci., 83 (1993) 199–209.

[3] M. Bodzek, K. Konieczny, The influence of molecular mass of poly (vinyl chloride) on the structure and transport characteristics of ultrafiltration membranes, J. Membr. Sci. 61 (1991) 131–156.

[4] S. Mei, C. Xiao, X. Hu, Preparation of porous PVC membrane via a phase inversion method from PVC/DMAc/water/additives, J. Appl. Polym. Sci., 120 (2011) 557–562.

[5] W.D. Liu, Y.H. Zhang, L.F. Fang, B.K. Zhu, L.P. Zhu, Antifouling properties of poly(vinyl chloride) membranes modified by amphiphilic copolymers P(MMA-bMAA), Chin. J. Polym. Sci., 30 (2012) 568–577.

[6] M. Yoshikawa, K. Tsubouchi, Specialty polymeric membranes. 9. Separation of benzene cyclohexane mixtures through poly(vinyl chloride)-graft-poly(butyl methacrylate), J. Membr. Sci., 158 (1999) 269–276.

[7] R. Patel, M. Patel, S.H. Ahn, Y.K. Sung, H.K. Lee, J.H. Kim, J.S. Sung, Bioinert membranes prepared from amphiphilic poly(vinyl chloride)-g-poly(oxyethylene methacrylate) graft copolymers, Mater. Sci. Eng. C-Mater. Biol. Appl., 33 (2013) 1662–1670.

[8] F. Liu, B.K. Zhu, Y.Y. Xu, Preparation and characterization of poly(vinyl chloride)-graft-acrylic acid membrane by electron beam, J. Appl. Polym. Sci., 105 (2007) 291–296.

[9] S. Rajabzadeh, R. Sano, T. Ishigami, Y. Kakihana, Y. Ohmukai, H. Matsuyama, Preparation of hydrophilic vinyl chloride copolymer hollow fiber membranes with antifouling properties, Appl. Surf. Sci., 324 (2015) 718–724.

[10] P.R. Babu, V.G. Gaikar, Preparation, structure, and transport properties of ultrafiltration membranes of poly(vinyl chloride) (PVC), carboxylated poly(vinyl chloride) (CPVC), and PVC CPVC blends, J. Appl. Polym. Sci., 73 (1999) 1117–1130.

[11] P.R. Babu, V.G. Gaikar, Preparation, structure, and transport properties of ultrafiltration membranes of poly(vinyl chloride) and poly(vinyl pyrrolidone) blends, J. Appl. Polym. Sci., 77 (2000) 2606–2620.

[12] X. Fan, Y. Su, X. Zhao, Y. Li, R. Zhang, J. Zhao, Z. Jiang, J. Zhu, Y. Ma, Y. Liu, Fabrication of polyvinyl chloride ultrafiltration membranes with stable antifouling property by exploring the pore formation and surface modification capabilities of polyvinyl formal, J. Membr. Sci., 464 (2014) 100–109.

[13] J.A. Xu, Z.L. Xu, Poly(vinyl chloride) (PVC) hollow fiber ultrafiltration membranes prepared from PVC/additives/solvent, J. Membr. Sci., 208 (2002) 203–212.

[14] Y.N.T. Uragami, M. Sugihara, Studies on synthesis and permeability of special polymer membranes, Polym. Bull., 10 (1981) 617–622.

[15] S.O. Mei, C.F. Xiao, X.Y. Hu, Interfacial microvoid formation of poly(vinyl chloride)/polyacrylonitrile blend hollow-fiber membranes, J. Appl. Polym. Sci., 124 (2012) E9–E16.

[16] L. Krishnamoorthy, P.M. Arif, R. Ahmedkhan, Separation of proteins from aqueous solution using cellulose acetate/poly (vinyl chloride) blend ultrafiltration membrane, J. Mater. Sci., 46 (2011) 2914–2921.

[17] Q.F. Alsalhy, Hollow fiber ultrafiltration membranes prepared from blends of poly (vinyl chloride) and polystyrene, Desalination, 294 (2012) 44–52.

[18] S. Molina, P. Carretero, S.B. Teli, J.G. de la Campa, A.E. Lozano, J. de Abajo, Hydrophilic porous asymmetric ultrafiltration membranes of aramid-g-PEO copolymers, J. Membr. Sci., 454 (2014) 233–242.

[19] J.F. Hester, P. Banerjee, Y.Y. Won, A. Akthakul, M.H. Acar, A.M. Mayes, ATRP of amphiphilic graft copolymers based on PVDF and their use as membrane additives, Macromolecules, 35 (2002) 7652–7661.

[20] J.F. Hester, A.M. Mayes, Design and performance of foul-resistant poly(vinylidene fluoride) membranes prepared in a single-step by surface segregation, J. Membr. Sci., 202 (2002) 119–135.

[21] F. Liu, Y.Y. Xu, B.K. Zhu, F. Zhang, L.P. Zhu, Preparation of hydrophilic and fouling resistant poly(vinylidene fluoride) hollow fiber membranes, J. Membr. Sci., 345 (2009) 331–339.

[22] M.C. Shen, L. Martinson, M.S. Wagner, D.G. Castner, B.D. Ratner, T.A. Horbett, PEO like plasma polymerized tetraglyme surface interactions with leukocytes and proteins: in vitro and in vivo studies, J. Biomater. Sci. Ed., 13 (2002) 367–390.

[23] W. Norde, D. Gage, Interaction of bovine serum albumin and human blood plasma with PEO-tethered surfaces: Influence of PEO chain length, grafting density, and temperature, Langmuir, 20 (2004) 4162–4167.

[24] B. Liu, C. Chen, W. Zhang, J. Crittenden, Y. Chen, Low-cost antifouling PVC ultrafiltration membrane fabrication with Pluronic F 127: effect of additives on properties and performance, Desalination, 307 (2012) 26–33.

[25] H. Sun, COMPASS: an ab initio force-field optimized for condensed-phase applications overview with details on alkane and benzene compounds, J. Phys. Chem. B, 102 (1998) 7338–7364.

[26] D.N. Theodorou, U.W. Suter, Shape of unperturbed linear polymers: polypropylene, Macromolecules, 18 (1985) 1206–1214.

[27] X.P. Chen, C.A. Yuan, C.K.Y. Wong, S.W. Koh, G.Q. Zhang, Validation of forcefields in predicting the physical and thermophysical properties of emeraldine base polyaniline, Mol. Simul., 37 (2011) 990–996.

[28] S. Nosé, A molecular dynamics method for simulations in the canonical ensemble, Mol. Phys., 52 (1984) 255–268.

[29] H.J.C. Berendsen, J.P.M. Postma, W.F. van Gunsteren, A. DiNola, J.R. Haak, Molecular dynamics with coupling to an external bath, J. Chem. Phys., 81 (1984) 3684–3690.

[30] G. Sauerbrey, The use of quartz oscillators for weighting thin layers and for microweighting, Z. Phys., 155 (1959) 206–222.

[31] G. Raffaini, F. Ganazzoli, Surface hydration of polymeric (bio) materials: a molecular dynamics simulation study, J. Biomed. Mater. Res. Part A , 92A (2010) 1382–1391.

[32] J.H. Lee, Interaction of PEO-containing polymeric surfactants with hydrophobic surfaces, University of Utah, 1988, Ph.D. thesis.

[33] F. Zhang, E.T. Kang, K.G. Neoh, P. Wang, K.L. Tan, Surface modification of stainless steel by grafting of poly(ethylene glycol) for reduction in protein adsorption, Biomaterials, 22 (2001) 1541–1548.

[34] Y.X. Qiu, D. Klee, W. Pluster, B. Severich, H. Hocker, Surface modification of polyurethane by plasma-induced graft polymerization of poly(ethylene glycol) methacrylate, J. Appl. Polym. Sci., 61 (1996) 2373–2382.

[35] Z.Y. Xi, Y.Y. Xu, L.P. Zhu, B.K. Zhu, Modification of polytetrafluoroethylene porous membranes by electron beam initiated surface grafting of binary monomers, J. Membr. Sci., 339 (2009) 33–38.

[36] D.G. Walton, P.P. Soo, A.M. Mayes, S.J.S. Allgor, J.T. Fujii, L.G. Griffith, J.F. Ankner, H. Kaiser, J. Johansson, G.D. Smith, J.G. Barker, S.K. Satija, Creation of stable poly(ethylene

oxide) surfaces on poly(methyl methacrylate) using blends of branched and linear polymers, Macromolecules, 30 (1997) 6947–6956.

[37] H. Bubert, J.C. Rivière, H.F. Arlinghaus, H. Hutter, H. Jenett, P. Bauer, L. Palmetshofer, L. Fabry, S. Pahlke, A. Quentmeier, K. Hinrichs, W. Hill, B. Gruska, R. Arthur, G. Friedbacher, Surface and thin-film analysis, Ullmann's Encyclopedia of Industrial Chemistry, Wiley-VCH Verlag GmbH & Co. KGaA, 2000, 21-25.

[38] H. Strathmann, K. Kock, Formation mechanism of phase inversion membranes, Desalination, 21 (1977) 241–255.

[39] B.H. Tan, H. Hussain, Y. Liu, C.B. He, T.P. Davis, Synthesis and self-assembly of brush-type poly poly(ethylene glycol)methyl ether methacrylate -block-poly (pentafluorostyrene) amphiphilic diblock copolymers in aqueous solution, Langmuir, 26 (2010) 2361–2368.

[40] S. Kang, A. Asatekin, A.M. Mayes, M. Elimelech, Protein antifouling mechanisms of PAN UF membranes incorporating PAN-g-PEO additive, J. Membr. Sci., 296 (2007) 42–50.

[41] A. Asatekin, S. Kang, M. Elimelech, A.M. Mayes, Anti-fouling ultrafiltration membranes containing polyacrylonitrile-graft-poly(ethylene oxide) comb copolymer additives, J. Membr. Sci., 298 (2007) 136–146.

[42] J. Peng, Y. Su, Q. Shi, W. Chen, Z. Jiang, Protein fouling resistant membrane prepared by amphiphilic pegylated polyethersulfone, Bioresour. Technol., 102 (2011) 2289–2295.

[43] I. Szleifer, Polymers and proteins: interactions at interfaces, Curr. Opin. Solid State Mater. Sci., 2 (1997) 337–344.

[44] X.R. Chen, Y. Su, F. Shen, Y.H. Wan, Antifouling ultrafiltration membranes made from PAN-b-PEG copolymers: effect of copolymer composition and PEG chain length, J. Membr. Sci., 384 (2011) 44–51.

[45] A. Halperin, Polymer brushes that resist adsorption of model proteins: design parameters, Langmuir, 15 (1999) 2525–2533.

[46] X. Fu, T. Maruyama, T. Sotani, H. Matsuyama, Effect of surface morphology on membrane fouling by humic acid with the use of cellulose acetate butyrate hollow fiber membranes, J. Membr. Sci., 320 (2008) 483–491.

[47] J. Mueller, R.H. Davis, Protein fouling of surface-modified polymeric microfiltration membranes, J. Membr. Sci., 116 (1996) 47–60.

[48] H.P. Chu, X.Y. Li, Membrane fouling in a membrane bioreactor (MBR): Sludge cake formation and fouling characteristics, Biotechnol. Bioeng., 90 (2005) 323–331.

[49] D.J. Miller, S. Kasemset, L. Wang, D.R. Paul, B.D. Freeman, Constant flux crossflow filtration evaluation of surface-modified fouling-resistant membranes, J. Membr. Sci., 452 (2014) 171–183.

Chapter III

Effect of surface properties on antifouling performance of poly(vinyl chloride-*co*-poly(ethylene glycol)methyl ether methacrylate)/PVC blend membrane

III.1 INTRODUCTION

In the last chapter, membranes with very low fouling propensities were prepared when poly(VC-*co*-PEGMA) with the highest available PEGMA percentage (9.8%) was used. Although membranes with considerable antifouling properties were obtained, PEGMA-based copolymer membranes have low mechanical strengths, limiting their practical applications. This is especially true if consider self-support membranes (i.e., hollow fiber membranes). Therefore, in the present study, poly(VC-*co*-PEGMA) with a PEGMA segment percentage of 9.8 mol% was blended with PVC by using the conventional non-solvent induced phase separation (NIPS) method to obtain membranes with an appropriate mechanical strength and antifouling performance. The effect of the copolymer/PVC blend ratios on the surface morphology, hydrophilicity, mechanical strength, and, in particular, the fouling propensity of the prepared membranes was evaluated. To understand the mechanism of membrane fouling, molecular dynamics (MD) simulations were carried out to assess the distribution of the copolymer in the membrane matrix in the presence of water.

III.2 COMPUTATIONAL METHODS

Molecular dynamics simulations were carried out using Gromacs 5.0.4 program. Poly(VC-co-PEGMA) copolymer, with the structure shown in Fig. III. 1, and PVC molecules

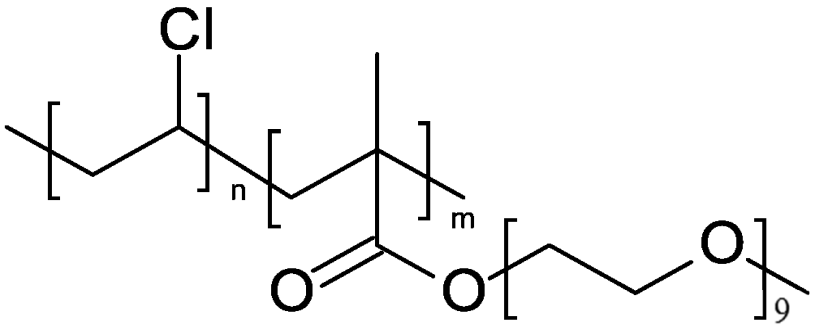

Fig. III. 1. Chemical structure of poly(VC-*co*-PEGMA)

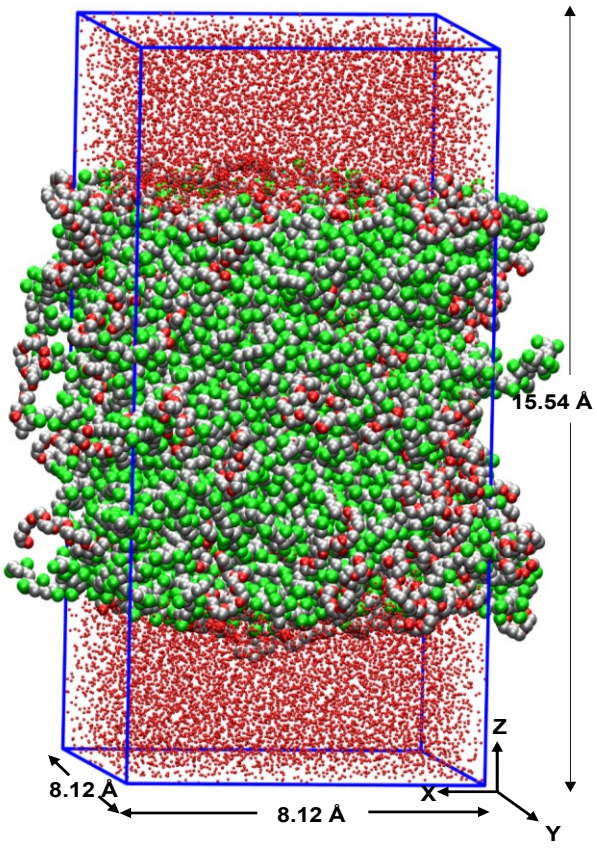

Fig. III. 2. A representative snapshot of the poly(VC-*co*-PEGMA)/PVC (blend 1:2) in the presence of water. The O atom of each water molecule is shown as a CPK model. The poly(VC-*co*-PEGMA)/PVC molecules are shown with their van der Waals radii and atom color coding is as follows: C, gray; Cl, green; O, red. For clarity, hydrogen atoms are not shown.

were constructed based on experimental information. Similar to our previous work [1, 2], model building and MD simulations were carried out and details has been reported in the appendices of this chapter. Table S1 shows degree of polymerization, number of atoms and box size for equilibrated structure in dry condition. A representative snapshot of the poly(VC-*co*-PEGMA)/PVC (blend 1:2) in the presence of water is shown in Fig. III. 2.

.

III.3 EXPERIMENTAL

III.3.1 Materials

PVC (M_w = 55,000) and poly(VC-*co*-PEGMA) (with a PEGMA segment percentage of 9.8 mol% and M_w of 180,000) were kindly supplied by Sekisui Chemical Co., Ltd. The chemical structure of this random copolymer was shown in Fig. III. 1. BSA, sodium dihydrogen phosphate (NaH_2PO_4), disodium hydrogen phosphate (Na_2HPO_4), and dimethylacetamide (DMAc) were purchased from Wako Pure Chemical Industries. The BSA solution was prepared by dissolving BSA in 0.1 mol/L phosphate buffer solution (PBS). Monodispersed polystyrene latex particles (diameter = 50 nm and size distribution < 3%) used for the rejection measurement were purchased from Duke Scientific Corporation (Thermo Fisher Scientific, Waltham, MA). Deionized water was produced in a Millipore Milli-Q unit. All reagents were used as received.

III.3.2 Flat-sheet membrane fabrication

The pure PVC copolymer membrane and three blended membranes with various copolymer/PVC blend ratios were prepared by a NIPS method. The compositions of the dope solutions used for membrane casting are shown in Table 1, where the blend membranes are labeled as Blend 1:4, 1:2, and 1:1, corresponding to their copolymer/PVC blend ratios. For the

prepared membranes, the dope compositions were adjusted so that they had similar pure water permeabilities to enable a better comparison of the fouling properties without the effects of different water permeabilities. To prepare flat sheet membranes, the polymers were dissolved in DMAc by stirring at 45 °C for one day to obtain homogeneous solutions and, then, degassed overnight at 25 °C. Then, the solution was cast onto a glass plate with a nonwoven support using a steel knife with a thickness of 200 μm to obtain the nascent polymeric film. The plate and film were subsequently immersed in a bath of deionized water at 24 ± 1 °C, leading to phase separation and formation of a porous membrane. All membranes were washed thoroughly with deionized water to remove residual solvent and stored in deionized water until use.

Table 1. Dope compositions for casting membranes.

Membrane	Copolymer/PVCblend ratio	Copolymer wt%]	PVC [wt%]	DMAc [wt%]	Total polymer conc. [wt%]
Pure PVC			14	86	14
Blend 1:4	1:4	3.6	14.4	82	18
Blend 1:2	1:2	6.5	13	80.5	19.5
Blend 1:1	1:1	10.8	10.8	78.4	21.6
Pure copolymer		22		78	22

III.3.3 BSA adsorption on polymer films

The amount of BSA adsorbed on the polymer film surface was measured using a quartz crystal microbalance with dissipation monitoring (QCM-D, Q-Sense E1, MEIWAFOSIS Co. Ltd, Japan). Piezoelectric quartz crystal sensors with a fundamental resonant frequency of around 5 MHz and a diameter of 14 mm (QSX 301, Q-Sense Co., Sweden) were used. Before each measurement, the sensor was cleaned by using an ultraviolet/ozone cleaner (Pro Cleaner 110; BioForce Nanosciences Co., USA). After spin coating with a 1.0 wt% polymer solution

at 3000 rpm for 1 min and drying on a hot stage (KATHERM C-MAG HP4' Kampmann GmbH, Germany) at 80 °C for 20 min, the sensor was placed in the QCM flow chamber. Then, the PBS solution was injected into the flow chamber at a flow rate of 50 μL/min for more than 1 h to stabilize the sensor and obtain the baseline. Next, the PBS solution was replaced with a 1000 ppm BSA solution. It is worth to mention that surface chemical composition of QCM-D samples would be different from that of the prepared membranes due to the different preparation conditions. QCM-D sample was prepared by the heating of polymer solution and the evaporation of solvent in air, while the membrane was obtained by the phase separation and the solidification of polymer solution in water. However, when the prepared sample contacted with PBS solution before BSA solution, the surface of the QCM-D sample can reconstruct to minimize the interfacial free energy, resulting in a similar surface chemical composition to that of the membrane [3]. Therefore, the measured interaction between the BSA and the QCM-D sample surface can be correlated to the interaction of BSA with the membrane surface. In accordance with the Sauerbrey equation (Eq. 1), the total amount of BSA adsorbed on the polymeric film surface was calculated by varying the sensor oscillation frequency during parallel flow of BSA solution at a constant temperature of 25 °C [4]:

$$\Delta m = -C\frac{\Delta f}{n} \qquad (1)$$

In Eq. 1, Δm is the adsorption amount ($ng \cdot cm^{-2}$), C is the mass sensitivity constant (17.7 $ng \cdot cm^{-2} \cdot Hz^{-1}$ at f = 4.95 MHz), Δf is the variation of frequency (Hz), and n is the overtone number (n = 7).

III.3.4 Membrane characterization

III.3.4.1 X-ray photoelectron spectroscopy analysis

X-ray photoelectron spectroscopy (XPS, PHI X-tool, ULVAC-PHI, Japan) was used to evaluate the surface chemical composition of the polymeric membranes. The system was equipped with an Al Kα radiation source (280 eV). Survey spectra were recorded over the range of 0 to 700 eV. The surface elemental composition was calculated from the peak area with a correction for atomic sensitivity. The photoelectron take-off angle was set at 45°.

III.3.4.2 Tensile strength measurements

For tensile strength measurements, I cast another batch of membranes directly onto the glass plate without using a nonwoven substrate. The composition of the dope solution and the preparation method were the same as those described in section 3.2. The tensile stresses at the break point were measured with a tensile testing apparatus (AGS-J, Shimadzu Co., Japan). At first, the thickness of the samples was measured using calipers. Then, the membrane samples (4 × 26 mm) were placed vertically between two pairs of pneumatic clamps, and a testing speed of 26 mm/min to the upper clamp was applied until the sample broke. Finally, I recorded the maximum tensile stress of the sample before it was broken. For each type of membrane, a minimum of three tensile stress measurements were averaged for reliability.

III.3.4.3 Membrane morphology observations

A field emission scanning electronic microscope (FE-SEM; JSF-7500F, JEOL Co. Ltd., Japan) was used to observe the surface morphology of the membranes. The prepared flat membranes were freeze-dried using a freeze dryer (FD-1000, EYELA, Japan) and then sputter coated with a 5 nm osmium tetroxide (OsO_4) layer using an osmium coater (Neoc-STB;

MEIWAFOSIS Co. Ltd., Japan). The coated samples were examined at an accelerating voltage of 8 kV at different magnifications.

III.3.4.4 Water permeability measurements

Water permeability was evaluated using a two-parallel-plate cross-flow module (C10-T; Nitto Denko Co. Ltd., Japan). The module channel had a clearance of 2.5 mm, a width of 45 mm, and a length of 180 mm. The flat membrane was installed on a permeable support. The effective membrane area inside the footprint of the O-ring was 6×10^{-2} m^2. Ultrapure water was pumped into the module using a peristaltic pump. The operating pressure at filtration was adjusted by a needle valve at the outlet. The mean pressure at the inlet and outlet of the membrane module was taken as the operating pressure. The feed water flow rate at the entrance of the membrane module was maintained at 190 $mL \cdot min^{-1}$. Before starting the measurements, the membrane was compacted at 0.1 MPa until the water flux became stable. Then, the membrane permeability was measured at 0.05 MPa every 3 min.

III.3.4.5 Polystyrene particle rejection measurement

The polystyrene particle rejection experiment was conducted in a cross-flow stainless cell with an effective filtration area of 8×10^{-4} m^2 using 300 ppm solution of latex particles. The feed solution was prepared by adding the monodisperse latex particles, which has a diameter of 50 nm, in an aqueous nonionic surfactant (mass fraction 0.1%, Triton X-100). This was then forced to permeate through the membrane under a pressure of 0.05 MPa. The filtrate was collected after 15 min of feed circulation. The concentration of both the feed and the filtrate was measured via a UV-vis spectrophotometry (U-2000, Hitachi Co., Tokyo, Japan) at a wavelength of 385 nm. The membrane rejection was calculated by the following equation:

$$R(\%) = (1 - \frac{C_p}{C_f}) \times 100 \qquad (2)$$

where R, C_p, and C_f are the rejection, latex particle concentration of permeate, and feed solution concentration, respectively.

III.3.4.6 Air bubble contact angle measurements

The air bubble contact angle of each membrane was measured with a contact angle goniometer (Drop Master 300, Kyowa Interface Science Co., Japan) to evaluate the surface hydrophilicity. A sample was prepared by cutting off a random part of the membrane of a suitable size and then placing this sample in a glass cell filled with deionized water. By using a special L-shaped syringe needle, an air bubble (5 μL) was released below the sample. The air bubble contact angle with the surface was measured automatically upon contact of the bubble with the membrane. To minimize experimental error, a minimum of seven measurements were carried out at different sample locations.

III.3.4.7 Membrane fouling experiments

The membrane fouling experiments was carried out using the same apparatus as that used for the membrane water permeability measurements. First, the membrane was compacted with Milli-Q water at a pressure of 0.1 MPa and a flow rate of 190 mL/min for at least 15 min until the water flux stabilized. Then, the initial water flux was set to 80 L/(m^2·h) by adjusting the filtration pressure. As described below, the prepared membranes had similar water permeabilities, and thus, their adjusted pressures did not differ significantly. Subsequently, the BSA fouling experiments were performed by replacing Milli-Q water by a 50 ppm BSA solution (pH 7.0 in PBS), and the flux was measured over the 2 h filtration time. The retentate was recycled into the feed tank, while the permeate was collected and weighed. The collected

permeate was returned to the feed tank every 10 min to maintain a constant concentration of the feed solution.

III.4 RESULTS AND DISCUSSION

III.4.1. XPS measurements

The surface chemical compositions of the prepared membranes were examined by using XPS wide scans, and the results are shown in Fig. III. 3. The prepared membranes show four major emission peaks at 201, 270, 284, and 530 eV due to Cl 2p, Cl 2s, C 1s, and O 1s emissions, respectively. The O 1s peak at the membrane surface is considered representative of the poly(VC-*co*-PEGMA) component because there is no oxygen in PVC. The appearance of a

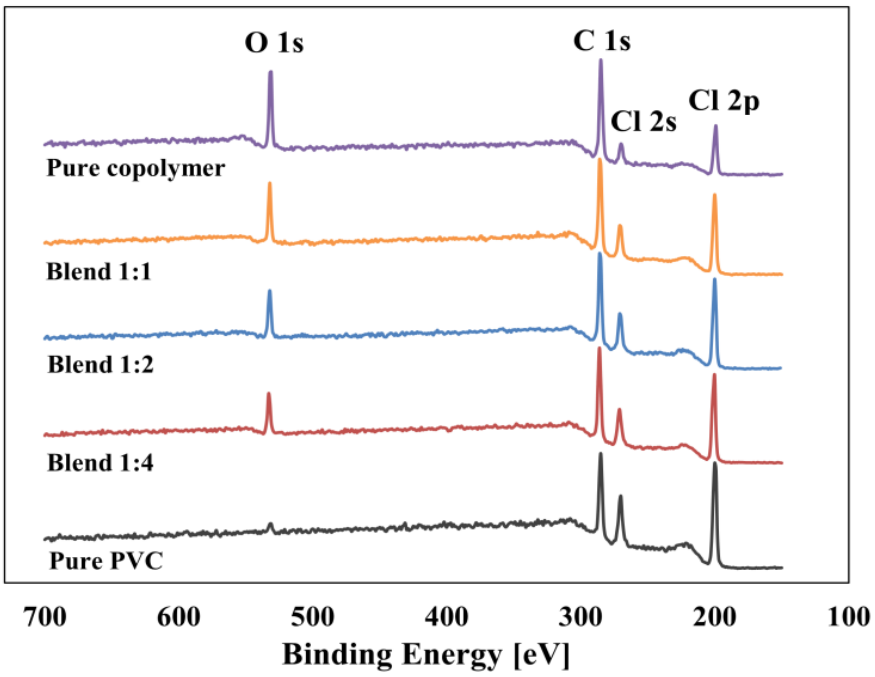

Fig. III. 3. XPS spectra for the prepared membranes with different copolymer/PVC blend ratios.

small O s1 peak in the pure PVC membrane is related to surface oxidation by environmental oxygen [5], and I believe that this surface oxidation occurs in all the prepared membranes.

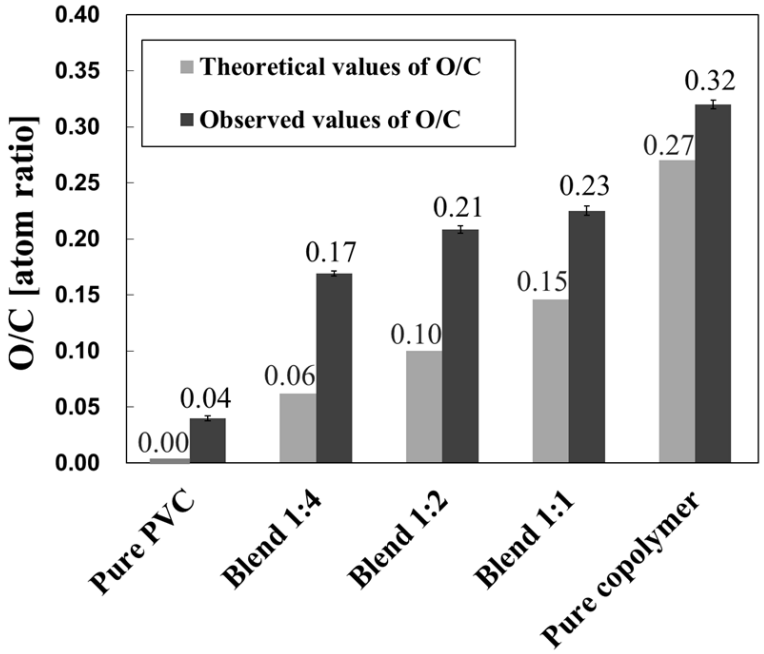

Fig. III. 4. Surface O/C atom ratios of the prepared membranes with different copolymer/PVC blend ratios.

The surface chemical compositions of the prepared membranes were evaluated by considering the O/C ratios. The O/C ratios from XPS measurements and the theoretical calculations are shown in Fig. III. 4. The theoretical O/C ratios of pure copolymer and PVC control membranes were simply calculated by considering the chemical structure of the copolymer. The theoretical results of the blend membranes were calculated by combining the results of pure copolymer and PVC membrane with their copolymer/PVC blend ratios, respectively. From Fig. III. 4, the experimental results showed that the O/C ratios increased as copolymer/PVC blending ratio increased. For all the prepared membranes, the measured O/C ratios were higher than the theoretical values, indicating that the copolymer was localized at

the membrane surface during the membrane preparation process due to the strong interactions between the PEGMA chains and the water molecules in the coagulation bath [6]. On the other hand, I observed that the differences between the calculated and measured O/C ratio of the blend membranes were completely considerable and were almost 2 times larger than that of the pure copolymer. For blend membranes, such large differences can attribute to the well-known surface segregation of copolymer during the membrane preparation process. However, for pure copolymer membrane, when PEGMA segment of the copolymer segregates to the membrane surface, it may drags the VC segment to the surface simultaneously, resulting in little change in O/C ratio and a smaller difference between XPS results and theoretical calculations.

III.4.2 MD simulation results

MD simulations are sophisticated atomistic simulation tools. The simulations can provide details about the atomic and nanoscale structural properties of the polymers that are crucial to understand the membrane transport and selectivity towards water molecules, ions, and other small solutes [7, 8]. The surface properties of polymers are often characterized at the macroscopic level to determine their hydrophilic or hydrophobic properties [9, 10]. In polymers, wettability mainly depends on the chemical nature and mobility of the exposed groups that undergo significant surface rearrangement on environmental change; that is, changes that occur if the membrane surface is surrounded by vacuum or solvent water. Because adsorption of the foulant on the surface of the membrane is dependent on the membrane surface properties, I analyzed the surface properties by MD simulation [1, 2]. In addition, the XPS results for surface analysis is for the depth of 50-100 Å, which mostly comes in the bulk of the membranes. While XPS shows mostly surface embedded in the bulk of the membrane, MD is a powerful tool to

analyze surface at the atomic level. Based on our studies [1], I believe that the only surface layer of the polymer interact with foulant that resulted in membrane fouling.

In our previous studies [1, 2], I showed that by increasing the PEGMA mol%, the O/C ratio on the membrane surface increased, indicating that the more hydrophilic PEGMA moieties were present at the surface. In the present study, I extended our study to analyze the effects of hydration on the surface chemical composition of poly(VC-*co*-PEGMA)/PVC blend membranes. MD simulations were carried out to understand the surface chemical composition of the blend polymers in the presence of water and to compare these results with those from experimental XPS results.

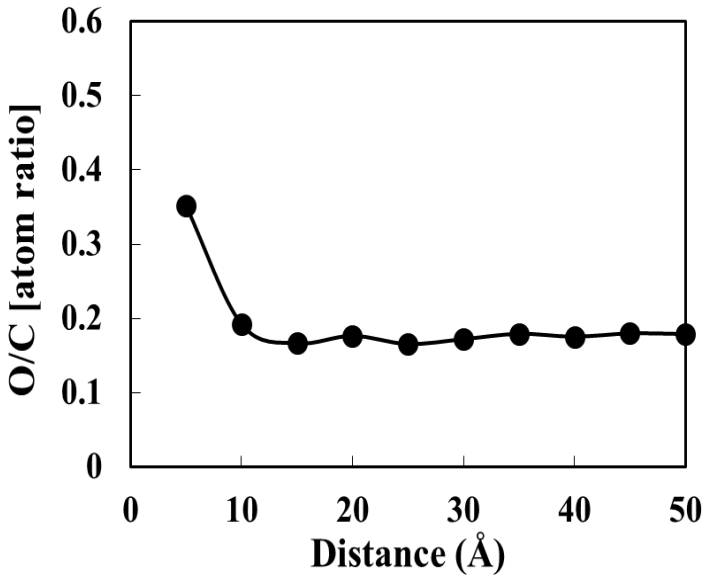

Fig. III. 5. O/C ratios of different distances in blend 1:1 membrane obtained by MD simulation.

To evaluate the distribution of PEGMA in the membrane matrix, the O/C ratio at different depths of the 1:1 blend membrane was calculated, and the results are shown in Fig. III. 5. Fig. III. 5 shows that, as distance from the membrane surface increases, the O/C ratio and, as a

consequence, PEGMA concentration decreases. Beyond 15 Å, the PEGMA concentration is equal to the bulk concentration. To further evaluate the membrane surface chemical composition by MD simulation, I considered the composition at 5 Å depth as the surface chemical composition.

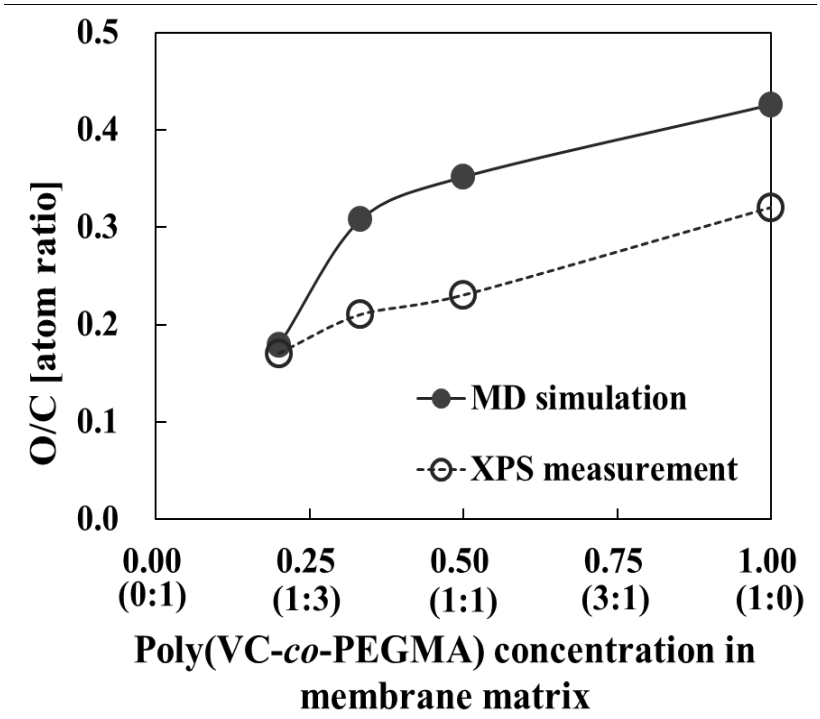

Fig. III. 6. Surface O/C atom ratios of the membranes with different copolymer/PVC blend ratios obtained from MD simulations and XPS measurements. The numbers inside the parentheses show the copolymer/PVC blend ratios.

Figure 6 shows the O/C ratio at a depth of 5 Å from the membrane surface obtained from MD studies. The results obtained by XPS measurements are also plotted. As expected, the O/C ratio at the membrane surface increased with increasing poly(VC-*co*-PEGMA)/PVC blend ratio. From Fig. III. 5, the O/C ratios calculated from MD simulations are higher than the experimental ratios. However, this may be due to the nature of the XPS analysis; that is, the

elemental composition is the average over a depth of several tens of angstroms from the surface [11]. In contrast, for MD simulations, the surface chemical composition results were obtained at equilibrium. For experimental results, the polymer was solidified after phase separation and before equilibrium was reached. Therefore, the localization of copolymer molecules on the membrane surface is expected to be higher in the MD simulations than in the experimental results. Consequently, the O/C ratio results derived from MD simulations would also be higher. If the fouling propensity of the membrane is controlled by the properties of the surface molecules, an analysis that shows the surface composition of the membranes in a very thin depth layer will be more useful to understand the BSA foulant interactions and, thus, will aid understanding of the fouling phenomena.

Fig. III. 6 shows that O/C ratios obtained by MD simulation increased sharply when the copolymer/PVC blending ratio increased from 1:4 (0.20 on the *x*-axis) to 1:2 (0.33 on the *x*-axis). Further increasing the copolymer/PVC blending ratio from 1:2 (0.33 on the *x*-axis) to pure copolymer, the O/C ratio increased slightly. This indicates that the membrane surface is almost covered by poly(VC-*co*-PEGMA) at the equilibrium state, even in case of the 1:2 blend ratio, because PEGMA interacts strongly with water. Thus, theoretically, only the 1:2 blend ratio is sufficient to produce a similar membrane surface to the pure copolymer membrane. On the other hand, the experimental data show a linear O/C ratio increase with increasing blend ratio. This is because polymer solution solidified before the equilibrium was reached and, thus, sufficient copolymer could move to the surface, as described above. Thus, the MD simulation results provide guidelines to decide the blend ratio.

III.4.3 BSA adsorption on polymer films

QCM-D analysis was performed to investigate the BSA adsorption on the different polymer films with different copolymer/PVC blend ratio. Fig. III. 7 shows the quantity of BSA adsorbed on different polymer films with different blending ratios. BSA adsorption on the pure PVC film was the highest due to the hydrophobic nature of BSA, whereas adsorption on the pure copolymers film was the lowest. The amount of BSA adsorbed on the blended copolymer films decreased with increasing copolymer/PVDF blending ratio. When the copolymer/PVC blend ratio increased to 1:1, the blend film showed similar BSA adsorption to that of the pure copolymer film. The results in Fig. III. 7 indicate that, due to the antifouling properties of poly(VC-*co*-PEGMA) [12-14], blending PVC with this copolymer is a promising method to prevent protein fouling. It is worth to mention that although nanometer-scale structure or roughness of the prepared film surfaces might affect the adsorption of protein in QCM-D test, polarity/hydrophilicity was the dominant factor affecting surface-protein interaction [15]. Therefore, I concluded the decreasing trend of the BSA adsorption amount shown in the Fig. III. 7 was the result of the change in hydrophilicity of the film surfaces. Consequently, the QCM-D analysis indicates that poly(VC-*co*-PEGMA)/PVC blend membranes with good antifouling properties can be obtained by use of an appropriate blend ratio.

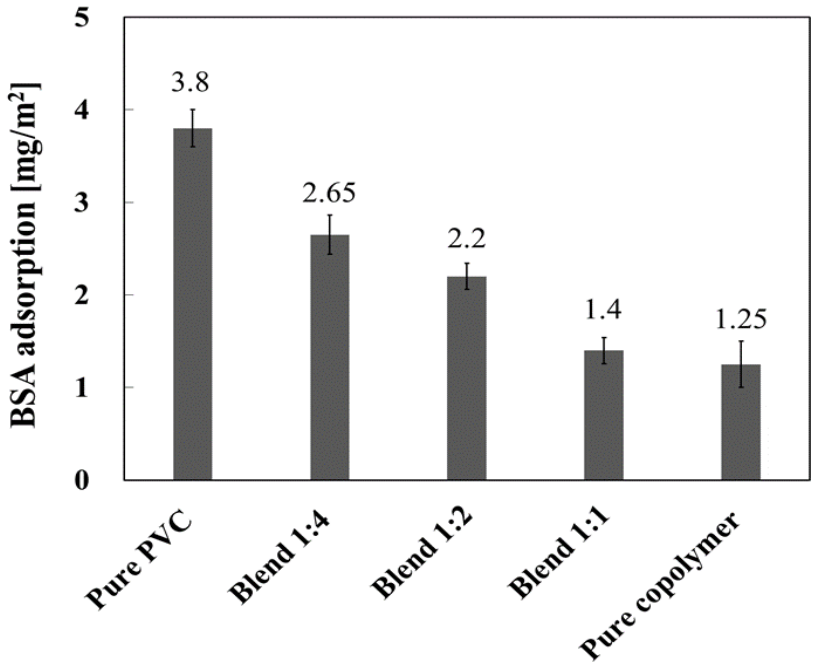

Fig. III. 7. BSA adsorption on different polymer films with different copolymer/PVC blend ratios.

III.4.4 Membrane surface morphology

FE-SEM images of the prepared membrane surfaces are shown in Fig. III. 8. For easy comparison of the pore size and pore density of the prepared membranes, FE-SEM images of at 10,000 and 50,000 magnification are shown in Fig. IIIs. 8 (a) and (b), respectively. Fig. III. 8 shows that by increasing the copolymer/PVC blend ratio, pore size increased and pore quantity decreased. A similar phenomenon was observed when PVC was blended with PES-*g*-PEGMA [16]. The higher the copolymer content in the dope solution, the higher the hydrophilicity of the dope solution. This leads to faster influx of water into the dope solution during membrane formation and a faster demixing process, resulting in the larger pores size at the selective-membrane layer surface [17].

(a)

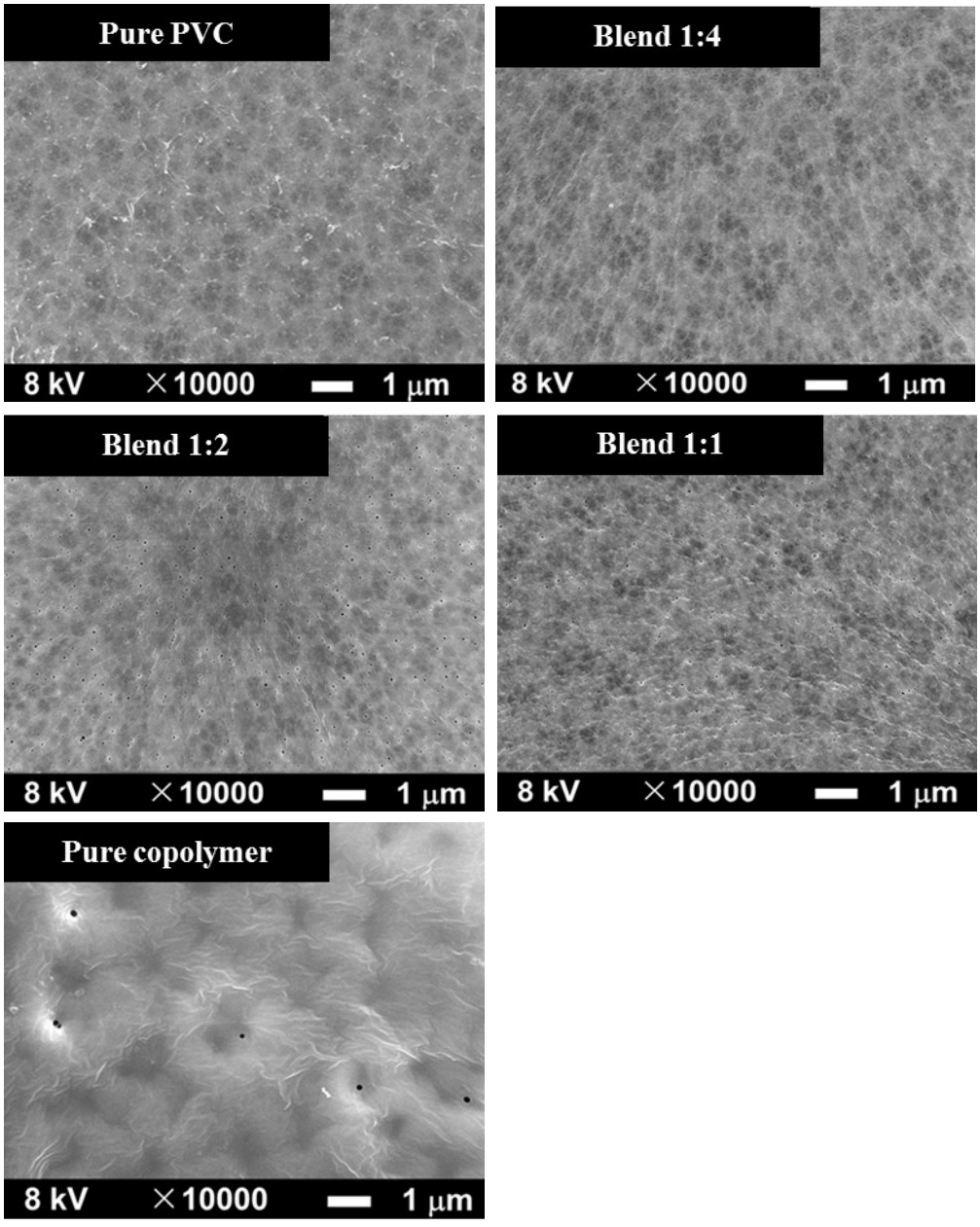
Pure PVC
8 kV ×10000 1 μm
Blend 1:4
8 kV ×10000 1 μm
Blend 1:2
8 kV ×10000 1 μm
Blend 1:1
8 kV ×10000 1 μm
Pure copolymer
8 kV ×10000 1 μm

(b)

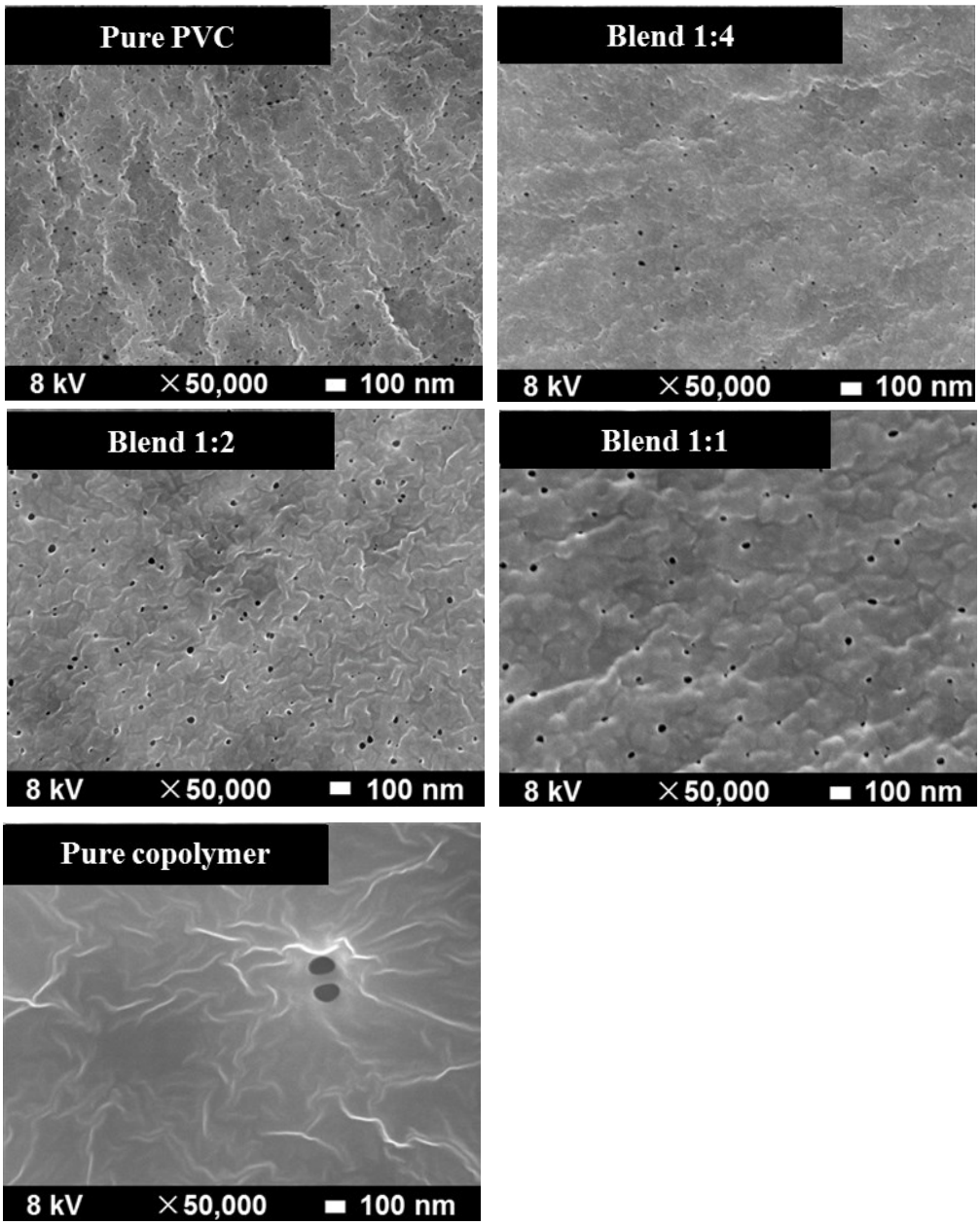

Fig. III. 8. Surface SEM images of the prepared membranes. (a) Low magnification (10,000) and (b) high magnification (50,000)

III.4.5 Pure water permeability and polystyrene particle rejection

Pure water permeabilities of the prepared membranes are shown in the Fig. III. 9. The prepared membranes have similar water permeabilities, around 180 ± 10 L/(m^2 atm h). It is important to prepare membranes with similar pure water permeabilities to avoid altering the hydrodynamic conditions (i.e., initial water flux and operating pressure) to allow evaluation of the effects of the membrane material properties only (i.e., hydrophilicity in this study) on the fouling properties [18, 19]. As shown in Fig. III. 8, the pore size increased and pore density decreased on increasing the copolymer/PVC blend ratio. Thus, these membranes expected to have similar surface porosity, and hence, similar pure water permeability, considering that the surface porosity is the most essential factor that affect the membrane water permeability [20].

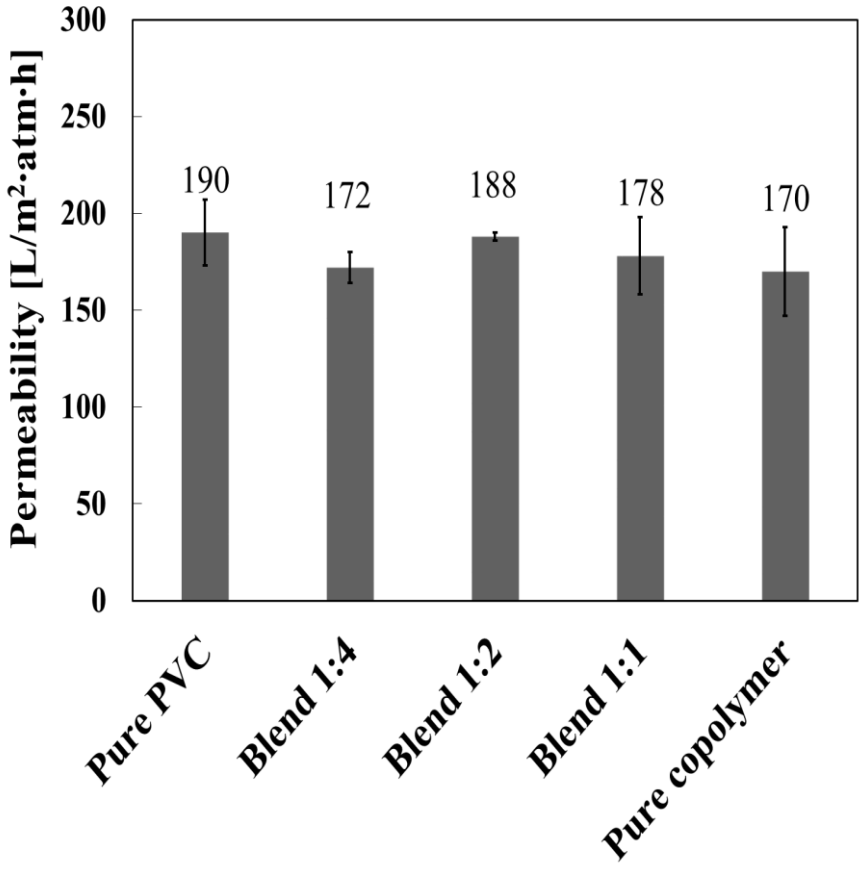

Fig. III. 9. Pure water permeabilities of the prepared membranes.

The rejection properties of the prepared membranes were investigated using polystyrene latex particles of 50 nm diameter. As shown in Fig. III. 10, increasing the copolymer/PVC blend ratio led to a decrease in membrane rejection, from 94% for pure PVC membrane to 76% for pure copolymer membrane. This is because the increase in blending ratio increases pore size at the membrane surface. However, I concluded that the rejection properties of the prepared membranes are not significantly different. Because the rejection properties of the membranes can affect the fouling properties [21], the membranes must have similar rejection properties to enable the evaluation of the effect of the membrane material only on the fouling propensity of the membranes.

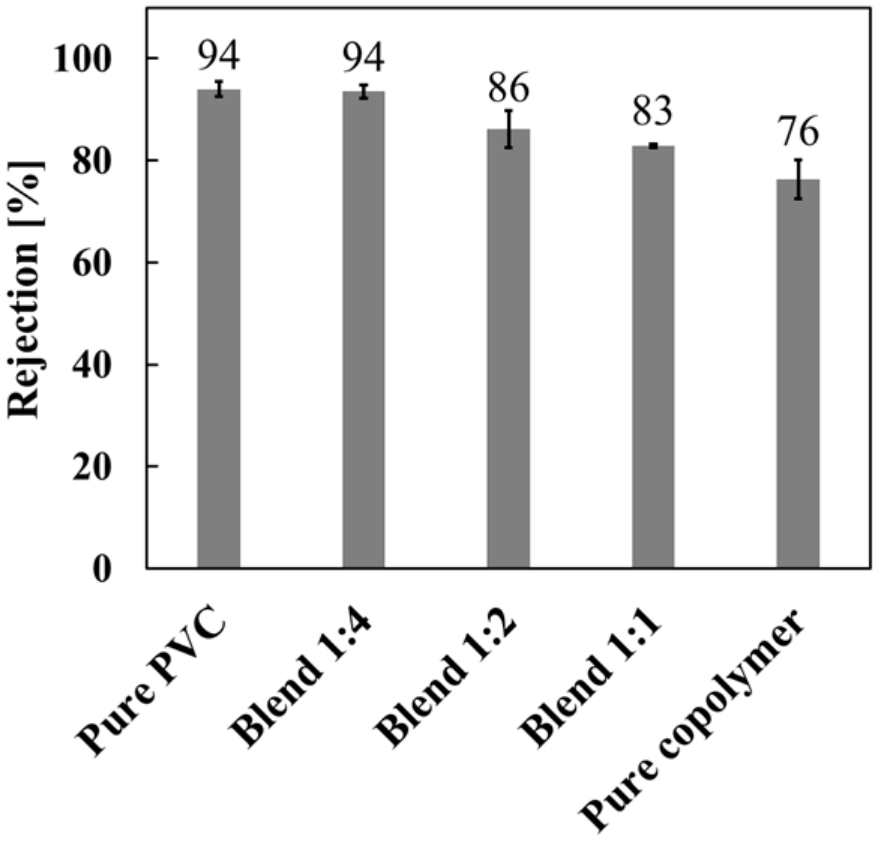

Fig. III. 10. Polystyrene rejection results of the prepared membranes. Polystyrene particles with 50 nm diameter were used.

III.4.6 Tensile strength

To evaluate the mechanical strength properties of the membranes, the tensile strengths at the break point were measured (without substrate), and the results of these measurements are summarized in Fig. III. 11. Increasing the copolymer/PVC blend ratio decreased the tensile strength sharply from 4.3 MPa for pure PVC to 0.2 MPa for the pure copolymer membrane. This sharp decrease in mechanical strength on increasing the copolymer/PVC blend ratio is related to the increase in the PEGMA content in the membrane matrix, and PEGMA is a well-known soft polymer [22]. In conclusion, adjusting the copolymer/PVC blend ratio allowed the preparation of membranes with appropriate mechanical strengths. Control over the tensile strength is crucial if preparation of self-supported membranes (i.e., hollow fiber membrane) is required.

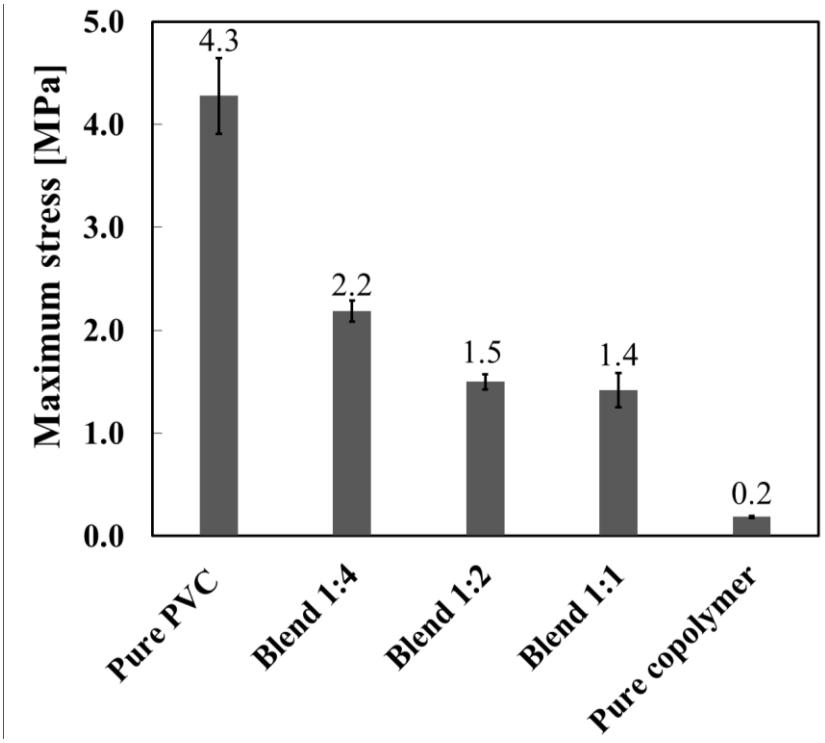

Fig. 11. Tensile strengths of the prepared membranes. All membranes used in this test were prepared without nonwoven supports.

III.4.7 Hydrophilicity of the membranes

Contact angle measurements have been widely used to characterize the hydrophilicity of the polymeric surfaces [23-26]. In this study, contact angle measurements were performed using captive air bubble method rather than sessile drop method, because our membranes were kept in Milli-Q water after preparation, and the membrane surface properties can keep constant during the air bubble contact angle measurement [27]. The air bubble contact angles of the prepared membranes are shown in Fig. III. 12. The air bubble contact angle did not increase when the copolymer/PVC blend ratio was less than 1:4, whereas it increased smoothly from 115º to 134º when the blend ratio increased from 1:4 to the pure copolymer, indicating an increase of the surface hydrophilic. Except the Blend 1:4, increase in hydrophilicity of the prepared membranes with an increase in copolymer/PVC blend ratio is consistent with increasing copolymer concentration at the membrane surfaces, as observed by XPS results and shown in Fig. III. 4. According to Fig. III. 4, in which the enrichment of the copolymer on the surface of Blend 1:4 membrane was observed, I expected the surface hydrophilicity and the air bubble contact angle of the Blend 1:4 would be larger than that of the Pure PVC membrane. However, Fig. III. 12 showed the similar air bubble contact angles for the Pure PVC and Blend 1:4, indicating that the hydrophilicity of the blend membrane seemed unchanged when the blend ratio increased to 1:4. It is well studied that many factors can affect the accuracy of the contact angle test, such as surface roughness, membrane pore size, and its distribution [21]. In Fig. III. 8 (b), Blend 1:4 exhibited different surface morphology compared with that of Pure PVC membrane. Therefore, I hypothesized here that the small difference in air bubble contact angle results of Blend 1:4 and Pure PVC membranes may attribute to the effect of their different surface morphologies rather than hydrophilicity.

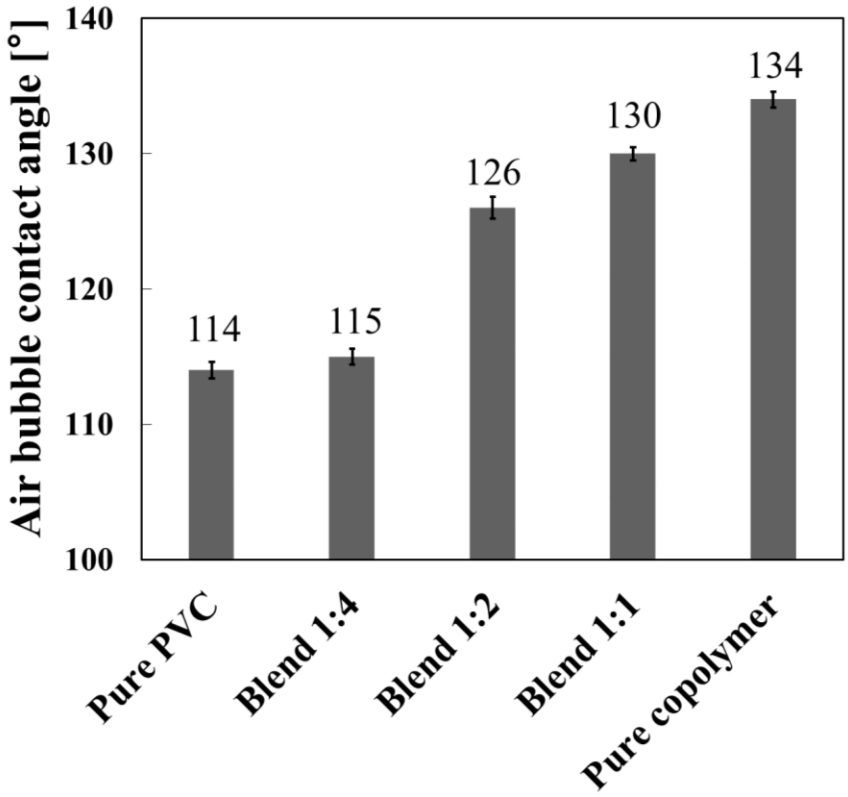

Fig. III. 12. Air bubble contact angle results for the prepared membranes.

III.4.8 Evaluation of the antifouling properties

The antifouling properties of the prepared membranes were evaluated by filtration experiments using a 50 ppm BSA solution. The initial water flux through the membranes was set to 80 L/(m^2·h) by adjusting the transmembrane pressure. Notably, the transmembrane pressures for the prepared membranes in the filtration experiments were almost the same due to similar membrane water permeabilities. Therefore, by removing the effect of the initial flux and transmembrane pressure, I can assess the net effect of the membrane material on BSA fouling. The changes in water flux during the BSA filtration process are plotted in Fig. III. 13. The antifouling properties of the prepared membranes increased with increasing

copolymer/PVC blend ratio, a consequence of the resistance to protein adsorption shown by poly(VC-*co*-PEGMA), consistent with the QCM-D results shown in Fig. III. 7. As shown in Fig. III. 13, the pure PVC membrane permeation flux sharply decreased to around 55% after 2 hours of BSA filtration. In contrast, the water fluxes of membranes with 1:4, 1:2, and 1:1 blend ratios were around 38, 20, and 12%, respectively, and that of the pure copolymer membrane was less than 10%. That is, by increasing the blending ratio from 0 (PVC) to 1:2, a sharp increase in the antifouling properties was observed, and further increasing the blending ratio from 1:2 to pure copolymer led to a slight increase in the membrane antifouling properties. Although the air bubble contact angle of the membrane prepared by blending copolymer/PVC in a 1:4 ratio was almost the same as the pure PVC membrane (Fig. III. 12), the antifouling performance of the 1:4 blend membrane improved by almost 20% compared to that of the pure PVC membrane. I would expect no differences in the antifouling properties of these two membranes if only the effect of the air bubble contact angles is considered. On the other hand, higher antifouling property of the Blend 1:4 membrane agreed well with the presence of the copolymer molecules at the membrane surface which is confirmed by XPS results in Fig. III.7, and resulted in the lower BSA interaction with the membrane surface (confirmed by QCM-D results in Fig. III.4). Thus, based on XPS and QCM-D results I strongly expect to observe higher antifouling property for Bled 1:4 membrane. Here I hypothesized that the similar air bubble contact angles of pure PVC and Blend 1:4 result from the effect of different surface morphologies rather than hydrophilicity [28]. As another phenomenon that might affect the fouling phenomena here, for the blend membranes in an aqueous environment, the brush like PEGMA chains on the membrane surface and in the pores create steric hindrance, preventing protein adsorption due to the large excluded volume of the hydrated PEGMA chains [29-31]. Thus, even though the membrane surface was partially covered by the PEGMA segments of

the copolymer, the steric repulsion due to PEGMA improves the membrane antifouling properties. Also, the denser PEGMA chain layer on the membrane surface that is formed by increasing the poly(VC-*co*-PEGMA)/PVC blend ratio prevents more effectively protein adsorption [32-37]. Thus, due to the hydrophilicity and steric repulsion of the PEGMA segments, further increasing the copolymer/PVC blend ratio increases the observed membrane antifouling properties.

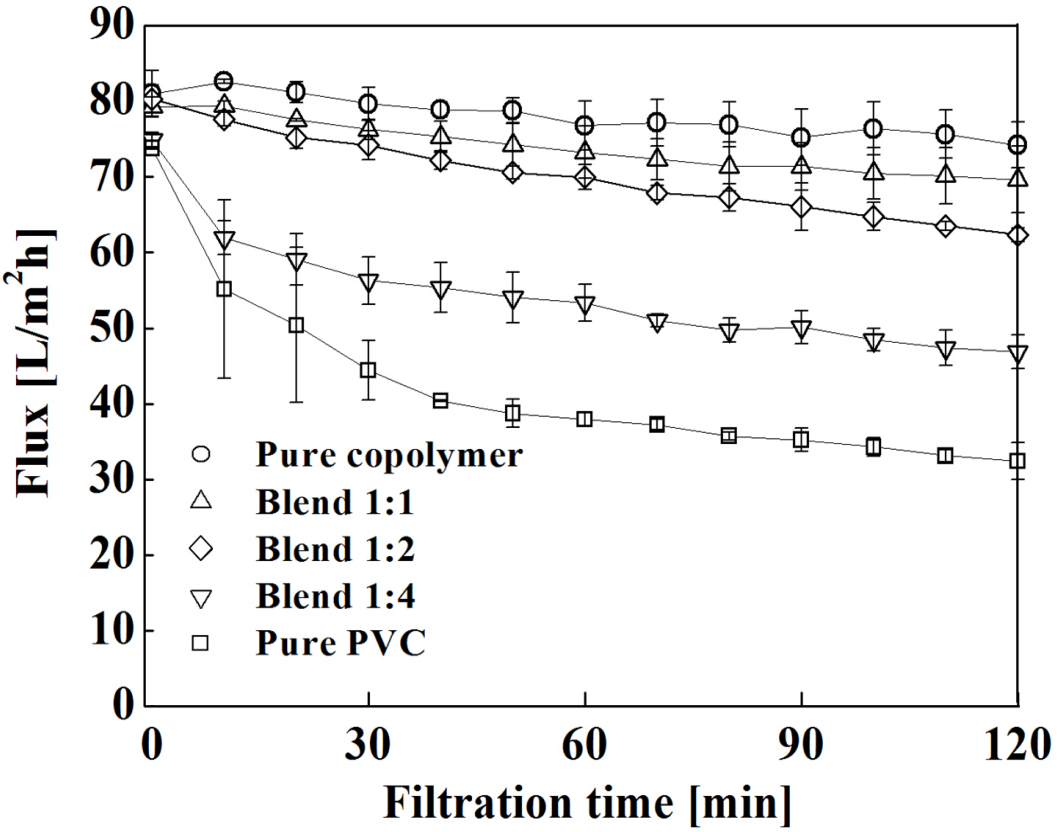

Fig. III. 13. BSA fouling results for the prepared membranes.

Fu et al. [21] showed that larger pore sizes at the membrane surface result in increased propensity for membrane fouling. Considering only the effects of their surface morphologies, because surface pore sizes increased with increasing copolymer content in the membrane (Fig.

III. 8 (b)), I expected that more severe fouling would occur for the pure copolymer membranes. However, the BSA fouling results indicate that the observed difference in the antifouling performance is related to the change in the membrane material properties, rather than their surface morphologies.

III.5 CONCLUSTIONS

Poly(VC-*co*-PEGMA)/PVC blend membranes were successfully prepared via a NIPS method. To evaluate the net effect of the membrane material on the fouling propensity of the prepared membrane, membranes with similar pure water permeabilities were prepared by adjusting the dope solution composition. Concerning the chemical compositions of the membrane surfaces, the O/C ratios obtained from MD simulations showed higher values than those measured by XPS due to differences in the analysis depths and because the MD simulations model a system at equilibrium, whereas the experimental measurements are made on membranes that have not reached equilibrium. Results from the MD simulations guide the choice of blending ratio to produce a membrane with reduced propensity to protein fouling. When copolymer/PVC blending ratio was greater than 1:2, considerable improvement in the hydrophilicity and antifouling propensity was observed. In conclusion, changes in the membrane material properties were more effective than changes to the surface structure in decreasing protein fouling.

REFERENCES

[1] Z. Zhou, et al., Preparation and characterization of antifouling poly(vinyl chloride-*co*-poly(ethylene glycol) methyl ether methacrylate)membranes, J Membr Sci (2015), 498 (2016) 414-422.

[2] A.R. Shaikh, S. Rajabzadeh, R. Matsuo, H. Takaba, H. Matsuyama, Hydration effects and antifouling properties of poly(vinyl chloride-co-PEGMA) membranes studied using molecular dynamics simulations, Appl. Surf. Sci. , 369 (2016) 241-250.

[3] Q. Shi, S. Ye, C. Kristalyn, Y. Su, Z. Jiang, Z. Chen, Probing molecular-level surface structures of polyether sulfone/Pluronic F127 blends using sum-frequency generation vibrational spectroscopy, Langmuir, 24, 7939-7946 (2008).

[4] G. Sauerbrey, The use of quartz oscillators for weighting thin layers and for microweighting, Z. Phys. 155 (1959) 206-222.

[5] Z.Y. Xi, Y.Y. Xu, L.P. Zhu, B.K. Zhu, Modification of polytetrafluoroethylene porous membranes by electron beam initiated surface grafting of binary monomers, J. Membr. Sci. 339 (2009) 33-38.

[6] D.G. Walton, P.P. Soo, A.M. Mayes, S.J.S. Allgor, J.T. Fujii, L.G. Griffith, J.F. Ankner, H. Kaiser, J. Johansson, G.D. Smith, J.G. Barker, S.K. Satija, Creation of stable poly(ethylene oxide) surfaces on poly(methyl methacrylate) using blends of branched and linear polymers, Macromolecules, 30 (1997) 6947-6956.

[7] Y. Luo et al. Computer simulations of water flux and salt permeability of the reverse osmosis FT-30 aromatic polyamide membrane, J. Membr. Sci. 384 (2011) 1-9.

[8] M. Shen et al. Dynamics of water and solute transport in polymeric reverse osmosis membranes via molecular dynamics simulations, J. Membr. Sci. 506 (2016) 95-108.

[9] K. Merrett, R.M. Cornelius, W.G. McClung, L.D. Unsworth, H. Sheardown, Surface analysis methods for characterizing polymeric biomaterials, J Biomat Sci-Polym E, 13 (2002) 593-621.

[10] G. Raffaini, F. Ganazzoli, Surface hydration of polymeric (bio)materials: A molecular dynamics simulation study, J. Biomed. Mater. Res. Part A, 92A (2010) 1382-1391.

[11] H. Bubert, J.C. Rivière, H.F. Arlinghaus, H. Hutter, H. Jenett, P. Bauer, L. Palmetshofer, L. Fabry, S. Pahlke, A. Quentmeier, K. Hinrichs, W. Hill, B. Gruska, R. Arthur, G. Friedbacher, Surface and thin-film analysis, in: Ullmann's Encyclopedia of Industrial Chemistry, Wiley-VCH Verlag GmbH & Co. KGaA, 2000.

[12] J.H. Lee, Interaction of PEO-containing polymeric surfactants with hydrophobic surfaces, Ph.D. thesis, University of Utah, (1988).

[13] F. Zhang, E.T. Kang, K.G. Neoh, P. Wang, K.L. Tan, Surface modification of stainless steel by grafting of poly(ethylene glycol) for reduction in protein adsorption, Biomaterials, 22 (2001) 1541-1548.

[14] Y.X. Qiu, D. Klee, W. Pluster, B. Severich, H. Hocker, Surface modification of polyurethane by plasma-induced graft polymerization of poly(ethylene glycol) methacrylate, J. Appl. Polym. Sci. 61 (1996) 2373-2382.

[15] B. Tan, H. Hussain, K. Chaw, G. Dickinson, C. Gudipati, W. Birch, S. Teo, C. He, Y. Liu, T. Davis, Barnacle repellent nanostructured surfaces formed by the self-assembly of amphiphilic block copolymers, Polym. Chem., 2010, 1, 276-279.

[16] R. Patel, M. Patel, S.H. Ahn, Y.K. Sung, H.-K. Lee, J.H. Kim, J.-S. Sung, Bioinert membranes prepared from amphiphilic poly(vinyl chloride)-g-poly(oxyethylene methacrylate) graft copolymers, Mater. Sci. Eng. C-Mater. Biol. Appl. 33 (2013) 1662-1670.

[17] H. Strathmann, K. Kock, Formation mechanism of phase inversion membranes, Desalination, 21 (1977) 241-255.

[18] R.W. Field, D. Wu, J.A. Howell, B.B. Gupta, Critical flux concept for microfiltration fouling, J. Membr. Sci. 100 (1995) 259-272.

[19] Q. She, C.Y. Tang, Y.N. Wang, Z. Zhang, The role of hydrodynamic conditions and solution chemistry on protein fouling during ultrafiltration, Desalination, 249 (2009) 1079-1087.

[20] A. Mehta, A.L. Zydney, Permeability and selectivity analysis for ultrafiltration membranes, J. Membr. Sci. 249 (2005) 245-249.

[21] X. Fu, T. Maruyama, T. Sotani, H. Matsuyama, Effect of surface morphology on membrane fouling by humic acid with the use of cellulose acetate butyrate hollow fiber membranes, J. Membr. Sci. 320 (2008) 483-491.

[22] L.T.J. Korley, B.D. Pate, E.L. Thomas, P.T. Hammond, Effect of the degree of soft and hard segment ordering on the morphology and mechanical behavior of semicrystalline segmented polyurethanes, Polymer, 47 (2006) 3073-3082.

[23] A.G. Fane, C.J.D. Fell, A review of fouling and fouling control in ultrafiltration, Desalination, 62 (1987) 117-136.

[24] D. Rana, T. Matsuura, Surface modifications for antifouling membranes, Chemical Reviews, 110 (2010) 2448-2471.

[25] V. Gekas, K.M. Persson, M. Wahlgren, B. Sivik, Contact angles of ultrafiltration membranes and their possible correlation to membrane performance, J. Membr. Sci. 72 (1992) 293-302.

[26] J.T.F. Keurentjes, J.G. Harbrecht, D. Brinkman, J.H. Hanemaaijer, M.A. Cohen Stuart, K. van't Riet, Hydrophobicity measurements of microfiltration and ultrafiltration membranes, J. Membr. Sci. 47 (1989) 333-344.

[27] W. Zhang, B. Hallström, Membrane characterization using the contact angle technique I. methodology of the captive bubble technique, Desalination, 79 (1990) 1-12.

[28] Q. She, C.Y. Tang, Y.N. Wang, Z. Zhang, The role of hydrodynamic conditions and solution chemistry on protein fouling during ultrafiltration, Desalination, 249 (2009) 1079-1087.

[29] S. Kang, A. Asatekin, A.M. Mayes, M. Elimelech, Protein antifouling mechanisms of PAN UF membranes incorporating PAN-g-PEO additive, J. Membr. Sci. 296 (2007) 42-50.

[30] M.K. Ko, J.J. Pellegrino, R. Nassimbene, P. Marko, Characterization of the adsorption-fouling layer using globular proteins on ultrafiltration membranes, J. Membr. Sci. 76 (1993) 101-120.

[31] B.H. Tan, H. Hussain, Y. Liu, C.B. He, T.P. Davis, Synthesis and self-assembly of brush-type poly poly(ethylene glycol)methyl ether methacrylate-block-poly (pentafluorostyrene) amphiphilic diblock copolymers in aqueous solution, Langmuir 26 (2010) 2361-2368.

[32] R. Gref, M. Lück, P. Quellec, M. Marchand, E. Dellacherie, S. Harnisch, T. Blunk, R.H. Müller, 'Stealth' corona-core nanoparticles surface modified by polyethylene glycol (PEG): influences of the corona (PEG chain length and surface density) and of the core composition on phagocytic uptake and plasma protein adsorption, Colloids and Surfaces B: Biointerfaces, 18 (2000) 301-313.

[33] W. Zhao, Y. Su, C. Li, Q. Shi, X. Ning, Z. Jiang, Fabrication of antifouling polyethersulfone ultrafiltration membranes using Pluronic F127 as both surface modifier and pore-forming agent, J. Membr. Sci. 318 (2008) 405-412.

[34] J. Peng, Y. Su, Q. Shi, W. Chen, Z. Jiang, Protein fouling resistant membrane prepared by amphiphilic pegylated polyethersulfone, Bioresour. Technol. 102 (2011) 2289-2295.

[35] I. Szleifer, Polymers and proteins: interactions at interfaces, Curr. Opin. Solid State Mater. Sci. 2 (1997) 337–344.

[36] X.R. Chen, Y. Su, F. Shen, Y.H. Wan, Antifouling ultrafiltration membranes made from PAN-b-PEG copolymers: effect of copolymer composition and PEG chain length, J. Membr. Sci. 384 (2011) 44-51.

[37] A. Halperin, Polymer brushes that resist adsorption of model proteins: design parameters, Langmuir, 15 (1999) 2525-2533.

III.6 APPENDICIES

S1. Model Building and Force Field:

S1.1. Initial Model Building

Polymer chains were first built using the Materials Studio 7.0 (BIOVIA DASSAULT SYSTEMS) from vinyl chloride (VC), ethylene glycol (EG), methyl acrylate (MA) repeat units, based on experimental information of PEGMA and PVC content in the blend membranes. Poly(VC-co-PEGMA) (Figure 1) with PEGMA content of 9.8 mol% was obtained from our previous studies [1]. Several blends were packed in order to get cubic simulation boxes constructed using Amorphous Cell Module of Materials Studio using experimental blending ratios of PVC and poly(VC-co-PEGMA). Amorphous Cell module is based on the packing technique of Theodorou and Suter [2, 3] and Meirovitch scanning method [4]. For each system, 100 configurations were constructed. The module builds molecules in a cell in a Monte Carlo technique by minimizing the close contacts between atoms, until a realistic distribution of torsion angles for any given forcefield is reached. It is desirable to use experimental degree of polymerization to build a polymer model, however due to complexity arising to prepare such a model, often smaller models were used in simulation. These models were able to reproduce experimental density as well other properties of polymer and useful information can be derived from such a models [5-8]. Similar to the commercial PVC, the atactic chain was used with

equal fractions of meso and racemic diads distributed randomly along the chain.[9-11] Starting with the realistic initial structure of blends obtained using Amorphous Cell module of Materials studio, further calculations were carried out using Gromacs 5.0.4 [12] program. Methods used for force field development and MD simulations were reported below.

S1.2. Force Field:

The topology of the monomer molecules required by Gromacs was generated by using the Antechamber software package [13] based on the generalized amber force field [14] (GAFF). In order to calculate RESP [15] charges for VC, EG, and methyl acrylate (MA) monomer units, density functional theory (DFT) calculations were performed with the Gaussian 03 program [16] using the B3LYP and 6-31G(d) basis sets. The electrostatic potential surface was generated by the Merz–Kollman method at the HF/6-31G(d) level of theory, followed by a multi-configurationally two-stage RESP fitting. The software code RED IV was used for electrostatic potential fitting [17]. The obtained copolymer replicated several times to get the bulk structure. Dimension has been chosen such that I have equilibrated structure of bulk surface with depth of at least 7 nm in Z-direction. The degree of polymerization, total number of atoms and box size of equilibrated structure is reported in Table S1. Validation of force field parameter and comparison with experimental properties was reported in our previous paper [1].

S 2. Simulation Protocol

S 2.1. Constructing a dry bulk polymer

Starting configurations were first minimized using the energy minimization routine in Gromacs. Simulated annealing was performed on the PVC/poly(VC-*co*-PEGMA) system, starting from 300 K and increasing to 600 K to achieve reliable energetically favorable states

molecular conformations, the assembly was then cooled to 300 K with 20 K of intervals. The temperature was maintained at 300 K using velocity rescaling with a coupling time of 0.1 ps. The pressure was maintained at 1 atm for NPT simulations using a Berendsen barostat with a coupling time of 2 ps. Production simulations were carried out using the NPT ensemble for 20 ns. A constant pressure of 1 bar (τ_P = 2.0 ps) and temperature of 300 K (τ_T = 0.1 ps) were maintained using the Noose-Hoover [18] thermostat and Parrinello-Rahman [19] barostat. All simulations were carried out for 2.0 fs time step.

The equilibrated box-size was shown in Table S1. In order to get polymer membrane surface, box size was extended in both side of z-axis followed by equilibration for another 50 ns using NVT ensemble to ensure system is stabilized at its equilibrium value. Previously, Kolev and Freger [20] successfully used similar method to build a polyamide membrane structure. Equation of motions were integrated with the leapfrog algorithm with a time step of 2.0 fs. The total electrostatic interactions were evaluated using particle mesh Ewald (PME) summation. Coulomb and van der Waals cutoffs of 1.0 nm were employed. Periodic boundary conditions in all directions were used to mimic bulk behavior. All bonds with hydrogen atoms were constrained with the LINCS algorithm.

S 2.2. Constructing a hydrated membrane

In order to calculate effect of hydration on blend membrane, the box size was extended along the *z*-axis at both ends. The *z*-axis was extended by a total of 10 nm (5 nm each side) to create reservoirs for bulk water. Further 50 ns equilibration was carried out as reported earlier. The box was then filled with TIP3P water molecules (Fig. 2). Water molecules were added on the surface using Gromacs Tool and water molecules within the membrane bulk were removed. Due to compatibility with Amber GAFF force field, TIP3P water model was chosen. TIP3P

Table S1: Degree of polymerization, total number of atoms and box size in dry condition.

Membrane	Degree of polymerization (DP)		Number of atoms	Box size (nm^3)
	PVC	Poly(VC-co-PEGMA)		
Pure PVC	100	-	32508	7.43 × 7.43 × 7.43
Blend 4:1	72	20	33013	7.73 × 7.73 × 7.73
Blend 2:1	36	20	44625	8.10 × 8.10 × 8.10
Blend 1:1	18	20	53352	8.53 × 8.53 × 8.53
Pure copolymer	110		20730	5.76 × 5.76 × 6.92

water model was widely used and has been validated in many polymeric membrane MD simulations [20-23]. MD simulations were carried out, as reported above, for the bulk system. The pressure was maintained at 1 atm using semi-isotropic pressure coupling to a Berendsen barostat with a time constant of 5.0 ps using NPT ensemble. The height of the simulation box (*z* direction) and the cross sectional area (*xy*-plane) were allowed to vary independently of each other, thereby allowing the area of the membrane surface and the distance between the interfaces to fluctuate independently. The equilibration was carried out for 20 ns using NPT simulation. Final MD simulations in NVT ensemble were carried out for 20 ns and last 10 ns trajectory was used for analysis. No additional constraints were applied, and all molecules were allowed to freely move during simulation. The Gromacs analysis tools were used for analysis.

VMD program [24] was used to visualize trajectories. Partial density along z-axis for representative atoms were calculated using gromacs analysis tools. The partial densities of C, O, and Cl was analyzed using simulated trajectory along the z-axis. Then at every 5 Å interval, partial densities were averaged. Further, ratio of O/C was plotted against the distance from the surface.

References

[1] A.R. Shaikh, S. Rajabzadeh, R. Matsuo, H. Takaba, H. Matsuyama, Hydration effects and antifouling properties of poly(vinyl chloride-co-PEGMA) membranes studied using molecular dynamics simulations, Appl. Surf. Sci. 369 (2016) 241-250.

[2] D.N. Theodorou, U.W. Suter, Detailed Molecular-Structure of a Vinyl Polymer Glass, Macromolecules, 18 (1985) 1467-1478.

[3] D.N. Theodorou, U.W. Suter, Atomistic Modeling of Mechanical-Properties of Polymeric Glasses, Macromolecules, 19 (1986) 139-154.

[4] H. Meirovitch, Computer-Simulation of Self-Avoiding Walks - Testing the Scanning Method, J. Chem. Phys. 79 (1983) 502-508.

[5] W.Y. Ahn, A.G. Kalinichev, M.M. Clark, Effects of background cations on the fouling of polyethersulfone membranes by natural organic matter: Experimental and molecular modeling study, J. Membr. Sci. 309 (2008) 128-140.

[6] Z.L. Luo, J.W. Jiang, Molecular dynamics and dissipative particle dynamics simulations for the miscibility of poly(ethylene oxide)/poly(vinyl chloride) blends, Polymer, 51 (2010) 291-299.

[7] Z. Zhou, S. Rajabzadeh, A.R. Shaikh, Y. Kakihana, T. Ishigami, R. Sano, H. Matsuyama, Preparation and characterization of antifouling poly(vinyl chloride-co-poly(ethylene glycol)methyl ether methacrylate) membranes, J. Membr. Sci. 498 (2016) 414-422.

[8] S. Mani, F. Khabaz, R.V. Godbole, R.C. Hedden, R. Khare, Structure and Hydrogen Bonding of Water in Polyacrylate Gels: Effects of Polymer Hydrophilicity and Water Concentration, J. Phys. Chem. B, 119 (2015) 15381-15393.

[9] B.F. Abu-Sharkh, Glass transition temperature of poly(vinylchloride) from molecular dynamics simulation: explicit atom model versus rigid CH2 and CHCl groups model, Comput. Theor. Polym. Sci. 11 (2001) 29-34.

[10] G.D. Smith, R.L. Jaffe, D.Y. Yoon, Conformations and Order in Atactic Poly(Vinyl Chloride) Melts from Molecular-Dynamics Simulations, Macromolecules, 26 (1993) 298-304.

[11] G.D. Smith, P.J. Ludovice, R.L. Jaffe, D.Y. Yoon, Conformations of 2,4-Dichloropentane and 2,4,6-Trichloroheptane and a Force-Field for Poly(Vinyl Chloride) Based Upon Ab-Initio Electronic-Structure Calculations, J. Phys. Chem. 99 (1995) 164-172.

[12] S. Pronk, S. Pall, R. Schulz, P. Larsson, P. Bjelkmar, R. Apostolov, M.R. Shirts, J.C. Smith, P.M. Kasson, D. van der Spoel, B. Hess, E. Lindahl, GROMACS 4.5: a high-throughput and highly parallel open source molecular simulation toolkit, Bioinformatics, 29 (2013) 845-854.

[13] J.M. Wang, W. Wang, P.A. Kollman, D.A. Case, Automatic atom type and bond type perception in molecular mechanical calculations, J. Mol. Graph. Model. 25 (2006) 247-260.

[14] J.M. Wang, R.M. Wolf, J.W. Caldwell, P.A. Kollman, D.A. Case, Development and testing of a general amber force field, J. Comput. Chem. 25 (2004) 1157-1174.

[15] J.M. Wang, P. Cieplak, P.A. Kollman, How well does a restrained electrostatic potential (RESP) model perform in calculating conformational energies of organic and biological molecules?, J. Comput. Chem. 21 (2000) 1049-1074.

[16] M.J. Frisch, G.W. Trucks, H.B. Schlegel, G.E. Scuseria, M.A. Robb, J.R. Cheeseman, et al., Gaussian 09, in, Gaussian, Inc., Wallingford, CT, USA, 2009.

[17] F.Y. Dupradeau, A. Pigache, T. Zaffran, C. Savineau, R. Lelong, N. Grivel, D. Lelong, W. Rosanski, P. Cieplak, The R.ED. tools: advances in RESP and ESP charge derivation and force field library building, Phys. Chem. Chem. Phys. 12 (2010) 7821-7839.

[18] V. Kolev, V. Freger, Hydration, porosity and water dynamics in the polyamide layer of reverse osmosis membranes: A molecular dynamics study, Polymer, 55 (2014) 1420-1426.

[19] W.L. Jorgensen, J. Chandrasekhar, J.D. Madura, R.W. Impey, M.L. Klein, Comparison of Simple Potential Functions for Simulating Liquid Water, J. Chem. Phys. 79 (1983) 926-935.

[20] Y. Luo, E. Harder, R.S. Faibish, B. Roux, Computer simulations of water flux and salt permeability of the reverse osmosis FT-30 aromatic polyamide membrane, J. Membr. Sci. 384 (2011) 1-9.

[21] M. Shen, S. Keten, R.M. Lueptow, Dynamics of water and solute transport in polymeric reverse osmosis membranes via molecular dynamics simulations, J. Memb. Sci. 506 (2016) 95-108.

[22] W. Humphrey, A. Dalke, K. Schulten, VMD: Visual molecular dynamics, J. Molec. Graphics, 14 (1996) 33-38.

Chapter IV

Preparation of robust braid-reinforced poly(vinyl chloride) ultrafiltration hollow fiber membrane with antifouling surface and application to filtration of activated sludge solution

IV.1 INTRODUCTION

According to the results in Chapter III, copolymer poly(VC-*co*-PEGMA) has shown promising potential to prepare antifouling copolymer/PVC blend flat sheet membrane. However, the mechanical strength of the PVC membrane will decrease with the addition of such copolymer. Considering that poor mechanical strength can limit membrane application, it is necessary to explore the approaches for preparing robust membranes [1].

Several methods have been proposed to improve the mechanical strength of PVC membranes. Some researchers have incorporated nano-size additives into the PVC matrix to obtain strong PVC membranes, such as graphene oxide [2] or TiO_2 [3]. In other studies, dual-layer PVC hollow fiber membranes, where PVC dope solution was coated onto the strong microfiltration matrix membranes, such as PVDF hollow fiber membranes, have been developed [4-6]. Recently, braid-reinforced hollow fiber membranes obtained by coating the dope solution onto tubular braids have attracted significant attention [7-9]. Different polymer braids have been used in the preparation of the braid-reinforced membranes. On the other hand, interfacial bonding strength between the coating layer and braid is more crucial, because the braid-reinforced hollow fiber membranes with low interfacial bonding strength could restrict the application and operating life of the membranes due to the detachment of the coating layer during the wastewater treatment [8, 10]. It has been revealed that for the preparation of braid-reinforced membranes, when the braid material is same/similar to coating solution, higher

bonding strength between the coating layer and braid can be obtained due to the good compatibility and interfacial affinity [8-10]. The interaction between the coating material and braids plays an important role in determining the bonding strength and the membrane mechanical properties.

In this chapter, in order to obtain a robust ultrafiltration hollow fiber membrane with antifouling surface, poly(VC-*co*-PEGMA)/PVC blend was used as coating material to prepare antifouling braid-reinforced hollow fiber membrane. To the best of our knowledge, the preparation of braid-reinforced PVC hollow fiber membranes with antifouling surface to effectively prevent actual foulants deposition, has not been studied yet. KOH treatment was performed to the PET braids and the effect of KOH treatment on braid properties was studied. The effect of the altered braids properties on the membrane properties and the interfacial bonding strength between the coating layer and substrate were investigated. The mechanical strength and bursting strength of the braid-reinforced membranes were compared with those of a self-supporting membrane. The effects of the copolymer/PVC blend ratio on the structure, hydrophilicity, tensile strength, and especially the fouling propensity of bovine serum albumin (BSA) and activated sludge solution were evaluated. The braid-reinforced poly(VC-*co*-PEGMA)/PVC blend membranes exhibited advanced properties, such as having the largest tensile strength among the reported PVC hollow fiber membranes, higher interfacial bonding strength between the coating layer and the surface of PET-braid compared to other reported coating materials, and promising antifouling surface that can prevent molecular irreversible adsorption during filtration of activated sludge solution. Such superior properties strongly suggested the good application potential of these membranes for wastewater treatment.

IV.2 EXPERIMENTAL

IV.2.1 Materials

PVC (M_w = 55,000) and poly(VC-*co*-PEGMA) (with 6.1 mol% PEGMA and M_w = 360,000) were supplied by Sekisui Chemical Co., Ltd. (Japan). The chemical structure of this random copolymer is shown in Fig. IV. 1. BSA, sodium dihydrogen phosphate, disodium hydrogen phosphate, and dimethylacetamide (DMAc) were purchased from Wako Pure Chemical Industries (Japan). The BSA solution was prepared by dissolving BSA in 0.1 M phosphate buffer solution (PBS). The monodispersed polystyrene latex particles (diameter = 20, 50, and 400 nm, size distribution < 3%) used for the rejection measurement were purchased from Duke Scientific Corporation (Thermo Fisher Scientific, Waltham, MA). Deionized water was produced by a Millipore Milli-Q unit. All the reagents were used as received. The activated sludge solution was obtained from Sekisui Chemical Co., Ltd., and the detailed compositions are listed in Table 1.

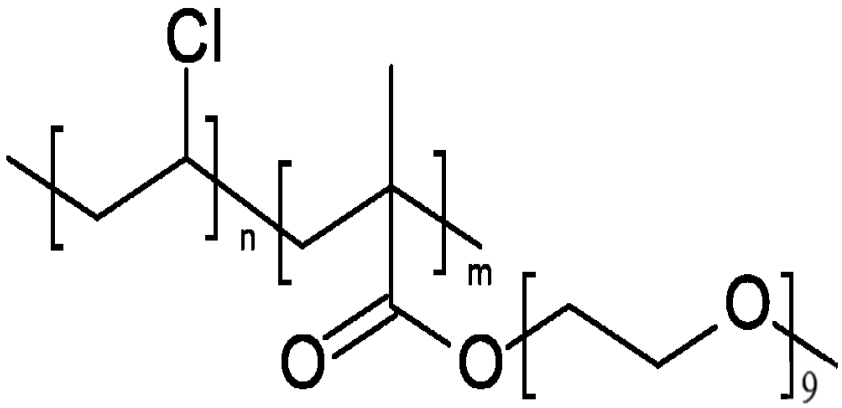

Fig. IV. 1. Chemical structure of poly(VC-*co*-PEGMA).

Table 1. Water analysis of the activated sludge solution.

Sample	TOC [mg/L]	DOC [ppb]	Biopolymer ppb]	Humics [ppb]	Building blocks [ppb]	Neutrals [ppb]
Activated sludge	88	9887	7138	1738	288	723

*TOC: total organic carbon, DOC: dissolved organic carbon. The data were measured using a TOC analyzer (TOC-VCSN, Shimadzu Co., Japan) and size-exclusion liquid chromatography system equipped with an organic carbon detector (LC-OCD, DOC-LABOR, Germany)

IV.2.2 Fabrication of braid-reinforced hollow fiber membrane

The braid-reinforced pure PVC membrane and 3 blended membranes with various blend ratios of copolymer/PVC were prepared using NIPS method. The compositions of the dope solutions used for the membrane casting are listed in Table 1, where the blend membranes are labeled as braid-reinforced blends 1:7, 1:3, and 1:1, corresponding to their copolymer/PVC blend ratios, respectively. For the prepared membranes, the dope compositions were adjusted to obtain similar PWPs for a better comparison of the fouling properties. The polymers were dissolved in DMAc by stirring at 45 °C for 1 day to obtain homogeneous solutions and were degassed overnight at 25 °C. As shown in Fig. 2, the solution was loaded in a vessel tank. After removing air bubbles under vacuum at room temperature for 2 h, the dope solution was pressed out from the nozzle using a gear pump and coated on a tubular braid that was flowed through the nozzle and wound up by a take-up roller. The outer and inner diameters of the PET tubular braid were 2 and 1 mm, respectively. The PET braid was provided by Sekisui Corp. The dope extrusion rate, air gap, and take-up speed were set at 5 g/min, 5 mm, and 5 m/min, respectively. When the coated braid went through a coagulation bath of deionized water at 24 ± 1 °C, the NIPS process occurred, and the porous braid-reinforced hollow fiber membrane was formed.

The prepared membranes were rinsed thoroughly with deionized water to remove residual solvent and were subsequently stored in deionized water until use.

The self-supporting hollow fiber membranes were prepared via NIPS using a batch-type extruder. The fabrication equipment and process were introduced in our previous work [25]. For the self-supporting hollow fiber membrane, the composition of the dope solution is also listed in Table 2, and this membrane was called self-supporting blend 1:1. The preparation process was the same as that for the braid-reinforced hollow fiber membrane except for the use of the tubular braid. The dope flow rate, bore flow rate, air gap, and take-up speed were set at 4 g/min, 4 g/min, 15 mm, and 4 m/min, respectively. After extracting the remaining solvent by immersing the prepared membranes in water, they were stored in deionized water until use.

Table.IV.2. Dope solution compositions for preparing braid-reinforced and self-supporting hollow fiber membranes.

Membrane ID	Copolymer: PVC blend ratio	Copolymer wt%	PVC [wt%]	DMAc [wt%]	Total polymer conc. [wt%]	PWP [L/atm m^2 h]	Rejection -20 [%]	Rejection-50 [%]
Braid-reinforced PVC control			15	86	14	290±10	76±0.4	100
Braid-reinforced blend 1:7	1:7	2.1	14.9	83	17	290±15	76±0.1	100
Braid-reinforced blend 1:3	1:3	4.8	14.3	81	19	300±11	79±0.5	100
Braid-reinforced blend 1:1	1:1	11.5	11.5	77	23	310±10	76±0.2	100
Self-supporting blend 1:1	1:1	9.5	9.5	81	19	300±20	0	10

* Rejection-20 and Rejection-50 refer to the results of the rejection measurements using polystyrene particles with average diameters of 20 and 50 nm, respectively.

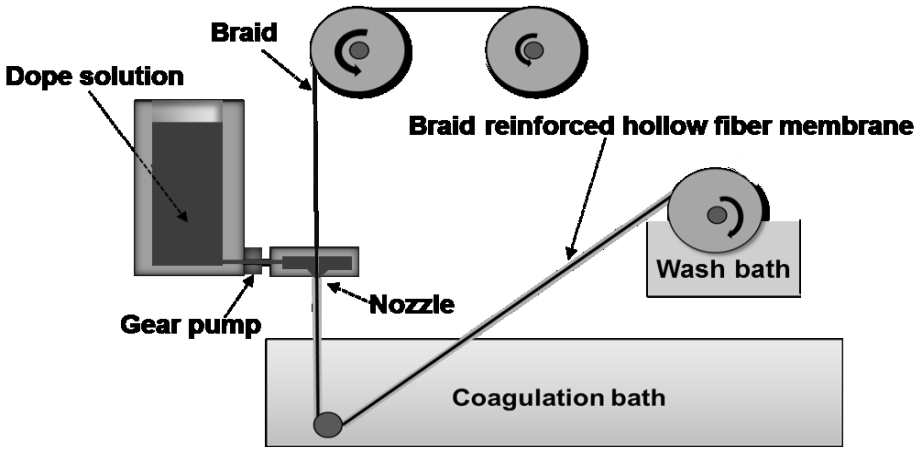

Fig. IV. 2. Schematic diagram for preparing braid-reinforced hollow fiber membranes.

Table IV.3. The dope solution compositions and the alkaline treatment conditions for the braids

Membrane ID	KOH treatments conditions for the braid		Compositions of the coating dope solution		
	KOH concentration [wt%]	Treatment time [h]	Poly(VC-*co*-PEGMA) [wt%]	PVC [wt%]	DMAC [wt%]
M0	0	0	10	5	85
M1	1	1	10	5	85
M2	1	6	10	5	85
M3	1	12	10	5	85
M4	3	1	10	5	85
M5	3	5	10	5	85
M6	3	12	10	5	85
M7	5	1	10	5	85
M8	5	6	10	5	85
M9	5	12	10	5	85

IV.2.3 PET braids characterization

IV.2.3.1 KOH treatment for the PET braids

The KOH and Milli-Q water were added in a beaker and then stirred by mechanical agitation to prepare 1000 mL KOH solution with different weight concentrations. The PET braid was soaked in the KOH solution at 90 ℃ over the treatment time ranging from 1 to 12 h. When the soaking time ended, the treated PET braid was thoroughly washed with Milli-Q to remove the residual alkaline. Then, the braid was vacuum dried at 60℃ for the further characterizations and the preparation of the braid-reinforced hollow fiber membranes. The braids KOH treatment conditions and the dope compositions for preparing the braid-reinforced membranes are listed in Table IV. 1. The membrane preparation procedure is the same as that mentioned in IV. 2. 2.

IV.2.3.2 Weight loss measurement

The weight loss measurement was carried out to evaluate the effect of KOH treatment on the physical properties of the PET braids [11-12]. The PET braids were cut by scissors to prepare the samples with 100 mm in length, and then the samples were weighed before immersed in 100 mL KOH solutions with different concentrations and treated time at 90℃. At the end of the predesigned time the samples were taken out and vacuum dried at 60℃. The treated samples were weighed again and the weight loss was calculated by following equation.

$$\text{Weight loss [\%]} = \frac{W_2 - W_1}{W_1} \times 100\ \% \qquad (1)$$

Where W_1 and W_2 are the weights of the samples before and after alkaline treatment, respectively.

IV.2.3.3 Water absorption of PET braids

To evaluate the effect of the KOH treatment on the chemical properties of the PET braids was evaluated by performing water adsorption measurement [12-13]. At first, the weight of all braids in dry condition was measured. Then, the wet weight was measured when the braids were soaked in the Milli-Q water. The relative water absorption rate was calculated according to the following equation.

$$\text{Relative water absorption ratio [\%]} = \frac{W2' - W1'}{W2 - W1} \times \frac{W1}{W1'} \times 100\% \qquad (2)$$

Where W_1 and W_1' are the dry weights of the original and treated braids, respectively; W_2 and W_2' are the wet weights of the original and treated braids, respectively.

IV.2.3.4 Pull-off test

Pull-out strength at the interface between the coating layer and the braid was tested to evaluate the interfacial bonding strength of the braid-reinforced hollow fiber membranes [***Fiber pull-out test and single fiber fragmentation test analysis and modelling***], [***An advanced equipment for single-fibre pull-out test designed to monitor the fracture process***]. The process of the single fiber pull-out test is described as follows. At first, a single pieces of braid-reinforced hollow fiber membrane was parallel put through a small PVC tube. The length and inner diameter of the tube were 50 and 14 mm, respectively. Then a rubber cap was used to block one end of the tube. The rubber cap had a small hole in center to make the hollow fiber membrane pass through and the hollow fiber was firmly fixed in the center of the tube. Then, the mixture of isocyanate resin and polyol (SANYU REC. CO. LTD, Japan) was slowly infected into the tube from the open end and subsequently blocked by another cap. After the resin solidified at room temperature over 1 day, the caps were removed from the ends and the sample for pull-off test was obtained (Fig. IV. 3). The fixed hollow fiber membrane was installed on the tensile testing apparatus (AG-X plus, Shimadzu Co., Japan).

The fiber was stretched along the fiber axis at a constant rate of 2 mm/min. The pull out force was recorded until the embedded hollow fiber membrane detached from the resin. The pull-out strength was calculated as following equation.

$$\text{Pull-out strength [N/mm}^2\text{]} = \text{Pull-out force/Interfacial area} = \frac{F}{\pi \times d \times L} \quad (3)$$

Where F (N) is the loaded pull-out force, L (mm) is the embedded length and d (mm) is the diameter of the braid-reinforced membranes.

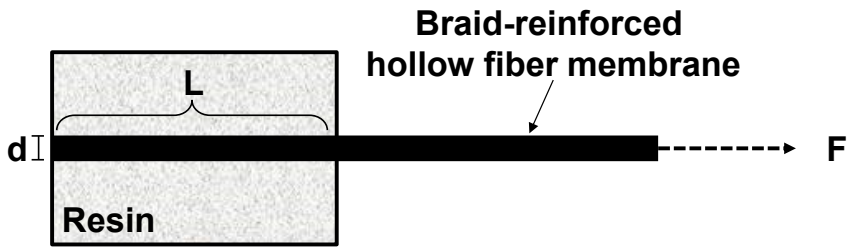

Fig. IV. 3 Single braid-reinforced hollow fiber membrane and resin composites

IV.2.4 BSA adsorption on polymer films surface

The amount of BSA adsorbed on the polymer film surface was measured using a quartz crystal microbalance with dissipation monitoring (QCM-D, Q-Sense E1, MEIWAFOSIS Co. Ltd., Japan). Piezoelectric quartz crystal sensors with a fundamental resonant frequency of approximately 5 MHz and diameter of 14 mm (QSX 301, Q-Sense Co., Sweden) were used. Before each measurement, the sensor was cleaned using an ultraviolet/ozone cleaner (Pro Cleaner 110; BioForce Nanosciences Co., USA). After spin coating with a 1.0 wt% polymer solution at 3000 rpm for 1 min and drying on a hot stage (KATHERM C-MAG HP4' Kampmann GmbH, Germany) at 80 °C for 20 min, the sensor was placed in the QCM flow chamber. Then, the PBS solution was injected into the flow chamber at a flow rate of 50 μL/min

for more than 1 h to stabilize the sensor and obtain the baseline. Next, the PBS solution was replaced with a 1000 ppm BSA solution. Using the Sauerbrey equation (Eq. 4), the total amount of BSA adsorbed on the polymeric film surface was calculated by varying the sensor oscillation frequency during parallel flow of the BSA solution at a constant temperature of 25 °C:

$$\Delta m = -C\frac{\Delta f}{n}, \qquad (4)$$

where Δm is the adsorption amount (ng·cm^{-2}), C is the mass sensitivity constant (17.7 ng·cm^{-2}·Hz^{-1} at f = 4.95 MHz), Δf is the variation of frequency (Hz), and n is the overtone number (n = 7).

IV.2.5 Membrane characterization

IV.2.5.1. Membrane morphology observation

A field-emission scanning electronic microscope (FE-SEM; JSF-7500F, JEOL Co. Ltd., Japan) was used to examine the surface morphology of the membranes. The prepared membranes were freeze-dried using a freeze dryer (FD-1000, EYELA, Japan). After the samples were immersed into liquid nitrogen and removed using a razor blade, a 5-nm-thick osmium tetroxide (OsO_4) layer was sputtered on the samples using an osmium coater (Neoc-STB; MEIWAFOSIS Co. Ltd., Japan). All the samples were examined at an accelerating voltage of 8 kV at different magnifications.

IV.2.5.2 Tensile strength measurements

The tensile stresses of the prepared membranes were measured using a tensile testing apparatus (AG-X plus, Shimadzu Co., Japan). The membrane samples with lengths of 20 mm were placed vertically between a pair of pneumatic clamps, and a stretching rate of 20 mm/min

was applied to the upper clamp. Finally, the maximum tensile stress of the sample was recorded until fracture. For each type of membrane, at least 7 measurements were averaged for reliability.

IV.2.5.3 X-ray photoelectron spectroscopy analysis

X-ray photoelectron spectroscopy (XPS, PHI X-tool, ULVAC-PHI, Japan) was used to evaluate the surface chemical composition of the polymeric membranes. The system was equipped with an Al Kα radiation source, the photoelectron take-off angle was set at 45°, and survey spectra were recorded over the range of 0 to 700 eV. The surface elemental composition was calculated from the peak area with a correction for atomic sensitivity.

IV.2.5.4 Water permeability measurements

The PWP was evaluated using a homemade module containing a single hollow fiber membrane. The membrane set inside the module had a length of 240 mm. The Milli-Q water was forced to permeate from the outside to the inside of the hollow fiber membrane. The operating pressure during filtration was adjusted using a needle valve at the outlet. The average pressure at the inlet and outlet of the membrane module was taken as the operating pressure. The feed water flow rate at the entrance of the membrane module was maintained at 1 $L \cdot h^{-1}$. Before the measurement, the membrane was compacted at 0.05 MPa until the water flux was stable. Then, the membrane permeability was measured at 0.02 MPa.

IV.2.5.5 Polystyrene particle rejection measurement

The polystyrene particle rejection experiment was conducted using a 100 ppm solution of latex particles. The feed solution was prepared by adding monodisperse latex particles with diameters of 20 and 50 nm to an aqueous nonionic surfactant of 0.1 wt% (Triton X-100). The

feed solution was then forced to permeate through the membrane under a pressure of 0.05 MPa. The filtrate was collected after 15 min of feed circulation. The concentrations of the feed and filtrate were measured using UV-vis spectrophotometry (U-2000, Hitachi Co., Tokyo, Japan) at a wavelength of 385 nm. The membrane rejection (R, %) was calculated using the following equation:

$$R(\%) = (1 - \frac{C_p}{C_f}) \times 100 \quad (2)$$

where C_p and C_f are the particle concentration of the permeate and feed solution, respectively.

IV.2.5.6 Interfacial bonding strength evaluation

The interfacial bonding strength between the coating layer and tubular braid was evaluated by measuring the bursting strength of the prepared membrane [14]. The test was performed using the same module described in Section 2.4.4. The bursting pressure was applied using pressurized Milli-Q water flowing through the inner surface of the prepared membrane to the outer surface. The PWP and rejection of 400-nm-diameter polystyrene particles were recorded for the prepared membrane for bursting pressures of 0.01 to 2.1 MPa. The tests were repeated at least 3 times.

IV.2.5.7 Air bubble contact angle measurements

Contact angle measurements have been widely used to characterize the hydrophilicity of polymeric surfaces. The air bubble contact angle was measured by a contact angle goniometer (Drop Master 300, Kyowa Interface Science Co., Japan). A sample was randomly cut from the prepared membrane with a suitable size and then placed in a glass cell filled with deionized water. Using a special L-shaped syringe needle, an air bubble (5 μL) was released below the sample. The air bubble contact angle with the surface was measured automatically. To

minimize experimental error, a minimum of 7 measurements were performed at different spots on the sample surface.

IV.2.5.8 Membrane fouling experiments

The membrane fouling experiments were performed using the same apparatus as that used for the PWP evaluation. First, the membrane was compacted with Milli-Q water at a pressure of 0.05 MPa and a flow rate of 1 L/h for at least 15 min until the water flux was stabilized. Then, the initial water flux was set to 90 and 30 L/(m^2·h) for the BSA and activated sludge filtration experiments, respectively, by adjusting the filtration pressure. As described below, the prepared membranes had similar PWPs, and thus, all their adjusted transmembrane pressures were approximately 0.01 MPa. Subsequently, the fouling experiments were performed using a 1000 ppm BSA solution (pH 7.0) or the activated sludge solution. The retentate was recycled into the feed tank while the permeate was collected and weighed. The collected permeate was returned to the feed tank every 10 min to maintain a constant concentration of the feed solution. After the filtration of the BSA solution or activated sludge for 2 or 1 h, respectively, backflushing was performed for 2 min at 0.01 MPa. This cycle of filtration for the activated sludge was performed continuously 4 times. All the fouling experiments were repeated at least 3 times for reproducibility.

IV.3 RESULTS AND DISCUSSION

IV.3.1 PET modification

IV.3.1.1 Weight loss measurement

The weight loss of the PET braids after the KOH treatment with different conditions are shown in Fig. IV. 24. The weight loss amount of all the treated PET braids increased linearly

with the treatment time ranging from 1 to 12 h. The weight loss amount increased more rapidly for the alkaline treatments using the KOH solution with higher concentrations. The increased weight loss results from the hydrolysis of the PET chains in the alkaline treatment [15], and such hydrolysis is promoted by the higher alkaline concentration and the longer reaction time [12]. However, the large weight lost will decrease the braids tensile strength [16] and affect the membranes mechanical strength, considering that the mechanical strength of the braid-reinforced membrane is mainly affected by braids mechanical properties [17].

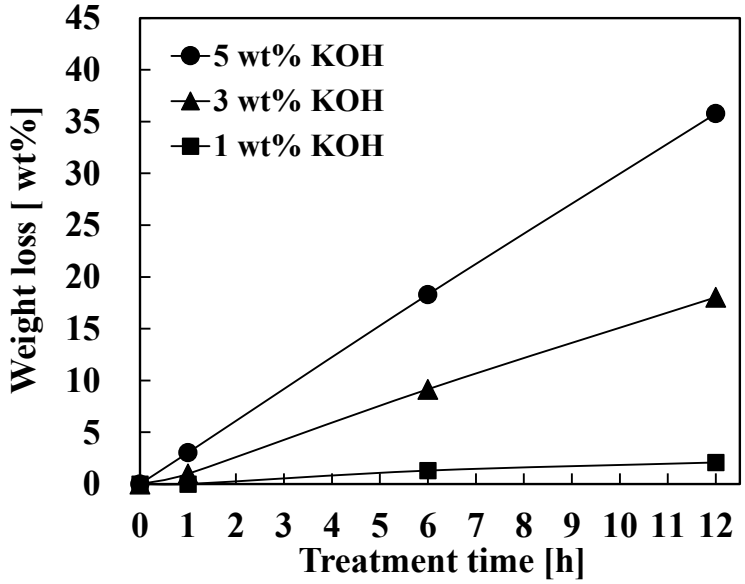

Fig. IV. 4 Effect of different KOH treatment condition on weight loss for the PET braids.

IV.3.1.2 Water absorption of PET braids

The water adsorption of the PET braids was measured to evaluate the PET surface hydrophilicity [11, 12, and 16]. Generally, the larger water adsorption indicates the higher surface hydrophilicity. Fig. IV. 5 shows the relative water adsorption ratio between the KOH treated and original PET braids. As exhibited in the Fig. IV. 5, the relative water adsorption

ratio increased with the increase of the treatment time and the concentration of the KOH solution, indicating that the increasing hydrophilicity/wettability of the PET braids. When 1 wt% of KOH solution was used in the treatment, the water adsorption increased linearly with the increase of the treatment time. For the braids treated by the KOH solutions with higher concentrations (3 and 5 wt%), the water adsorption increased sharply over 1h treatment and

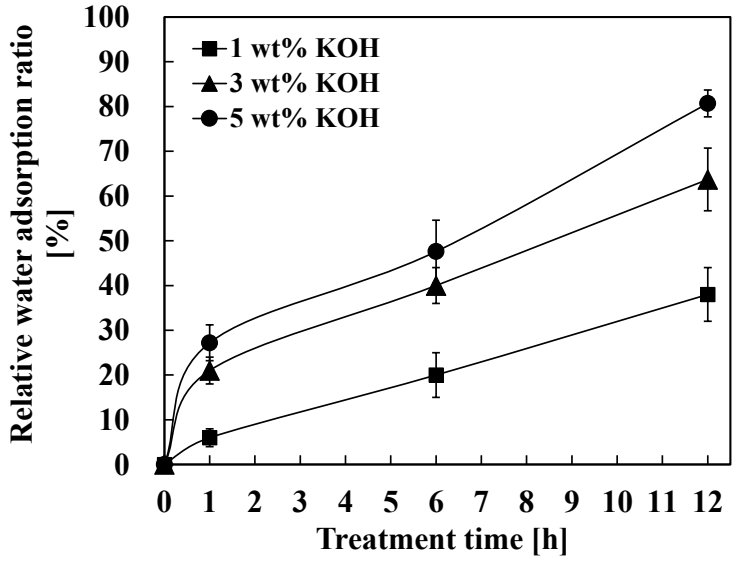

Fig. IV. 5 Effect of KOH treatment conditions on water adsorption of the PET

then increased steadily with longer treatment time. The improved water adsorption of the PET braids can be attributed to the PET hydrolysis in the alkaline treatment, where esters group in the PET are hydrolyzed to COOH and OH groups. In the KOH treatment, the higher alkaline concentration and longer treatment time accelerate the hydrolysis, leading to more COOH and OH groups on the PET surface, increasing the hydrophilicity of the PET braids. Furthermore, it is worth to note that the water adsorption of the braid can also be affected by the changed physical properties (porosity) after the KOH treatment, because the porous material with larger pore size or porosity might have higher water adsorption [18, 19]. However, the increase of the

water adsorption (in Fig. IV. 5) is greater than that of the weight loss (in Fig. IV. 4) after the same KOH treatment. For example, the weight loss for using 1 and 3 wt% KOH solution hardly changed over 1h treatment (in Fig. IV. 4), whereas the water adsorption of them increased 5 and 20% (in Fig. IV. 5). When increase the KOH concentration from 1 to 3 wt%, the water adsorption of the PET braids increased from 5 to 20 % after 1h alkaline treatment, while the weight loss of them are similar (almost zero). This indicate that the larger water adsorption was attributed to the more hydrophilic surface that resulted from the accelerated hydrolysis by the higher alkaline concentration. Therefore, it can be concluded that the increased water adsorption of the PET braids mainly resulted by the improved surface hydrophilicity.

IV.3.1.3 Effect of the KOH treated braid on the membrane permeability

Fig. IV. 6 shows the pure water permeability (PWP) of the braid-reinforced membranes prepared using different treated braids. The PWPs of the braid-reinforced membranes showed the overall decline tendencies over the treatment time after the braid treated by the different KOH solutions. For the braid treated by 1 wt% of KOH solution, the PWP of the braid-reinforced membrane remained stable when the treatment time was lower than 6 h, while that decreased 36 % when the treatment was performed over 12h. For alkaline treatment using 3 wt% of KOH solution, the membrane PWP started to decline when the treatment time was higher than 1h. For the treatment using 5 wt% of KOH solution, the PWP sharply declined even when the alkaline treatment was only carried out for 1h. Because all the test membranes shown in the Fig. IV. 6 are prepared from the same coating material and preparation conditions (in Table IV. 3), the different PWP of these membranes can only be resulted from the braids properties. As descripted in Fig. IV. 4, the membranes showed the changed weight loss after the alkaline treatment with different conditions, indicating the altered physical properties and

porosities. Comparing the PWP results (in Fig. IV. 6) with the weight loss of the braids (in Fig. IV. 4), it can be found that the membrane PWP decline occurred when the weight loss of the braids was larger than 2 %. It has been reported that the braid with enlarged pore size or porosity can reduce the membranes permeability, because the polymer solution might infiltrate into the bore of the braid and enclose or firmly fix in the braids [17]. Hence, it can be concluded

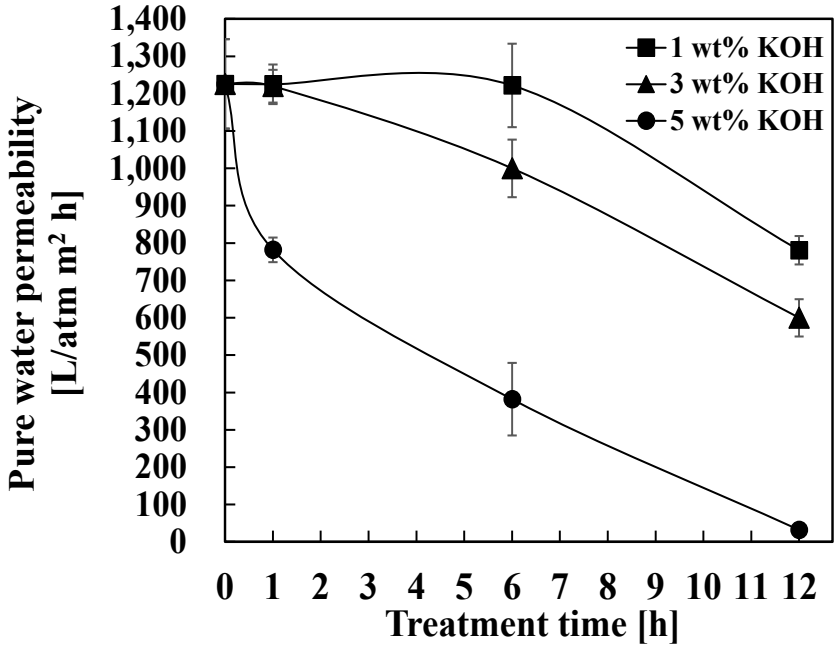

Fig. IV. 6 Effect of different KOH treatment conditions on the PWP for the braid-reinforced hollow fiber membranes.

that the declined membrane PWP are attributed to the altered braid structure (physical properties). Although performing KOH treatment increased the hydrophilicity of the braids, the effect of the alkaline hydrolysis on the physical properties of the braid should be controlled to some extent for preventing membrane permeability decline. Therefore, in this work the weight loss of the KOH treated braids should be limited 2 % by controlling the treatment conditions to avoid the effect on membrane PWP.

IV.3.1.4. Pull-out strength evaluation

Considering the membrane PWPs (in Fig. IV. 5) and the braids hydrophilicity (in Fig. IV. 4), M0, M2 and M4 membranes (in Table IV. 1) were used to evaluate the effect of KOH treatment on the bonding strength at the interface of the coating layer and braids by pull-out test. Fig. IV. 7 shows that the M2 and M4 membranes had the similar pull-out strength of around 1.1 N/mm^2, while the M0 exhibited only 0.6 N/mm^2. The pull-out strength of membranes prepared from KOH treated braids is almost 2 times larger than that of the original membranes, indicating that the interfacial bonding strength between the coating layer and KOH treated PET braid was stronger than that of the membrane used original PET braid. After the KOH treatment, numbers of the OH or COOH group are formed on the PET surface. These new formed polar groups endow the PET braids with higher surface energy to form polar attraction to another polar surface [20, 21]. The copolymer poly(VC-*co*-PEGMA) has high polarity. Hence, the KOH tread braids showed stronger bonding interaction with the poly(VC-*co*-PEGMA) incorporated coating layer.

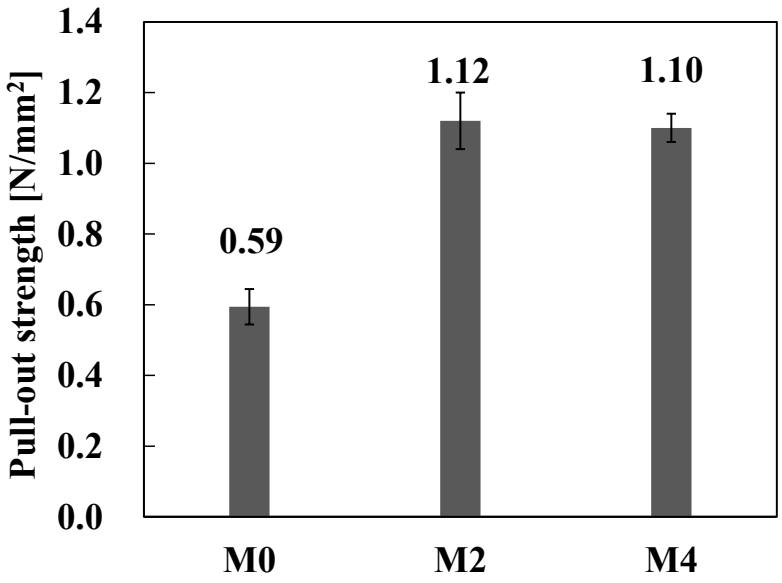

Fig. IV. 7 Pull-out strength of the M0, M2 and M4 membranes.

Because of the similar physical property of the braids for these three membranes, the increased pull-off strength of M2 and M4 membrane is attributed to the braid hydrophilic/polar surface (chemical properties). Thus, we concluded that increasing the hydrophilicity of the braids effectively improved the pull-out/bonding strength for the braid-reinforced membranes prepared using hydrophobic coating material.

IV.3.2 Membrane morphology

FE-SEM images were obtained to examine the membrane morphology. The surface and cross-sectional structures of the prepared membrane are shown in Fig. IV. 8 and Fig. IV. 9, respectively. Although the braid-reinforced membranes were prepared with different copolymer/PVC blend ratios, the outer surface structures are similar (Fig. IV. 8). Note that PEG or PEG-based copolymers exhibit strong pore forming ability, generally leading to enlarged pore size or increased surface porosity [22]. Increasing the copolymer content in the dope solution results in improved hydrophilicity of the dope solution. This improvement leads to a faster influx of water into the dope solution during membrane formation and a faster demixing process, resulting in a larger pore size at the selective-membrane layer surface [23]. However, increasing the total polymer concentration can effectively decrease the porosity of the membrane surface because of the effect of delayed demixing. Therefore, a similar surface structure of the braid-reinforced membranes is obtained because of the increased blend ratio and total polymer concentration (Table 2). The similar pore structure of the 4 types of membranes is critical to verify the effect of the membrane materials on the fouling property because the effect of the pore structure can be disregarded in this situation. Moreover, the pores on the inner and outer surface of the self-supporting blend 1:1 membrane were larger than those on the surface structure of the braid-reinforced blend 1:1 membranes, which is mainly

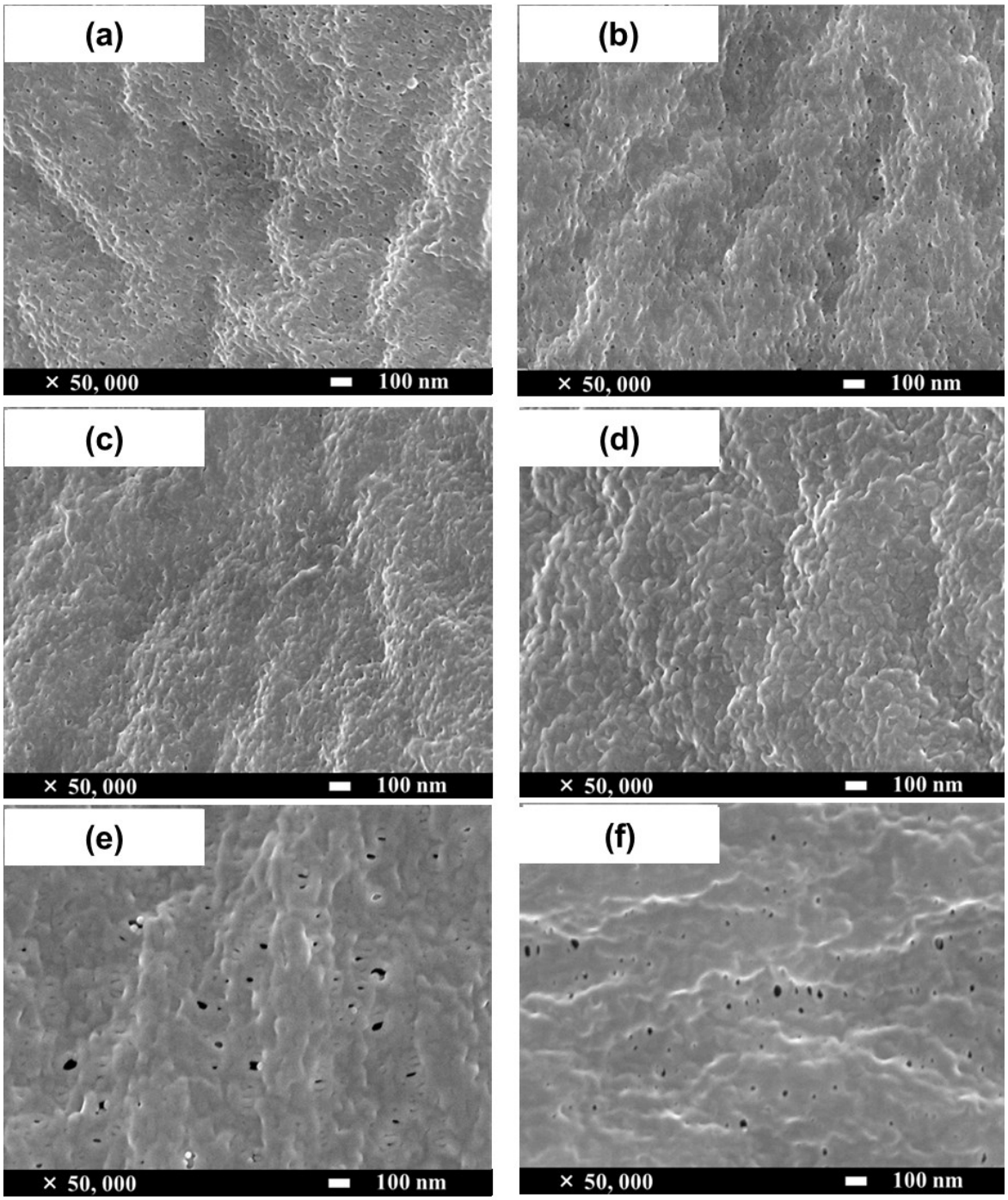

Fig. IV. 8. FE-SEM images of the membrane surfaces: (a) braid-reinforced PVC control, (b) braid-reinforced blend 1:7, (c) braid-reinforced blend 1:3, (d) braid-reinforced blend 1:1, (e) self-supporting blend 1:1 inner surface, (f) self-supporting blend 1:1 outer surface.

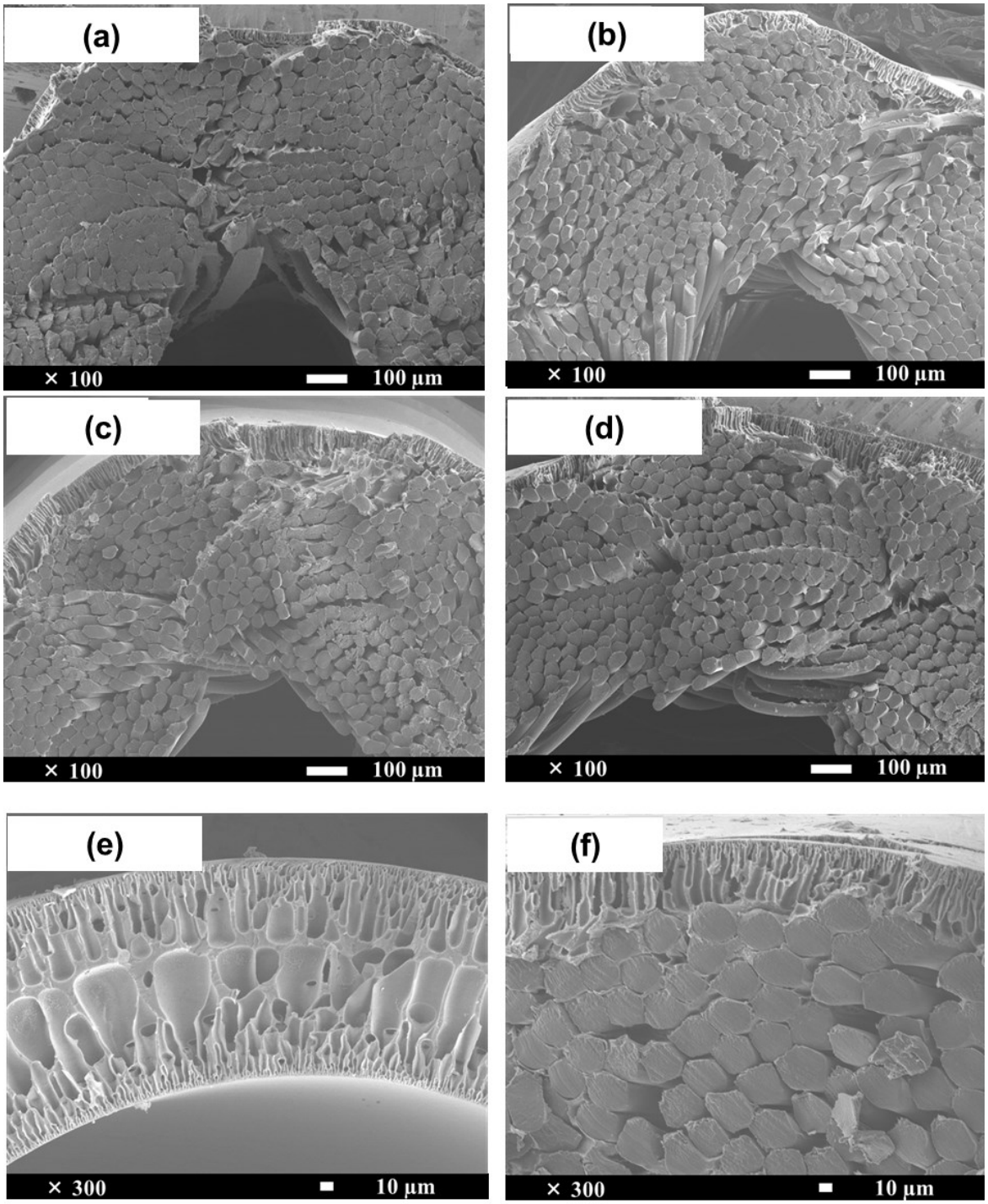

Fig. IV. 9. FE-SEM images of the membrane cross-sections: (a) braid-reinforced PVC control, (b) braid-reinforced blend 1:7, (c) braid-reinforced blend 1:3, (d) braid-reinforced blend 1:1, (e) self-supporting blend 1:1, (f) braid-reinforced blend 1:1 with same magnification as that for self-supporting blend 1:1 to compare the coating layer thickness.

attributed to the lower total polymer concentration in the dope solution (Table 2) and the different fabrication processes.

The cross-sectional structures of the prepared hollow fiber membrane are shown in Fig. IV. 9. For the braid-reinforced hollow fiber membranes, porous coating layers with narrow finger-like macrovoids formed on the top surface of the tubular braid, and a small amount of the coating solution penetrated into the substrate. The thickness of the coating layer and length of the macrovoids for the copolymer/PVC blend membranes were larger than those of the PVC control membrane, indicating the strong pore-forming ability of the hydrophilic poly(VC-*co*-PEGMA). In addition, 2 skin layers were observed in the cross-section of the self-supporting membrane, whereas only 1 skin layer was observed for the braid-reinforced membranes. The coating layer thickness of the braid-reinforced membranes was approximately 1/3 of the membrane thickness of the self-supporting membrane. In general, a thinner membrane thickness and reduced number of skin layers can reduce the membrane filtration resistance, resulting in improvement of the membrane permeability.

IV.3.3 Mechanical strength and interfacial bonding strength

To evaluate the mechanical strength, the tensile stress and elongation of the membranes and tubular braid were measured, and the data are plotted in Fig. IV. 10. The braid-reinforced membranes exhibited super-high tensile stress at break (higher than 170 MPa), which was much higher than that of the self-supporting membrane and previously reported PVC hollow

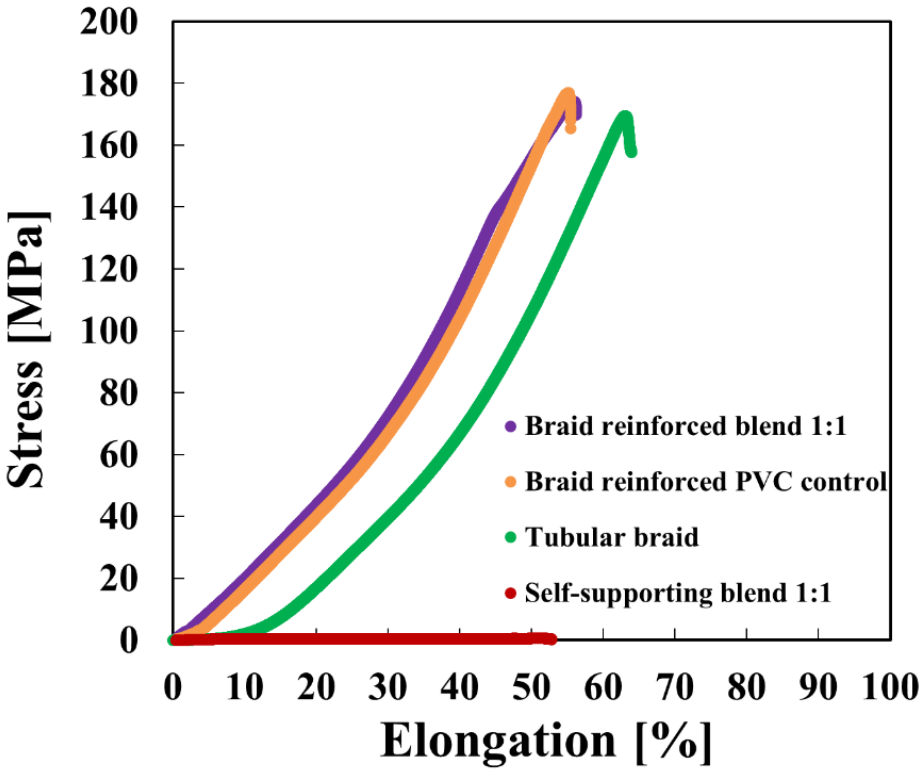

Fig. IV. 10. Mechanical strength of self-supporting and braid-reinforced hollow fiber membranes and tubular braid.

fiber membranes (Table 2). Note that the increase of the PEG-based copolymer content in the dope solution can decrease the membrane mechanical strength, because of the softness of PEG.

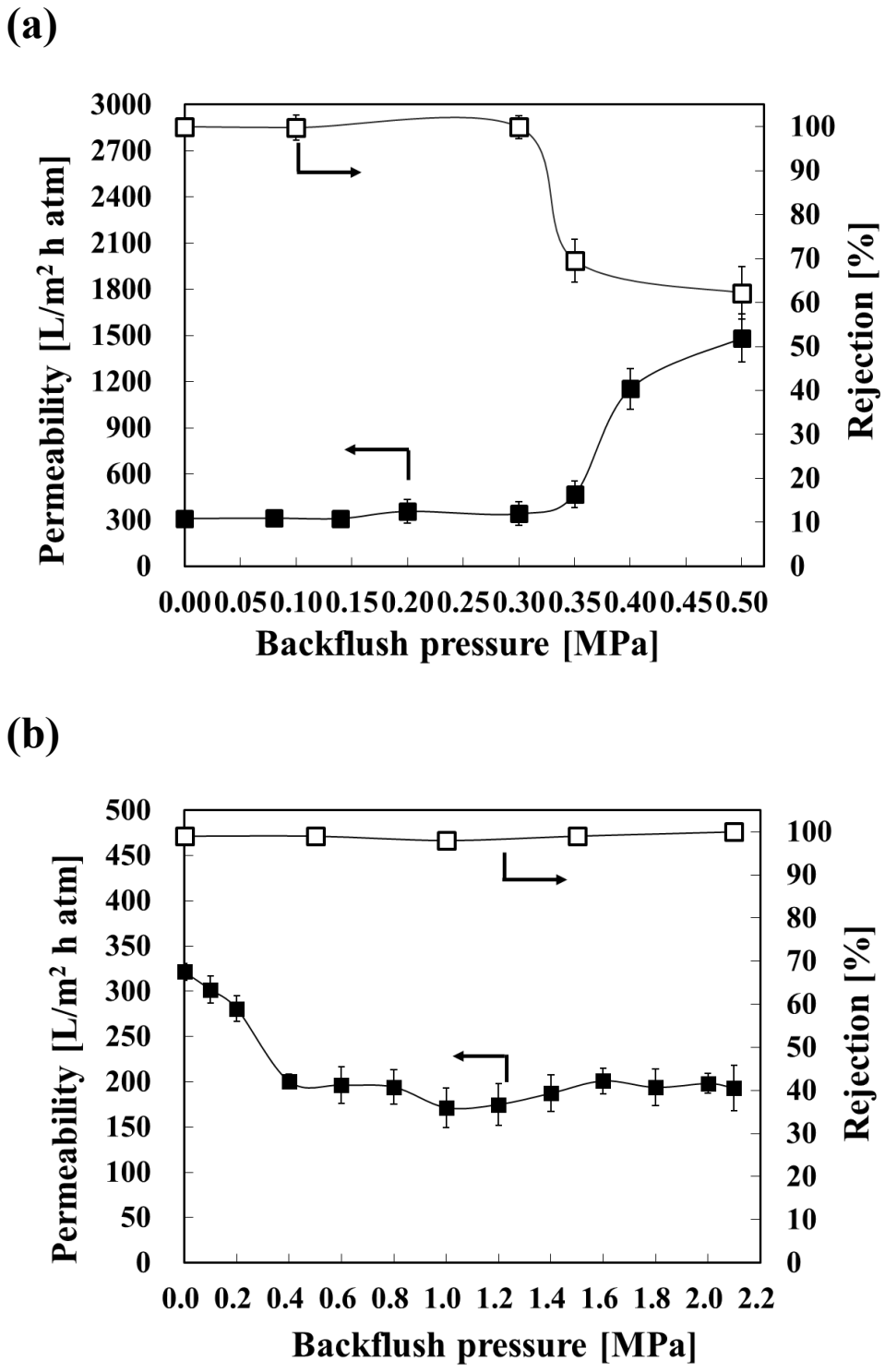

Fig. IV. 11. PWP and rejection for various backflush pressures for (a) self-supporting blend 1:1 and (b) braid-reinforced blend 1:1. The rejection measurements were performed using polystyrene particles with average diameters of 400 and 50 nm, respectively.

Table IV 4. Mechanical properties of previously reported PVC hollow fiber membranes and our braid-reinforced PVC hollow fiber membranes.

Dope solution material	Membrane type	Tensile strength at break [MPa]	Elongation at break [%]	Ref	Publication year
PDMAE-BC/PVC	self-supporting	2.3	62	[36]	2016
TEOS/PVC	self-supporting	1.5–3.8	56–80	[37]	2015
PVP/PVC	dual-layer reinforced	9.0–10.6	95–120	[20]	2015
PEG or PVP/PVC	dual-layer reinforced	12–21	32–49	[18]	2014
PEG/PVC	dual-layer reinforced	19–22	93–102	[38]	2013
Polystyrene/PVC	self-supporting	2.4–4.1	37–54	[39]	2012
PAN/PVC	self-supporting	2.8–5	-	[40]	2012
PAN/SiO_2/PVC	self-supporting	4–4.8	18–42	[41]	2011
PVC	self-supporting	2–4	58–84	[42]	2011
PEG or PEG/PVC	self-supporting	1.8–4.3	9–47	[43]	2002
Present work	braid-reinforced	170±0.5	50±0.8		

* PDMAE-BC, poly(methacryloxylethyl benzyl dimethyl ammonium chloride); TEOS, tetraethoxysilane

In Fig. IV. 10, the braid-reinforced blend membrane, PVC control membrane, and tubular braid exhibited similar maximum forces of approximately 170 MPa, indicating that the mechanical strength of the braid-reinforced membranes was determined by the properties of the selected braid rather than those of the coating layer. Furthermore, it can be observed that the elongations of the braid-reinforced membranes were lower than that of the braid itself because the formed coating layer on the braid limited the deformation of the braid, which can inhibit the straining of the braid membranes [17].

Although braid-reinforced membranes exhibit extremely high tensile strength at break, many researchers have noted that the interfacial bonding strength between the coating layer and braid is more crucial for reinforced hollow fiber membranes, which could restrict the application and operating life of the membranes [24]. The interfacial bonding strength of reinforced hollow fiber membranes was investigated by testing the membrane bursting pressure [7]. The changes of the PWP and rejection with the backflush pressure for the self-supporting and braid-reinforced blend membranes are plotted in Fig. IV. 11 (a) and (b), respectively. The rejection tests for the self-supporting and braid-reinforced membranes were performed using polystyrene particles with average diameters of 400 and 50 nm, respectively. Fig. IV. 11 demonstrates that even though the coating material of the 2 types of membranes was the same, the PWP increased and the rejection decreased sharply for the self-supporting membrane when the backflush pressure was over 0.3 MPa, whereas those of the braid-reinforced membrane remained stable even for a backflush pressure of 2.0 MPa. The bonding strength of the braid-reinforced membranes was at least 3 times larger than that of the PAN-braid-reinforced CA membrane [8], indicating the better interfacial bonding strength between the poly(VC-*co*-PEGMA)/PVC coating layer and the PET-braid. Thus, considering the super-high mechanical

properties, braid-reinforced membranes are expected to be useful for long-term application for the frequent backwashing process in wastewater treatment [24, 25].

IV.3.4 XPS measurements

The surface chemical compositions of the prepared membranes were examined using XPS, and the results are presented in Fig. IV. 12. The prepared membranes exhibited 4 major emission peaks at 201, 270, 284, and 530 eV, which were attributed to Cl 2p, Cl 2s, C 1s, and O 1s emissions, respectively. The O 1s peak at the membrane surface is considered representative of the poly(VC-*co*-PEGMA) component because of the non-oxygen atom in PVC.

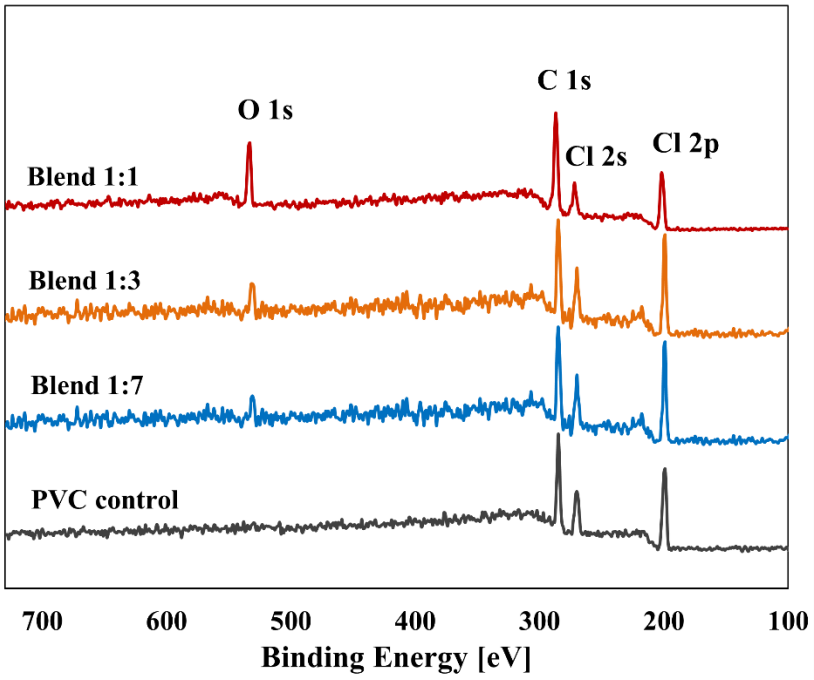

Fig. IV. 12. XPS spectra for the prepared braid-reinforced membranes with different copolymer/PVC blend ratios.

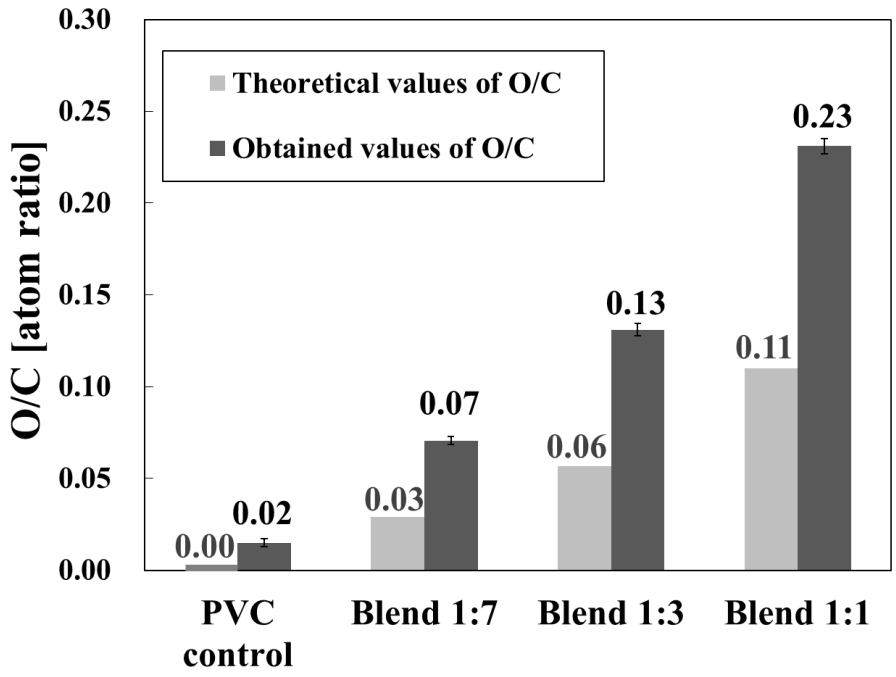

Fig. IV. 13. Surface O/C atom ratios of the prepared braid-reinforced membranes with different copolymer/PVC blend ratios.

The surface chemical compositions of the prepared membranes were evaluated by considering the O/C ratios. The O/C ratios from XPS measurements and the theoretical calculations are presented in Fig. IV. 13. The calculation method for the theoretical values of the O/C ratio is same as that described in Chapter III. The experimental results indicated that the O/C ratios increased as the copolymer/PVC blending ratio increased. In addition, the measured O/C ratios were 2 times larger than the theoretical values for all the prepared blend membranes. This finding indicates that the copolymer poly(VC-*co*-PEGMA) was localized at the membrane surface during the membrane fabrication process because of the strong interactions between the PEGMA chains and water in the coagulation bath. The small O/C ratio of 0.02 for the PVC control membrane can be attributed to surface oxidation by environmental oxygen, and this surface oxidation may occur in all the prepared membranes.

IV.3.5 PWP and polystyrene particle rejection

The PWPs for the prepared membranes are listed in Table 2. All the prepared membranes including the self-supporting membrane have similar PWPs of approximately 300 ± 10 L/(m^2 atm h). Note that the preparation of membranes with similar PWPs can be used to evaluate the effect of the membrane material properties alone (i.e., hydrophilicity in this study) on membrane fouling and avoids the effect of hydrodynamic conditions on fouling tendency (i.e., initial water flux and operating pressure) [26].

The rejection properties of the prepared membranes were investigated using polystyrene latex particles with diameters of 20 and 50 nm. As indicated in Table 2, all the braid-reinforced hollow fiber membranes had similar 76% rejections of the 20-nm particles and 100% rejections of the 50-nm particles, whereas the self-supporting blend 1:1 exhibited no rejection of the 20-nm particles and only 10% rejection of the 50-nm particles. The rejection results agree well with the surface structures (Fig. IV. 8), where the pore size of the self-supporting membrane was much larger than those of the braid-reinforced membranes. Note that although the PWPs and materials of the braid-reinforced and self-supporting membranes were almost the same, a much higher rejection property and smaller surface pore size were obtained for the braid-reinforced membrane, which can lead to reduced fouling propensity during the filtration process.

IV.3.6 Hydrophilicity of the membranes

Air bubble contact angle measurements were performed to evaluate the surface hydrophilicity of the braid-reinforced membranes, and the results are presented in Fig. IV. 14. The air bubble contact angles of the prepared membranes increased with increasing

copolymer/PVC blend ratio, indicating an increase of the surface hydrophilicity. Compared with the air bubble contact angle for the PVC control membrane, those of the blend membranes increased to 138° and 142° for copolymer/PVC blend ratios of 1:7 and 1:3, respectively; in addition, the air bubble contact angle increased slightly upon further increasing the blend ratio over 1:3. The increase in contact angle is consistent with the increased copolymer concentration at the membrane surfaces, as observed by XPS and illustrated in Fig. IV. 8. Where enrichment of the copolymer on the surface of braid-reinforced blend 1:1 membrane was observed, I expected the surface hydrophilicity and air bubble contact angle to be larger than that of the blend 1:3 membrane. However, the blend 1:3 and blend 1:1 membranes exhibited similar contact angles, suggesting that the hydrophilicity of the blend membrane was unchanged as the blend ratio increased over 1:3. Considering that some factors (such as surface roughness and membrane pore distribution) could affect the contact angle results, I hypothesized that the small contact angle difference of the blend 1:3 and blend 1:1 membranes could be attributed to the multiple effects of the hydrophilicity and surface morphologies.

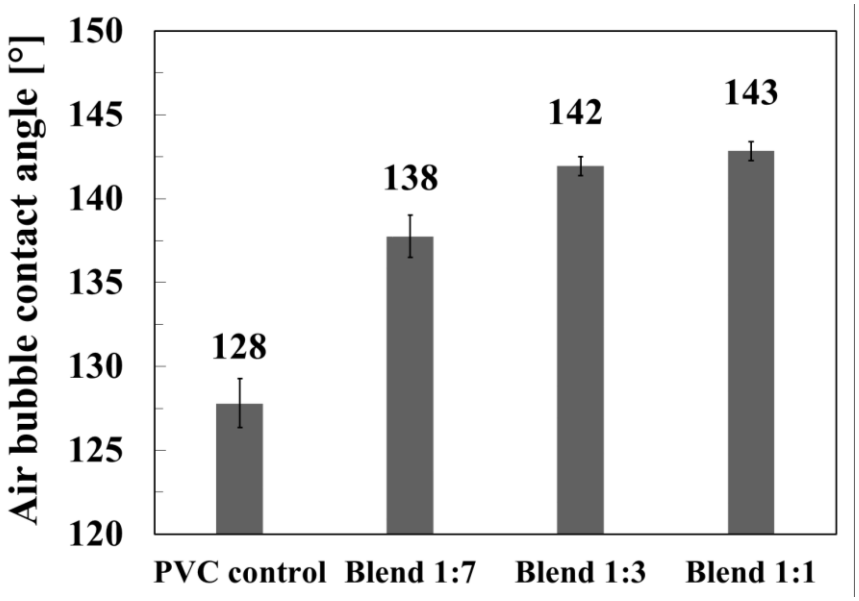

Fig. IV. 14. Air bubble contact angles for the braid-reinforced membranes.

IV.3.7 Fouling resistance to BSA and activated sludge solutions

IV.3.7.1 BSA adsorption on polymeric films

QCM-D analysis was performed to evaluate the interaction between the BSA molecule and surface of the polymer films. Fig. IV. 15 demonstrates that the BSA adsorption amount decreased as the copolymer content in the copolymer/PVC blends increased from 0 to 50 wt% and remained constant upon further increasing the copolymer content. These results indicate that blending poly(VC-*co*-PEGMA) into PVC film can significantly weaken the interaction with BSA molecules, enhancing the resistance to BSA adsorption. Therefore, good resistance to BSA fouling can be expected when using an appropriate blend ratio.

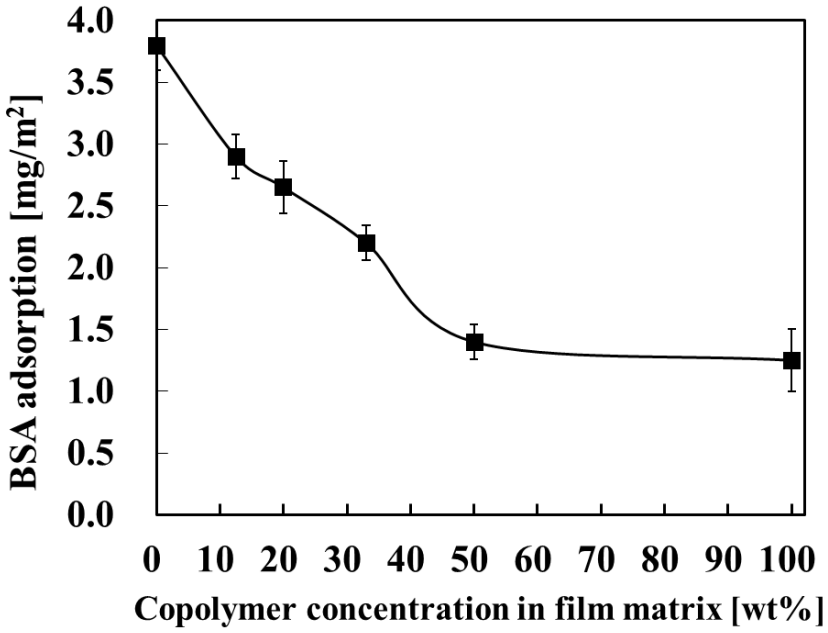

Fig. IV. 15. BSA adsorption on polymeric films for copolymer/PVC blends with various copolymer contents.

IV.3.7.2 BSA fouling property

Protein fouling experiments were performed on the membranes using a 1000 ppm BSA solution. The initial water flux through the membranes was set to 90 L/(m^2·h) by adjusting the transmembrane pressure. The transmembrane pressures for the prepared membranes in the filtration experiments were almost the same because of the similar membrane PWPs, as observed in Table 2. Therefore, the net effect of the membrane material on BSA fouling could be evaluated by removing the effects of the initial flux and transmembrane pressure. The water flux values of the prepared membranes as a function of filtration time are plotted in Fig. IV. 16. The permeation flux of the blend 1:7 and 1:3 membranes and the PVC control membrane decreased to approximately 30% because of the fouling. However, the flux of the blend 1:1 membrane remained at approximately 70% after120 min of BSA filtration. After backflushing, the water fluxes of the blend 1:7, 1:3, and 1:1 membranes notably recovered to 75%, 80%, and 90% of the initial fluxes, respectively, whereas that of the PVC control membrane only recovered to 50%. The blend 1:1 membrane exhibited the best antifouling performance during the filtration of the BSA solution. However, even though the total BSA fouling performances of the blend 1:7 and 1:3 membranes and PVC control membrane were similar, the blend membranes exhibited improved flux recovery abilities and decreased irreversible fouling, indicating their better antifouling properties. This result is consistent with the increased resistance of protein adsorption observed in the QCM-D characterization. Thus, I can conclude that the improved antifouling properties of the blend membranes resulted from their fouling-resistant surfaces.

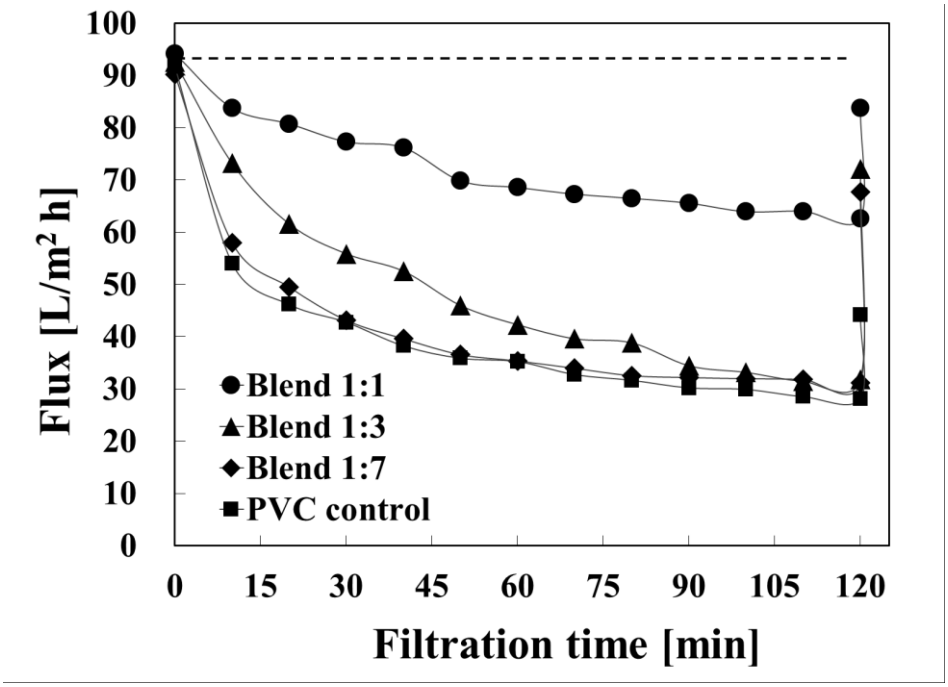

Fig. IV. 16. BSA fouling performance of the braid-reinforced hollow fiber membranes.

IV.3.7.3 Activated sludge fouling property

The performance of the membranes in filtrating activated sludge solution is shown in Fig. IV. 17. During the filtration experiment, the initial water flux was set to approximately 30 L/(m^2·h) by adjusting the transmembrane pressure. The backflush was performed every 30 min during the filtration process, which is close to the backflush conditions in a practical MBR [1]. As depicted in Fig. IV. 17, the blend membrane also exhibited considerable antifouling property compared with that of the PVC control membrane for the filtration of activated sludge solution; however, the fouling tendency of the activated sludge solution was much more severe than that of the 1000 ppm BSA solution (Fig. IV. 16). The permeation flux of the blend membrane decreased to nearly 45% of the initial flux after just over 30-min filtration of the activated sludge solution, whereas that of the PVC control membrane dramatically dropped to 25%. After the first backflush, the water flux of the blend membrane recovered to almost 77%

of the initial flux, whereas that of the PVC control membrane only recovered to approximately 35%. The blend membrane exhibited much lower fouling propensity and higher resistance to irreversible fouling. All 4 filtration circles exhibited similar flux decline tendencies and flux recoveries, suggesting the unchanged antifouling performance. Thus, the blend membrane could be expected to be used in practical MBR processes with stable antifouling properties, which will be examined in our future work.

The good antifouling performance of the copolymer/PVC braid-reinforced membrane can be attributed to the existence of a PEG layer at the outer surface of the membrane and pores. Because the hydrated PEG chains have a large excluded volume in an aqueous environment, the PEG layer tends to repel the foulant molecules approaching the membrane surface, serving as a steric barrier to foulant adsorption. However, as observed in Table 1, the major component in the activated sludge is a biopolymer substance (72%), which can lead to more severe membrane fouling [27, 28]. Nevertheless, the considerable antifouling performance of the

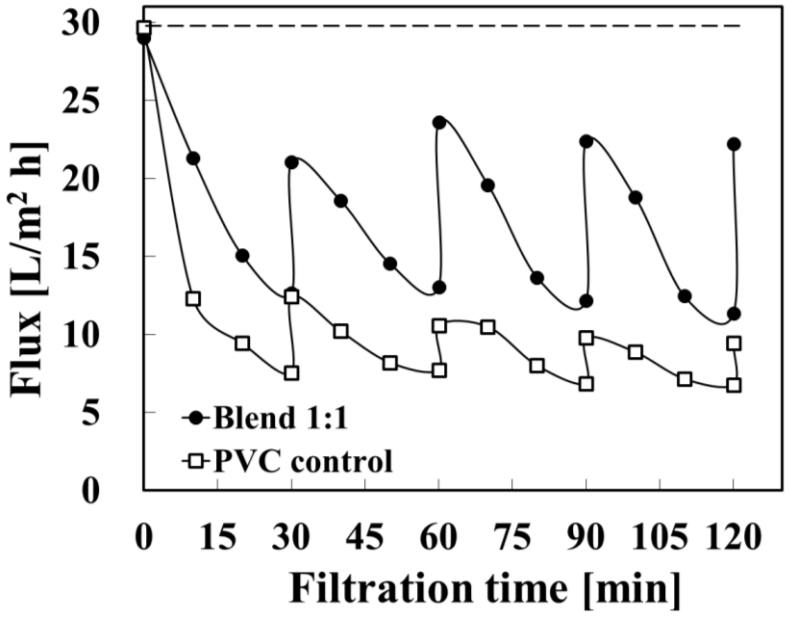

Fig. IV. 17. Activated sludge fouling performance of braid-reinforced 1:1 blend and PVC control hollow fiber membranes.

copolymer/PVC blend membranes was apparent even in the filtration of such activated sludge solution.

In summary, considering the super-high mechanical strength and good fouling resistance to activated sludge solution, braid-reinforced poly(VC-*co*-PEGMA/PVC hollow fiber membranes show great potential for application in wastewater treatment, including MBR treatment [1, 29].

IV.4 CONCLUSTIONS

Braid-reinforced poly(VC-*co*-PEGMA)/PVC hollow fiber membranes were successfully prepared via NIPS. The braid physical and chemical properties affect the membrane permeability and bonding strength between the coating and the braids. The membrane with stronger bonding strength was obtain after performing the KOH treatment to the PET braids and increased braids surface wettability/hydrophilicity. These membranes exhibited thinner polymer coating layer thicknesses and smaller surface pore sizes than those of a self-supporting hollow fiber membrane (same membrane material and PWP). The tensile strength and bursting strength of the braid-reinforced hollow fiber membranes were higher than 170 and 2.1 MPa, respectively, which were significantly larger than those of the self-supporting hollow fiber membrane and the various reported PVC hollow fiber membranes. Owing to the copolymer surface segregation, the copolymer incorporated membrane surface showed the improved hydrophilicity and antifouling properties. When the copolymer/PVC blending ratio reached 1:1, considerable improvement of the antifouling propensity and flux recovery after water backflush were observed for the filtration of BSA solution and activated sludge solution. In conclusion, the newly prepared braid-reinforced poly(VC-*co*-PEGMA)/PVC hollow fiber membranes exhibited great mechanical properties and surface antifouling resistance to activated sludge

solution, suggesting their potential for application in practical wastewater treatment. According to this work, the fabrication of braid-reinforced hollow fiber membrane can be suggested, when the soft amphiphilic copolymers is used to prepare robust hollow fiber membrane.

REFERENCE

[1] S. Judd, The MBR Book (Second Edition): Principles and Applications of Membrane Bioreactors for Water and Wastewater Treatment, in: Commercial Technologies, Butterworth-Heinemann Inc., Oxford, 2011, pp. 289-357.

[2] Y. Zhao, J. Lu, X. Liu, Y. Wang, J. Lin, N. Peng, J. Li, F. Zhao, Performance enhancement of polyvinyl chloride ultrafiltration membrane modified with graphene oxide, J. Colloid Interface Sci., 480 (2016) 1-8.

[3] A. Behboudi, Y. Jafarzadeh, R. Yegani, Preparation and characterization of TiO2 embedded PVC ultrafiltration membranes, Chem. Eng. Res. Des., 114 (2016) 96-107.

[4] H. Liu, C. Xiao, Q. Huang, X. Hu, W. Shu, Preparation and interface structure study on dual-layer polyvinyl chloride matrix reinforced hollow fiber membranes, J. Membr. Sci., 472 (2014) 210-221.

[5] H. Liu, C. Xiao, Q. Huang, X. Hu, Structure design and performance study on homogeneous-reinforced polyvinyl chloride hollow fiber membranes, Desalination, 331 (2013) 35-45.

[6] H. Liu, C. Xiao, Q. Huang, Z. Fan, X. Hu, W. Shu, Study on interface structure and performance of homogeneous-reinforced polyvinyl chloride hollow fiber membranes, Iranian Polymer Journal, 24 (2015) 491-503.

[7] Z.W. Fan, C.F. Xiao, H.L. Liu, Q.L. Huang, J. Zhao, Structure design and performance study on braid-reinforced cellulose acetate hollow fiber membranes, J. Membr. Sci., 486 (2015) 248-256.

[8] Q. Quan, C.F. Xiao, H.L. Liu, Q.L. Huang, W. Zhao, X.Y. Hu, G.L. Huan, Preparation and characterization of braided tube reinforced polyacrylonitrile hollow fiber membranes, J. Appl. Polym. Sci., 132 (2015), pp, 41795-41805.

[9] Z.W. Fan, C.F. Xiao, H.L. Liu, Q.L. Huang, Preparation and performance of homogeneous braid reinforced cellulose acetate hollow fiber membranes, Cellulose, 22 (2015) 695-707.

[10] Z. Fan, C. Xiao, H. Liu, Q. Huang, J. Zhao, Structure design and performance study on braid-reinforced cellulose acetate hollow fiber membranes, J. Membr. Sci., 486 (2015) 248-256.

[11] J.H. Lee, S.H. Park, K.W. Oh, C.H Lee, S.H. Kim, Effect of pretreatment conditions on the hydrolysis and water absorption behavior of poly(ethylene terephthalate) fibrous assembly, Polymer International, 61 (2012) 657-663.

[12] M.Y. Li, T.T. Deng, S.X. Liu, F.X. Zhang, G.X. Zhang, Superhydrophilic surface modification of fabric via coating with nano-TiO2 by UV and alkaline treatment, Appl. Surf. Sci. 297 (2014) 147–152

[13] F.S. Kim, C.H. Lee, S.H. Kim, Effects of pretreatment reagents on the hydrolysis and physical properties of PET fabrics, J. Appl. Polym. Sci., 112 (2009) 3071-3078.

[14] Z.W. Fan, C.F. Xiao, H.L. Liu, Q.L. Huang, J. Zhao, Structure design and performance study on braid-reinforced cellulose acetate hollow fiber membranes, J. Membr. Sci., 486 (2015) 248-256.

[15] G.P. Karayannidis, A.P. Chatziavgoustis, D.S. Achilias, Poly(ethylene terephthalate) recycling and recovery of pure terephthalic acid by alkaline hydrolysis, Adv. Polym. Tech., 21 (2002) 250-259.

[16] S. H. Zeronian, M.J. Collins, Surface modification of polyester by alkaline treatment, Textile Progress, 20 (1989) 1-26.

[17] M. Mahendran, K.P. Goodboy, L. Fabbricino, Hollow fiber membrane and braided tubular support therefor, U.S. Patent 6,354,444 (2002).

[18] H. Furukawa, F. Gandara, Y.B. Zhang, J. Jiang, W.L. Queen, M. R. Hudson, O.M. Yaghi, Water adsorption in porous metal–organic frameworks and related materials, J. Am. Chem. Soc., 2014, 136 (11), pp 4369–4381

[19] M. Thommes, J.Morell, K.A. Cychosz, M. Fröba, Combining nitrogen, argon, and water adsorption for advanced characterization of ordered mesoporous carbons (CMKs) and periodic mesoporous organosilicas (PMOs), Langmuir, 2013, 29 (48), pp 14893–14902.

[20] J. Kloubek, Interaction of polar forces and their contribution to the work of adhesion, J. Adhesion, 6 (1974) pp. 293-301.

[21] S. Takeda, M. Fukawa, Y. Hayashi, K. Matsumoto, Surface OH group governing adsorption properties of metal oxide films, Thin Solid Films, 339 (1999) 220-224.

[22] J. Xu, Z.L. Xu, Poly(vinyl chloride) (PVC) hollow fiber ultrafiltration membranes prepared from PVC/additives/solvent, J. Membr. Sci., 208 (2002) 203-212.

[23] H. Strathmann, K. Kock, The formation mechanism of phase inversion membranes, Desalination, 21 (1977) 241-255.

[24] N.S.A. Mutamima, Z.Z. Noora, , M.A.A Hassana, G. Olsson, Application of membrane bioreactor technology in treating high strength industrial wastewater: a performance review, Desalination, 305 (2012) 1-11.

[25] T. Zsirai, P. Buzatu, P. Aerts, S. Judd, Efficacy of relaxation, backflushing, chemical cleaning and clogging removal for an immersed hollow fibre membrane bioreactor, Water Research, 46 (2016) 4499-4507.

[26] H. Huang, , N. Lee, , T. Young, , A. Gary, J.C. Lozier, J.G. Jacangelo, Natural organic matter fouling of low-pressure, hollow-fiber membranes: Effects of NOM source and hydrodynamic conditions, Water Research, 41 (2007) 3823–3832.

[27] Z. Wang, J. Ma, C.Y. Tang, K. Kimura, Q. Wang, X. Han, Membrane cleaning in membrane bioreactors: A review, J. Membr. Sci., 468 (2014) 276-307.

[28] J.Y. Tian, M. Ernst, F. Cui, M. Jekel, Correlations of relevant membrane foulants with UF membrane fouling in different waters, Water Res., 47 (2013) 1218-1228.

[29] A. Drews, Membrane fouling in membrane bioreactors - Characterisation, contradictions, cause and cures, J. Membr. Sci., 363 (2010) 1-28.

Chapter V

Conclusion

Antifouling membranes were prepared using copolymer poly(VC-*co*-PEGMA) via nonsolvent induced phase separation (NIPS). The membrane properties of the flat sheet copolymer membranes were evaluated by testing the membrane characterizations, such as the surface chemical composition, water permeability, particle rejection, membrane morphology, air bubble contact angle, fouling resistance, etc. The relationship between the fouling propensities with the membrane material, morphology, filtration conditions was revealed. Moreover, the molecular dynamics (MD) simulation was also carried out to study the membrane surface properties to clarify the fouling mechanism.

To improve membrane mechanical properties, poly(VC-*co*-PEGMA)/PVC blend was used to prepare flat sheet membranes via NIPS. Effect of the poly(VC-*co*-PEGMA)/PVC blend ratio on membrane properties was evaluated. The copolymer distribution in the membrane matrix was determined by MD simulations.

In order to further increase the antifouling membranes mechanical properties and applications, novel braid-reinforced poly(VC-*co*-PEGMA)/PVC hollow fiber membranes were prepared. The membrane with stronger bonding strength was obtain after performing the KOH treatment to the PET braids and increased braids surface wettability/hydrophilicity. The mechanical strength of the membranes is significantly larger than that of the reported various types of PVC hollow fiber membranes. The effect of the poly(VC-*co*-PEGMA)/PVC blend ratio on the membrane surface properties was evaluated. The membrane performance in the filtration of activated sludge solution was studied.

The conclusions of this work are summarized as follows:

In Chapter II, poly(VC-*co*-PEGMA) copolymer membranes were successfully prepared via a NIPS method. The membrane characterization was carried out using XPS, air contact angle, QCM, and SEM observation. MD simulation was performed to evaluate the state of PEGMA segment at the membrane surface. XPS measurement and MD simulation revealed that the PEGMA segment was prefer to be present at the membrane surface rather than membrane bulk. The surface hydrophilicity and antifouling property of the copolymer membranes improved, owing to the higher concentration of PEGMA segment on the membrane surface. When the PEGMA segment percentage was up to 9.8 mol%, the copolymer membrane showed desired antifouling property and restrained irreversible fouling.

In Chapter III, poly(VC-*co*-PEGMA)/PVC blend membranes were successfully prepared via NIPS method. For evaluating the net effect of the membrane material on the fouling propensity of the prepared membrane, the dope solution composition was adjusted to obtain the membranes with similar pure water permeabilities. MD simulation was performed to study the chemical compositions of the membrane surfaces. The O/C ratios obtained from MD simulations showed higher values than those measured by XPS, because of the differences in the analysis depths and because the MD simulations model a system at equilibrium, while the experimental measurements are made on membranes that have not reached equilibrium. The results of the MD simulations suggested the choice of blending ratio to prepare a membrane with inhibited propensity to protein fouling. When copolymer/PVC blending ratio was than more than 1:2, the hydrophilicity and antifouling propensity of the prepared membranes considerable increased. For decreasing protein fouling, the changes in the membrane material properties were more effective than those in the surface structure.

In chapter IV, braid-reinforced poly(VC-*co*-PEGMA)/PVC hollow fiber membranes were successfully prepared via NIPS. The PET braid showed hydrophilic surface after the KOH

treatment with different conditions. For the PET braid-reinforced copolymer/PVC hollow fiber membrane, the bonding strength between the coating layer and the hydrophilicity modified PET braid was almost 2 times higher than using original hydrophobic PET braids. The braid-reinforced hollow fiber membranes exhibited thinner polymer coating layer thicknesses and smaller surface pore sizes than those of a self-supporting hollow fiber membrane (same membrane material and PWP). The tensile strength and bursting strength of the braid-reinforced hollow fiber membranes were higher than 170 and 2.1 MPa, respectively. The mechanical properties of the new prepared membranes were much larger than those of the various reported PVC hollow fiber membranes. The copolymer incorporated membrane surface showed the improved hydrophilicity and antifouling properties because of the copolymer surface segregation. In the filtration test of the BSA and activated sludge solution, the blend membranes exhibited the considerable improvement of the antifouling propensity and flux recovery after water backflush. The prepared braid-reinforced poly(VC-*co*-PEGMA)/PVC hollow fiber membranes showed much improved mechanical properties and surface antifouling resistance to activated sludge solution, suggesting their wide application potentials, such as the wastewater treatment. According to this work, the fabrication of braid-reinforced hollow fiber membrane can be recommended, when the soft hydrophilic materials are incorporated in the preparation of the hollow fiber membrane.

List of publications:

Z. Zhou, S. Rajabzadeh, A.R. Shaikh, Y. Kakihana, T. Ishigami, R. Sano, H. Matsuyama, Preparation and characterization of antifouling poly(vinyl chloride-co-poly(ethylene glycol) methyl ether methacrylate)membranes, J. Membr. Sci., 498 (2016) 414-422.

Z. Zhou, S. Rajabzadeh, A.R. Shaikh, Y. Kakihana, W. Ma, H. Matsuyama, Effect of surface properties on antifouling performance of poly(vinyl chloride-co-poly(ethylene glycol)methyl ether methacrylate)/PVC blend membrane, J. Membr. Sci., 514 (2016) 537-546.

Z. Zhou, S. Rajabzadeh, L.F. Fang, M. Taro, Y. Kakihana, H. Matsuyama, Preparation of robust braid-reinforced poly(vinyl chloride) ultrafiltration hollow fiber membrane with antifouling surface and application to filtration of activated sludge solution, Mater. Sci. Eng., C., submitted.

Acknowledgment

This thesis is the result of work that I have completed in three-year doctoral study. With all my pleasure, I want to express my deepest gratitude for all the people who have accompanied and supported me.

Foremost, I would like to express my sincere gratitude to my supervisor Prof. Hideto Matsuyama for the continuous support of my Ph.D study for his guidance, support and encouragement. His extreme enthusiasm and integral view on research always impressed me. I owe him a great debt of gratitude for showing me the way of research.

I truly thank Prof. Saeid for the kind help and guidance since I joined the Matsuyama Laboratory. Without your guidance, I would never achieve my accomplishments here.

My sincere thanks also goes to Dr. Fang, Dr. Kakihana of Kobe University for their kindness during the reviewing and examining of this thesis and giving many constructive comments to make it better.

My sincere gratitude is also to other assistant professors and students in the lab that I met in these four years. Thank you for your constructive comments for my research and your kindness. The time we shared together really means a lot to me.

Finally, I am forever indebted to my family: my parents and my wife. Without their whole-heartedly support and understanding, I could not accomplish my PhD thesis.

Zhuang Zhou

January, 2017

Graduate School of Science and Technology

Kobe University

Doctoral Dissertation, Kobe University

Preparation of antifouling poly(vinyl chloride) membranes for application in wastewater treatment, 147 pages

Submitted on January, 20. 2017

The date of publication is printed in cover of repository version published in Kobe University Repository Kernel.